Engineering
Library

MAY 12 '49

Journal of Research

of the

National Bureau of Standards

APRIL 1949

VOLUME 42 NUMBER 4

PERIODICALS OF THE NATIONAL BUREAU OF STANDARDS

Journal of Research

The National Bureau of Standards is the principal agency of the Federal Government for fundamental research in physics, chemistry, and engineering. It has the custody of the national standards of physical measurement in terms of which all working standards in research laboratories and industry are calibrated, and carries on necessary research leading to improvement in such standards and methods of measurement. It also has a general responsibility for basic research in physics, chemistry, and engineering, and for development of improved methods for testing materials and equipment. It determines physical constants and properties of materials, tests and calibrates standard measuring apparatus and reference standards, and studies technical processes. The results of the Bureau's research and investigations are published in the JOURNAL OF RESEARCH.

Research Papers

Reprints of individual articles appearing in the JOURNAL OF RESEARCH. They are made available to serve the needs of research workers, technical groups, and others for the separate papers relating to the special subjects in which they are interested.

Technical News Bulletin

Contains short but complete summaries of research, development, and testing in progress at the Bureau, accounts of the Bureau's national and international activities, scientific and technical announcements of new plans and programs, and a list of publications by members of the staff. It is a prompt and reliable source of official information of value to those who desire to keep in touch with the general activities of the Bureau.

Basic Radio Propagation Predictions

The CRPL–D series, Basic Radio Propagation Predictions, is issued as a monthly publication for those concerned with radio communication in determining the best sky-wave frequencies over any path at any time of day for average conditions for the month of prediction, which is made 3 months in advance. Charts of extraordinary-wave critical frequency for the F2 layer, of maximum usable frequency for a transmission distance of 4,000 km, and of percentage of time occurrence for transmission by sporadic E in excess of 15 Mc, for a distance of 2,000 km, are included.

ANNUAL SUBSCRIPTION Send order, with remittance, to Superintendent of Documents, U. S. Government Printing Office, Washington 25, D. C.	United States, Canada, Cuba, Mexico, Newfoundland, Republic of Panama	Other countries
JOURNAL OF RESEARCH of the National Bureau of Standards:		
12 monthly issues (2 volumes), paper covers	$4.50	$5.50
Bound volume (½ year, 1 volume), blue buckram	3.00	3.50
RESEARCH PAPERS	(*)	(*)
TECHNICAL NEWS BULLETIN, 12 monthly issues	1.00	1.35
BASIC RADIO PROPAGATION PREDICTIONS, 12 monthly issues	1.00	1.25

* The prices of the separate Research Papers appearing in this JOURNAL are given in the Contents. If 100 or more copies of any separate are ordered, a discount of 25 percent is allowed. Those who desire copies of separate Research Papers should send their orders and remittances without delay to the Superintendent of Documents, U. S. Government Printing Office, Washington 25, D. C. This will aid him to determine the number of copies to be printed for sale. Research Papers are not printed from electrotypes and usually no more reprints can be had when the first and only printing is exhausted.

The printing of this publication has been approved by the Director of the Bureau of the Budget, April 23, 1947

U. S. DEPARTMENT OF COMMERCE
Charles Sawyer, Secretary
NATIONAL BUREAU OF STANDARDS
E. U. Condon, Director

APRIL 1949
VOLUME 42
NUMBER 4

JOURNAL OF RESEARCH

of the

NATIONAL BUREAU OF STANDARDS

Contents

RP		Page
1972.	Characterization of some commercial soaps by X-ray diffraction. Gopal S. Hattiangdi. (Price 10 cents)	331
1973.	Characterization of alkali soaps by electron microscopy. Gopal S. Hattiangdi and Max Swerdlow. (Price 15 cents)	343
1974.	Some physical-chemical properties of aqueous solution of soap and soapless detergents. Gopal S. Hattiangdi, William W. Walton, and James I. Hoffman. (Price 10 cents)	361
1975.	Doubly charged ion spectra in mass spectra of hydrocarbons. Fred L. Mohler, Evelyn G. Bloom, Edmund J. Wells, Jr., Jonathan H. Lengel, and C. Edward Wise. (Price 10 cents)	369
1976.	Heats, equilibrium constants, and free energies of formation of cyclopentene and cyclohexene. Morton B. Epstein, Kenneth S. Pitzer, and Frederick D. Rossini. (Price 10 cents)	379
1977.	Preparation of calcium melibionate. William W. Walton and Horace S. Isbell. (Price 10 cents)	383
1978.	Polarographic limiting currents. John Keenan Taylor, Roberta E. Smith, and Irvin L. Cooter. (Price 10 cents)	387
1979.	Stress distribution near reinforced circular hole loaded by pin. Samuel Levy and Frank C. Smith. (Price 10 cents)	397
1980.	Volumetric determination of columbium. Howard B. Knowles and G. E. F. Lundell. (Price 10 cents)	405
1981.	Effect of concentration on the viscosity of dilute solutions. Robert Simha. (Price 10 cents)	409

For sale by the Superintendent of Documents, U. S. Government Printing Office, Washington 25, D. C. · Price 50 cents
$4.50 per year on subscription

UNITED STATES GOVERNMENT PRINTING OFFICE, WASHINGTON : 1949

UNIVERSITY OF MICHIGAN LIBRARIES

U. S. Department of Commerce
National Bureau of Standards

Research Paper RP 1972
Volume 42, April 1949

Part of the Journal of Research of the National Bureau of Standards

Characterization of Some Commercial Soaps By X-Ray Diffraction[1]

By Gopal S. Hattiangdi[2]

The diffraction of X-rays by 29 commercial soaps was investigated. The patterns indicate that the soaps are crystalline, and the data have been used to identify the various phases in the solid soaps. The single long-spacing value obtained for the toilet, medicated, glycerin, coco, and washing soaps is indicative of the existence of a single crystal type in these soaps. The exhibition of two or three sets of long-spacing values by the shaving soaps is indicative of the presence in these soaps of two or three individual phases.

The moisture content of these soaps indicates that the toilet and medicated soaps are either hemihydrates or monohydrates; the coco soaps, dihydrates; and the shaving soaps, monohydrates.

I. Introduction

The purpose of this paper is to present X-ray diffraction data for numerous types of commercial soaps manufactured in India and in the United States, and to correlate these with data for pure single soaps with a view to obtaining information, insofar as possible, regarding the degree of crystallinity and phase nature of these systems. It is hoped ultimately to correlate these X-ray data with the physical-chemical properties of aqueous soap solutions and their washing (cleansing) action. Results pertaining to these latter properties and also some information relating to phase nature, as revealed by electron microscopy, are presented in RP1973 and RP1974 [23].

Soaps are the metal salts of the higher saturated and unsaturated fatty acids and of rosin acids; they are sometimes understood to include salts of naphthenic acids and of synthetic "fatty" acids. Only the alkali and ammonium soaps, and some organic-base salts like triethanolamine soaps, are freely soluble in water and therefore suitable as detergents in aqueous solution. In the case of the saturated fatty acids, the property of detergency of the corresponding soaps is limited to those containing at least 8 and not more than 22 carbon atoms.

Several workers [2, 4, 6, 12, 13][3] have emphasized the importance of thermal and mechanical treatment given to pure sodium soaps, inasmuch as their transformation from one phase to another is readily achieved. Although the composition of the fatty stock used in the manufacture of soaps may vary from batch to batch, and certainly from manufacturer to manufacturer, it may be well to consider briefly the soap-boiling process so as to understand the extent and nature of mechanical and thermal treatment that a commercial soap receives.

Soap is obtained by saponification of fats or oils, the nature of the fatty stock largely determining the characteristics of the resultant soap. The

[1] Part of this work was conducted by the author in the Chemistry Department, University of Southern California, Los Angeles 7, Calif.

[2] Guest worker, Surface Chemistry Section.

[3] Figures in brackets indicate the literature references at the end of this paper.

UNIVERSITY OF MICHIGAN LIBRARIES

soap-boiling process involves the fact that soaps are soluble in dilute aqueous solutions of electrolytes but become quite insoluble when the concentration of the electrolyte is increased. Consequently, after saponification of the fat or oil is completed, salt is added, which separates the system into the hydrous soap and "lye." The actual boiling process requires 2 to 8 days, depending upon the method used and the size of the charge, and involves at least five important stages or changes: (a) killing, (b) graining, (c) washing, (d) strengthening, and (3) fitting or pitching. Stages (a) and (b) of the soap-boiling process involve heating or "boiling" the charge with the aid of "open" or "closed" steam; stages (c) and (d) involve successive addition of water and vigorous boiling with open steam, whereas in stage (e) heating is discontinued, and slow separation of neat soap and "nigre" takes place. Nigre is a dark-colored layer intermediate between neat soap and lye and contains a high concentration of soap and salts. The soap thus obtained is vigorously boiled again with closed steam before it is permitted to settle, the latter process being carried out at approximately 65° C for 1 or 2 days, or even longer. The following four layers form in the final "settle": (1) a foamy top layer, called fob; (2) the main layer of soap, which, in the hot fluid condition, is known as neat soap; (3) nigre; and (4) a small amount of lye, called pitch-water.

The important types of commercial soaps manufactured by the full-boiling process are milled soaps (toilet and shaving soaps), form-made soaps (household bar soaps and floating soaps), flake soaps (chipped and powdered soaps), and sprayed soaps (spray-dried and spray-crystallized soaps). Paste, cold-made coco, and liquid soaps are manufactured by the semiboiling process, the cold process, etc., in which the thermal and mechanical treatment given to the soaps is different from that in the full-boiling process.

Several years ago, McBain [14] presented an interpretation of the manufacture of soap by the boiling process on the basis of phase-rule diagrams derived by him and his collaborators. Since then, several workers have investigated systems of single and mixed soaps by employing different techniques. Investigations of binary and commercial-soap systems by X-ray diffraction revealed that commercial soaps crystallize as solid solutions with no evidence of fractional crystallization into the constituent single soaps [10]. Ferguson, et al. [12] have shown from X-ray diffraction studies that sodium soaps exist in four crystalline phases (alpha, beta, delta, and omega), which can be identified by the positions and intensities of the long and short spacings. When two or more phases are present simultaneously, however, the long spacing changes, but the short spacings retain their values and seem to be independent also of the fatty stock and moisture content. These characteristic short spacings are at 3.65 and 2.45 A for the alpha form, 2.75 A for beta, 3.55 and 2.85 A for delta, and 2.95 A for omega. Ferguson, et al., found that commercial milled soap containing 80 percent of tallow and 20 percent of coconut oil can be transformed into (a) the beta form by milling and plodding operations, (b) the omega form by heating in a sealed tube to 190° F and slow cooling, and (c) the delta form by reworking the original soap at a temperature around 50° to 60° F.

II. Experimental Procedure

1. Materials Used

Of the 29 soaps investigated, 9 were manufactured in the United States and 20 in India. All the soaps were purchased in the retail market in the form supplied to customers, the soaps manufactured in India being mailed to the author about a month before they were X-rayed.

Of the 9 soaps manufactured in the United States, 6 were popular brands of toilet soaps, 2 were coco soaps, and 1 was a "medicinal" soap. Of the 20 soaps manufactured in India, 6 were toilet soaps, 2 were glycerin soaps, 2 were "medicated" soaps, 4 were washing, or laundry, soaps, and 6 were shaving soaps.

The soaps used for X-ray investigation were in the "air-dry" state. Their moisture content was determined by drying them to constant weight in an air oven at 107° C. The results are presented on a percentage basis in tables 1 to 4.

TABLE 1. *X-ray diffraction data for some commercial toilet soaps*

	Soap—																							
	T1		T2		T3		T4		T5		T6		T7		T8		T9		T10		T11		T12	
Color	White		White		White		White		Pale grey-green.		White		Dark mauve		White		Dark mauve		Green		Green		Bright orange-brown.	
Feel	Soft waxy		Soft waxy		Dry waxy		Soft waxy		Soft waxy.		Soft waxy		Dry		Dry		Dry		Dry		Dry		Soft.	
Moisture content (%)	4.32		5.12		5.32		5.14		6.81		6.87		3.42		3.80		3.86		4.37		4.74		6.23.	
Long spacings:																								
Number of peaks	4		3		3		3		5		3		4		4		5		4		4		4.	
Intensity of third-order peak	29		13		36		19		33		11		28		31		28		34		32		23.	
Width at half intensity of third-order peak	0.60		0.70		0.60		0.65		0.75		0.80		0.70		0.60		0.65		0.60		0.55		0.75.	
$c \sin \beta$ (A)	41.4		42.0		42.2		41.9		42.5		41.7		42.3		41.6		42.5		40.6		42.0		41.1	
Short spacings	*d/n*	*I/29*	*d/n*	*I/20*	*d/n*	*I/36*	*d/n*	*I/33*	*d/n*	*I/33*	*d/n*	*I/20*	*d/n*	*I/28*	*d/n*	*I/31*	*d/n*	*I/28*	*d/n*	*I/34*	*d/n*	*I/32*	*d/n*	*I/25*
													4.753	0.11			4.791	0.11	4.769	0.15	4.713	0.19	4.801	0.09
	4.632	0.14	4.683	0.45	4.678	0.17	4.676	0.27			4.695	0.25	4.606	.14	4.661	0.16								
									4.587	0.18	4.582	.45					4.511	.11	4.587	.12			4.592	.39
	4.450	.21	4.431	.25	4.442	.25	4.457	.18	4.413	.21	4.473	.35			4.439	.23					4.462	.12		
			4.279	.30	4.230	.08							4.394	.11			4.210	.18	4.328	.09			4.230	.09
	4.118	.62					4.120	1.00					4.148	.21	4.137	.90	4.118	.50	4.185	.35	4.166	.56	4.105	.22
			4.062	1.00	4.082	.28			4.068	.85	4.090	1.00	4.019	.64					4.037	.21				
					3.997	.28															3.960	.19	3.960	.35
	3.847	.07	3.883	.15	3.870	.14	3.870	.12	3.837	.12	3.847	.15	3.872	.18			3.880	.21	3.717	.06	3.818	.09		
							3.607	.15	3.626	.12			3.670	.18	3.619	.10	3.681	.21	3.648	.06	3.691	.09	3.663	.09
	3.560	.17	3.553	.20	3.560	.14	3.509	.12			3.569	.20			3.548	.13			3.565	.09	3.587	.19	3.556	.13
													3.490	.11	3.486	.10			3.496	.09				
	3.240	.07	3.215	.10	3.249	.08	3.220	.06	3.230	.12	3.187	.15	3.201	.07	3.230	.06								
	2.993	.21	2.976	.45	2.980	.17	2.993	.45	2.986	.18	2.987	.40	2.974	.07	2.982	.32	2.961	.21	2.982	.06	2.990	.06	3.012	.09
	2.927	.14											2.925	.14	2.936	.26			2.919	.15	2.949	.09	2.955	.17
							2.862	.06					2.882	.07	2.854	.06			2.863	.12	2.868	.12	2.880	.09
	2.790	.10	2.781	.15	2.773	.08	2.778	.12	2.776	.12	2.774	.15	2.778	.11	2.780	.06	2.782	.11	2.767	.09	2.775	.06		
	2.675	.07	2.660	.10							2.617	.10												
			2.556	.10																				
	*2.5 to 2.2	.14			*2.5 to 2.15	.14			*2.5 to 2.15	.09			*2.5 to 2.2	.14	*2.5 to 2.2	.13	*2.5 to 2.15	.14	*2.5 to 2.15	.12	*2.5 to 2.2	.09	*2.5 to 2.2	.26
															2.085	.06	2.007	.11	2.01	.06			2.156	.09

* Band.

UNIVERSITY OF MICHIGAN LIBRARIES

TABLE 2. *X-ray diffraction data for some miscellaneous commercial toilet soaps*

	Coco soaps				Glycerin soaps				"Medicated" soaps					
	C1		C2		G 1		G 2		M 1		M 2		M 3	
Color	Dull whitish cream.		Lemon		Pale violet		Pale violet		Pale green		Dark green		Orange-red	
Feel	Very soft		Very soft		Soft		Soft		Dry		Soft		Very soft.	
Moisture content (%)	13.96		13.99		15.20		17.03		3.30		4.18		5.46.	
Long spacings:														
Number of peaks	3		4		3		4		4		4		3.	
Intensity of third-order peak	18		21		10		12		31		20		14.	
Width at half intensity of third-order peak	0.95		0.95		0.80		1.10		0.60		0.70		0.75.	
$c \cdot \sin \beta$ (A)	34.1		34.5		37.8		38.9		42.2		39.5		41.8.	
	d/n	*I/18*	*d/n*	*I/21*	*d/n*	*I/18*	*d/n*	*I/12*	*d/n*	*I/31*	*d/n*	*I/20*	*d/n*	*I/25*
Short spacings	4.723	0.61	4.753	0.57			4.735	0.58	4.703	0.19	4.730	0.55		
					4.671	0.61							4.685	0.84
	4.409	.17	4.448	.24			4.409	.42	4.450	.19			4.437	.36
	4.216	.56	4.232	.29					4.212	.16	4.297	.10		
									4.110	.74	4.185	.15	4.144	1.00
	4.053	.94	4.095	.81	4.064	1.00	4.051	.25			4.092	.35		
							3.955	1.00			3.960	.25		
			3.842	.10									3.818	.08
	3.770	.28			3.764	.28	3.720	.33			3.706	.25		
			3.619	.10	3.644	.28	3.613	.25	3.629	.06				
	3.582	.17					3.500	.33	3.565	.13	3.527	.15	3.587	.12
													3.370	.08
	3.238	.11					3.224	.25	3.261	.06	3.283	.10		
									3.052	.06				
									3.013	.10	3.105	.10		
	2.984	.33	2.996	.38	3.005	.11	2.983	.25	2.981	.13	2.980	.10	2.971	.60
	2.920	.28	2.923	.14	2.948	.28	2.927	.33			2.939	.35		
	2.832	.17	2.825	.10	2.860	.28	2.863	.33	2.894	.10	2.840	10		
					2.701	.17			2.806	.10			2.793	.08
							2.685	.17						
	* 2.43 to 2.15	.22	* 2.5 to 2.15	.14	* 2.5 to 2.2	.17	* 2.5 to 2.2	.25	* 2.5 to 2 2	.13	* 2.5 to 2.15	.20		
									2.016	.06	2.049	10	* 2.2 to 1.93	.12

* Band.

TABLE 3. *X-ray diffraction data for some commercial washing soaps*

	Soaps							
	W1		W2		W3		W4 (see page 339)	
Color	Yellow ochre		Pale yellow		Pale yellow		Pale yellow	
Feel	Very soft		Dry		Very dry		Soft.	
Moisture content (%)	11.46		13.39		14.60		17 40.	
Long spacings:								
Number of peaks	6		3		4		3	2.
Intensity of third-order peak	15		7		9		6	3.
Width at half intensity of third-order peak	0. 65		0. 70		0. 55		0. 70	0. 55.
$c. \sin \beta$(A)	36. 7		33. 1		37. 8		34. 3	41. 3.
Short spacings	*d*/*n*	*I*/15	*d*/*n*	*I*/7	*d*/*n*	*I*/9	*d*/*n*	*I*/7
			4. 804	0. 29	4. 848	0. 22	4. 874	0. 43
	4. 748	0. 13	4. 690	. 43	4. 671	. 33	4. 713	. 43
	4. 594	. 13					4. 518	. 29
	4. 349	. 27			4. 353	. 22	4. 339	. 29
			4. 279	. 29			4. 210	. 29
	4. 120	. 53	4. 064	. 86	4. 101	. 89	4. 069	1. 00
	3. 978	. 47	3. 882	. 29	3. 929	. 33	3. 938	0. 29
	3. 658	. 40	3. 673	. 43	3. 623	. 33	3. 652	. 29
	3. 494	. 27	3. 472	. 29	3. 473	. 33	3. 449	. 29
	3. 030	. 13	3. 019	. 29	3. 098	. 33	3. 016	. 29
	2. 942	. 42	2. 969	1. 00	2. 962	. 56	2. 960	. 86
	2. 862	. 20	2. 907	0. 29			2. 866	. 43
					2. 671	. 44		
					2. 452	. 33		
	[a] 2.5 to 2.2	. 27	2. 337	. 29	[a] 2.43 to 2.2	. 33	[a] 2.43 to 2.2	. 29

[a] Band.

UNIVERSITY OF MICHIGAN LIBRARIES

TABLE 4. *X-ray diffraction data for some commercial shaving soaps*

	Soap—											
	S1		S2			S3		S4		S5		S6		
Color	White		Muddy-green			Green		Pale yellow		Whitish-yellow		Yellow-white,		
Feel	Very soft		Soft			Very soft		Very soft		Very soft		Soft,		
Moisture content (%)	6.69		6.79			7.72		8.13		8.26		8.57.		
Long spacings:														
Number of peaks	4	4	3	4	4	5	5	3	4	4	3	4	4	4
Intensity of third-order peak	19	12	3	7	23	35	6	7	11	43	5	7	14	6
Width at half intensity of third-order peak	0.50	0.65	0.20	0.35	0.80	0.50	0.80	0.50	0.65	0.45	0.50	0.45	0.70	0.40
$c \sin \beta$ (A)	46.7	43.4	43.7	41.8	39.5	45.4	40.9	46.9	42.3	45.0	41.6	43.8	40.6	37.7
Probable phase of Napalmitate	α	β	β	δ	ω	α	δ	α	β	α	δ	β	δ	ω
Short spacings	d/n	I/I_0	d/n	I/I_0		d/n	I/I_0	d/n	I/I_0	d/n	I/I_0	d/n	I/I_0	
	.....	.....	.....	.....		.....	.....	.....	.....	4.733	0.07	4.763	0.13	
	4.651	0.26	.....	.....		4.681	0.04	4.676	0.09	.....	.....	4.642	.20	
	.....	.....	4.618	0.35		.....	.....	4.604	.41	.....	.....	.....	.....	
	.....	.....	.....	.....		.....	.....	.....	.....	.....	.....	4.571	.27	
	4.309	.21	.....	.....		.....	.....	4.318	.10	.....	.....	4.312	.20	
	.....	.....	4.218	.09		.....	.....	4.248	.14	4.216	.16	.....	.....	
	4.114	.21	4.103	.09		4.135	.45	4.134	.17	4.158	.37	4.154	.27	
	4.035	.74	3.972	.52		4.068	1.00	4.058	1.00	4.047	.35	4.047	1.00	
	.....	.....	.....	.....		3.992	0.21	.....	.....	3.987	.14	3.974	0.33	
	.....	.....	3.854	.22		3.878	.11	.....	.....	3.849	.19	3.875	.27	
	3.731	.16	.....	.....		3.737	.09	.....	.....	3.705	.07	3.723	.20	
	.....	.....	3.627	.17		3.607	.04	3.623	0.28	.....	.....	3.603	.20	
	3.545	.21	.....	.....		.....	.....	.....	.....	.....	.....	.....	.....	
	.....	.....	3.462	.09		3.480	.06	3.449	.07	.....	.....	.....	.....	
	.....	.....	.....	.....		3.302	.06	.....	.....	.....	.....	.....	.....	
	.....	.....	.....	.....		3.247	.09	.....	.....	3.281	.12	.....	.....	
	.....	.....	3.187	.13		3.159	.06	.....	.....	.....	.....	.....	.....	
	3.022	.11	3.055	.09		2.994	.06	3.075	.07	.....	.....	2.995	.13	
	2.936	.11	2.970	.13		2.942	.06	2.948	.07	.....	.....	.....	.....	
	.....	.....	.....	.....		.....	.....	2.903	.07	.....	.....	.....	.....	
	2.864	.16	2.887	.13		2.877	.11	2.847	.10	2.861	.07	2.885	.20	
	2.779	.11	2.760	.09		2.793	.04	2.744	.10	.....	.....	.....	.....	
	.....	.....	2.660	.13		.....	.....	2.641	.10	.....	.....	.....	.....	
	[a] 2.56 to 2.15	.21	2.562	.13		2.572	.04	.....	.....	.....	.....	.....	.....	
	.....	.....	[a] 2.53 to 2.08	.26		2.541	.09	2.531	.10	2.523	.05	.....	.....	
	.....	.....	.....	.....		2.481	.04	.....	.....	.....	.....	[a] 2.43 to 2.1	.13	
	.....	.....	.....	.....		2.372	.04	.....	.....	.....	.....	.....	.....	

[a] Band.

2. X-ray Diffraction Technique

X-ray diffraction patterns were obtained by using a North American Philips Co. Geiger-Müller X-ray spectrometer with Cu Kα radiations, the intensity of the diffracted rays and the diffraction angle being recorded automatically on an electronic strip-chart recording potentiometer. Samples for X-ray examination were packed into a circular hole $\frac{1}{8}$ in. in diamater cut in a 1- by 3-in. microscope slide, and smoothed off with a glass plate. More elaborate procedural details are described elsewhere [21, 22].

Bragg spacings (d/n), corresponding to interplanar distances of the crystal lattice, were calculated from the positions of the peaks in the curves according to the relation $n\lambda = 2d \sin \theta$, using the weighted average wavelength of Cu Kα_1 and Cu Kα_2 radiations from the copper X-ray target tube, namely, $\lambda = 1.5418$ A. The weighted average was used because the positions of the centers rather than of the maxima of the peaks were determined. Measurements were made to 0.01° in the value of the diffraction angle 2θ. Values of d/n calculated from the measurements were reproducible to 0.02 A at large angles and 0.2 A at angles as small as $2\theta = 5°$.

The long spacings given in tables 1 to 4 represent the length $c.\ \sin\beta$ and were determined by averaging values calculated from the positions of peaks corresponding to the third and successive orders. Values were not calculated from the positions for the first and second order long-spacing peaks, because their positions cannot be determined accurately by the present experimental set-up. The intensities of the short spacing peaks are expressed as their amplitudes above the baseline divided by that of the most intense peak in the pattern, which is frequently the third order of the long spacing, or the short spacing around 4.1 A. Relative intensities from line to line are directly comparable for a given soap pattern but are not comparable

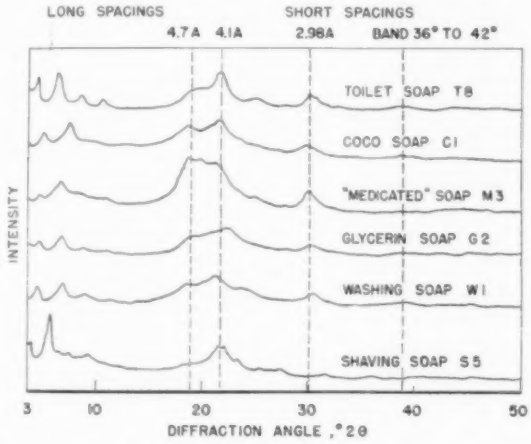

FIGURE 1. *X-ray diffraction patterns of some commercial soaps*

from soap to soap because of different reference intensities in different cases, as well as because of the difficulty of reproducing sample surface sufficiently closely to obtain reproducible values of absolute intensities.

Data for all the soaps, including the positions and relative intensities of the lines, bands, etc., are given in tables 1 to 4. However, since the degree of crystallinity can best be seen in terms of the sharpness of the pattern, representative one-fifth reductions of the original curves of intensity versus diffraction angle are given for six soaps in figure 1. The choice of the soaps and the order of their presentation is purely arbitrary. Values of the width at half intensity of the third order long-spacing peaks are also presented in tables 1 to 4.

III. Discussion

1. Appearance and Origin of the Diffraction Pattern

Examination of a typical X-ray diffraction pattern, such as that for soap T8 in figure 1, shows that it consists of a series of sharp, fairly intense peaks between $2\theta=3°$ and 10°, a second group of sharp, intense peaks between 20° and 30°, and a number of fainter peaks (not very evident on the reduced drawings) spread over the whole range.

The peaks at small angles arise from diffraction of X-rays by planes of atoms whose separation is proportional to the length of the soap molecule, $c.\sin\beta$. In all the soaps investigated, successive orders of this distance, $d/3$, $d/4$, etc., appear as peaks in the diffraction pattern; $d/1$, and $d/2$ generally occur at such small angles that values obtained with the present instrumental set-up are not accurate. The relative intensities of the several orders of the long spacing vary from soap to soap, being a function both of the crystal type and the scattering power of the various atoms for X-rays.

The peaks in the intermediate angle range arise from the diffraction of X-rays from planes of atoms separated by much smaller distances than those described above and are referred to as short spacings. The numerical values give distances between planes in the crystal lattice and can be related directly to the distances between the molecules by making assumptions about the crystal type.

Individual peaks vary considerably in their angular width at half maximum intensity. A good example is to be seen in comparing the peak at around 4.1 A for soaps T8 and G2 in figure 1. A wide peak, such as that for the latter soap, may be referred to as a "halo". The occurrence of halos in these patterns is indicative either of a molecular arrangement less orderly than that of a three-dimensional crystal, a very small size of crystallites, or small spatial extent of crystallized regions within a different phase.

2. Toilet Soaps

The toilet soaps are all characterized by relatively low moisture content, varying from 3.42 to 6.87 percent. The theoretical hemihydrate composition for sodium stearate, sodium palmitate,

UNIVERSITY OF MICHIGAN LIBRARIES

and sodium oleate is 2.86, 3.12, and 2.87 percent of H_2O, respectively. Toilet soaps commonly utilize a stock consisting of two-thirds tallow or high-grade fat and one-third coconut oil or other kernel oil, and thus have a high palmitate content. It seems reasonable therefore to assume that all the toilet soaps investigated here are hydrated to an extent of about 0.5 to 1 mole of H_2O per mole of soap.

For pure single soaps, each crystal modification has its own field of stability with respect to hydration or moisture. Its composition and temperature range, and the possible equilibria with other soap phases, constitute the phase diagram for the particular soap-water system. On the contrary, commercial soaps are convenient mixtures made from fats and oils containing both saturated and unsaturated components of varying chain lengths, and thus have complex phase diagrams. It is interesting, however, to test the applicability of Ferguson's hypothesis [12] regarding the absence of the alpha phase and the presence of only three phases (beta, omega, and delta) in commercial soaps to the present data.

The long-spacing value for the toilet soaps varies from 40.6 A for T10 to 42.5 A for T5 and T9; the mean average for the soaps manufactured in India is 41.7 A, and for those manufactured in the United States is 42 A. The long-spacing values for pure single sodium soaps reported in the literature are presented in table 5, in which the nomenclature used to designate the various phases is the same as that adopted by Ferguson, et al. [12]. Accordingly, Buerger's [6] kappa and eta phases and McBain's [7, 8] gamma correspond to Ferguson's omega, and Buerger's epsilon and zeta correspond to Ferguson's beta.

It is seen that the closest agreement of the long-spacing values for the toilet soaps seems to be with that for beta sodium palmitate, the values for sodium stearate and sodium oleate being rather high, and those for sodium laurate and sodium myristate being low. It is interesting to confirm the presence of beta sodium palmitate in these toilet soaps by comparing their short-spacing values with those reported by Thiessen and Ehrlich [18], Ferguson, et al. [12], and McBain, et al. [15]. It will be evident from table 5 that the agreement among the four sets of data is fair: the strong lines around 4.3, 3.9, 3.2, 3.1, and 2.7 A seem to match pretty well, and so do a number of other weaker lines. (The italicized values in this table are for the very strong, strong, and medium lines reported by the authors; the other lines are weak or very weak.) There also seems to be good agreement between these values for beta sodium palmitate and the short spacings obtained for the toilet soaps. It should be noted that the rather prominent "halo" around 2.95 A for the toilet soaps is characteristic of sodium oleate [20]. The halo from 36° to 42° in 2θ (centering around 2.4 A) seems to be more characteristic of sodium oleate than of sodium palmitate [20].

TABLE 5. *Short spacings for beta sodium palmitate*

Thiessen and Ehrlich [18]	Ferguson, et al. [12]	McBain et al. [15]	Thiessen and Ehrlich [18]	Ferguson, et al. [12]	McBain et al. [15]
A	A	A	A	A	A
		4.43		*3.13*	3.10
		4.38		*2.80*	2.81
4.28	*4.28*	*4.26*	*2.76*		*2.73*
		4.18		2.62	2.64
		3.99		2.48	2.50
3.88	*3.85*	*3.90*		2.35	2.36
		3.70			*2.25*
		3.64			2.15
	3.48	3.49			2.11
3.19		*3.19*			1.95
		3.18		1.78	*1.77*

In commercial soaps of low moisture content, simple cooling of neat soap produces the omega phase, which, in many cases, can be transformed into the beta phase by agitation at temperatures where the beta form is stable. The beta crystals are rapidly soluble and form lather easily, and thus have a direct and significant involvement in commercial soaps.

3. Coco, Glycerin, and "Medicated" Soaps

Both of the coco soaps investigated have an almost identical moisture content, namely, 13.96 and 13.99 percent, corresponding to about 2 moles of water per mole of soap. Their X-ray diffraction patterns are also identical in respect to the position, number, intensity, and sharpness of both the long- and short-spacing peaks. Both these soaps are reported by their manufacturers to have been made from pure coconut oil: the small long-spacing value of 34 A confirms the high laurate-myristate content to be expected from this oil stock; the main short spacings also agree reasonably well

with the values reported by McBain, et al. [1] for sodium laurate.

The glycerin soaps have the highest moisture content among these soaps. Soap G2 has a moisture content of 17.03 percent and a long-spacing value of 38.9 A, which is about 1 A longer than that for G1 (37.8 A), whose moisture content is 15.2 percent. These values of the long spacing are substantially lower than those for Pear's soap [17]. The long-spacing value for both G1 and G2 does not correspond to that for any single pure sodium soap, and it is therefore presumed that these are tallow-rosin soaps of rather indefinite fatty acid composition. The agreement between the short-spacing values for these two soaps and that for Pear's soap is relatively good. The glycerol halo, which should normally occur around 4.3 A [17], is not reported for both G1 and G2, because it is not clearly resolved; it probably is present, but the relatively high intensity of the closely situated peaks at 4.6 to 4.7 A and at 3.96 to 4.06 A evidently smears the glycerol halo.

The medicated soaps have a relatively low moisture content, corresponding to 0.5 mole of H_2O per mole of soap. The values of the long spacing for all the three soaps lie close to that for beta sodium palmitate and, like the toilet soaps, many of the strong short spacings correspond to those for beta sodium palmitate and a few to those for sodium oleate. The general nature and characteristics of the X-ray diffraction patterns for these soaps are similar to those for the toilet soaps. It seems therefore that the incorporation of medicative materials does not alter the crystal habit of the soap molecule, although their presence seems to soften the "feel" of the products.

The single long-spacing value obtained for both the toilet and the medicated soaps is indicative of a single-crystal type rather than a mixture of individual components, which would exhibit several sets of long spacings.

4. Washing Soaps

Washing soap bars are characterized by high moisture content of the order of 11 to 17 percent, and a value of $c.\sin\beta$ which ranges from 33.1 to 37.8 A. One of these soaps (W4 special washing soap) exhibits two distinct sets of long-spacing peaks corresponding to values of 34.3 and 41.3 A. These soaps are evidently derived from tallow acids of rather indefinite and variable fatty acid composition, and the values of $c.\sin\beta$ therefore do not correspond with those for any single pure soap of the acetic series.

There is good general agreement between the positions, relative intensities, and half-widths of peaks in the region of the short spacings for the washing soaps considered together. Since lines corresponding to 2.75, 2.85, and 3.55 A are missing in all the patterns, one is inclined to predict from Ferguson's phase-identification scheme [12] that the beta and delta phases are not present. On the contrary, lines corresponding to 2.45, 3.65, and 2.95 A are present; although it seems most unlikely that the alpha phase is present in these form-made washing soaps, the chances are that the omega phase is present to a predominating extent and contributes these above-mentioned lines.

The omega phase is believed to occur in commercial-framed and in most milled soaps, the proportion present depending on temperature, moisture, stock composition, and other processing conditions. This phase is obtained ordinarily by rapid chilling of neat soap without agitation, and always tends to form when low-moisture soaps of usual formulas are slow-cooled from the molten condition. In general, formation of the omega phase is favored by higher temperatures, lower moisture content, and low molecular weights. In commercial sodium oleate, it is perhaps the only stable form under most conditions [12].

5. Shaving Soaps

All of the six soaps investigated were in stick form and had a moisture content ranging from 6.7 to 8.6 percent, which is equivalent to about 1 mole of water per mole of soap. Four of these soaps had two separate sets of long-spacing peaks each, and two soaps, S2 and S6, exhibited three different sets. The lowest value of $c.\sin\beta$ among these was 37.7 A, and the longest was 46.9 A. The most intense short spacing is around 4.0 A for each soap, and relatively weaker lines are present up to about 2.4 A.

Shaving soaps are manufactured usually by the soap boiler's full-boiling process and are milled soaps. On the basis of the long-spacing values for sodium palmitate given in table 6, it seems that the shaving soaps are mixtures of two or more phases of this soap. The probable phases in each soap are given in table 4. The persistent exhibition of a long-spacing value corresponding approximately

UNIVERSITY OF MICHIGAN LIBRARIES

to that of alpha sodium palmitate is rather surprising, since this phase, unlike beta, omega, and delta, is rarely encountered in the usual commercial soaps. The alpha phase is usually the starting point for the formation of the other phases, however, and its presence in the shaving soaps is indicative of incomplete transformation to the other three phases. Transformation of the alpha form to the beta form is achieved by removal of water either by heating to about 52° C in an open or closed tube, by evacuation at room temperature, or by grinding at room temperature [4]. Also, water can be incorporated with the omega form to produce beta, and water can be driven off from beta to reduce it to omega. The formation of the delta phase is favored by high molecular weights, low soap content, and low temperatures. It is obtained in sodium palmitate by quenching nigre and in sodium stearate by ordinary cooling. Delta is also formed spontaneously at room temperature in 50 percent aqueous mixtures of alpha, beta, and omega palmitates. In addition, extrusion of sodium palmitate of high moisture content at and somewhat above room temperature converts the beta to the delta phase [12].

TABLE 6. *Literature values of long spacing c.sin β, for sodium soaps*

Soap	Phase			
	Alpha	Beta	Omega	Delta
Na-Laurate			31.5 [12] 31.8 [1] 31.9 [9, 10]	
Na-Myristate			36.0 [10] 36.2 [12]	36.5 [12]
Na-Palmitate	45.7 [3] 46.6 [12]	41.9 [15] 42.1 [12] 42.3 [11]	39.6 [12] 40.2 [10]	40.6 [12]
Na-Stearate	51.4 [12] 51.8 [3] 51.9 [16] 52.7 [16]	45.8 [12] 46.2 [16] 46.3 [19] 46.5 [16]	44.1 [16] 44.4 [12] 44.6 [7, 8] 44.9 [9, 10] 45.0 [16] 45.6 [15]	45.0 [12]
Na-Oleate			44.9 [20]	

6. Particle Size, Degree of Crystallinity, and Crystal Form

A crystalline soap, well developed in three dimensions, exhibits a sharp, rather intense long spacing and several short spacings that are well defined and that lead to sharp peaks in the X-ray diffraction pattern. Symmetry of the crystal lattice in certain cases may reduce the number of short spacings, but the spacings remain sharp and fairly intense. Several sharp short-spacing peaks combine to give a broad peak of a sort referred to as a halo, but when this occurs, it is usually found that this peak is more asymmetric than the halos obtained for liquids and for less-crystalline arrangements.

The decrease in the degree of regularity may take place along one dimension at a time. If the regularity along the *c*-axis falls off, the long spacing decreases in intensity to the point of disappearance. If the decrease in regularity occurs along the other axes of the crystal arrangement, the long spacing remains relatively intense, but the number of the sharp short spacings decreases. In the extreme case, random orientation of the chains within sharply defined layers leads to sharp long spacings plus a liquid like halo (broad and nearly symmetrical) centered at an angle corresponding to the average separation of the hydrocarbon chains within the layers.

Different crystal forms are characterized by different unit cells, the most easily observed characteristic being perhaps the value of the long spacing, $c.\sin\beta$, from which the angle of tilt, β, can be evaluated. The short spacings obtained for any arrangement of ions are not so easily correlated with structure. However, it might be that the translations along the *a*- and *b*-axes of the unit cell should essentially be the spacings obtained, except for their absence due to extinctions corresponding to symmetry properties of the given crystal.

A decrease in the intensity of the different maxima, but with no change in the sharpness or number of the peaks, may be interpreted as being caused by dilution or by a decrease in the size of the crystalline particles present. An increase in the half-widths of ordinarily sharp peaks, but with no change in their intensity or number, is usually caused by the transformation of an orderly crystal form into a relatively disorganized liquid-crystalline form. A decrease in the number of lines with no change in the intensity, or sharpness, of the peaks may be interpreted as being due to the transformation of the material from one phase state to another.

IV. Summary

1. The diffraction of X-rays by 29 commercial soaps, including toilet, glycerin, medicated, coco, washing (laundry), and shaving soaps, was investigated. The degree of sharpness of the long- and short-spacing peaks for the various soap patterns, including those for the glycerin soaps, indicates that the soaps are crystalline.

2. On the basis of their moisture content, the toilet and medicated soaps were found to be either hemihydrates or monohydrates, the coco soaps dihydrates, and the shaving soaps monohydrates.

3. The X-ray diffraction data have been used to identify the various phases present in the solid soaps. The values of the long and short spacings for the toilet and medicated soaps seem to indicate that these soaps consist essentially of beta sodium palmitate and to a smaller extent of omega sodium oleate. The glycerin soaps are evidently tallow-rosin soaps of rather indefinite composition; they are not amorphous or undercooled liquids but contain very fine crystalline material. The coco soaps have a high laurate-myristate content of the omega phase. The washing (laundry) soaps exhibit long spacings that do not correspond to values for any single pure sodium soap, but their short spacings indicate the presence of the omega phase. The shaving soaps are characterized by the existence of two or more individual phases, probably of sodium palmitate, as evidenced by the presence in the X-ray diffraction patterns of two or more distinct sets of long-spacing lines.

The author is very grateful to Robert D. Vold, University of Southern California, Los Angeles, Calif., for use of the X-ray spectrometer and for general discussions on the interpretation of soap phases.

V. References

[1] O. E. A. Bolduan, J. W. McBain, and S. Ross, J. Phys. Chem. **47,** 528 (1943).
[2] M. J. Buerger, Proc. Nat. Acad. Sci. **28,** 529 (1942).
[3] M. J. Buerger, Am. Mineral. **30,** 551 (1945).
[4] M. J. Buerger, L. B. Smith, A. DeBretteville, Jr., and F. V. Ryer, Proc. Nat. Acad. Sci. **28,** 526 (1942).
[5] M. J. Buerger, L. B. Smith, and F. V. Ryer, J. Am. Oil Chem. Soc. **24,** 193 (1947).
[6] M. J. Buerger, L. B. Smith, F. V. Ryer, and J. E. Spike, Jr., Proc. Nat. Acad. Sci. **31,** 226 (1945).
[7] A. DeBretteville, Jr. and J. W. McBain, Science **96,** 470 (1942).
[8] A. DeBretteville, Jr. and J. W. McBain, J. Chem. Phys. **11,** 426 (1943).
[9] R. H. Ferguson, Oil & Soap **21,** 6 (1944).
[10] R. H. Ferguson and H. Nordsieck, Ind. Eng. Chem. **36,** 748 (1944).
[11] R. H. Ferguson, F. B. Rosevear, and H. Nordsieck, J. Am. Chem. Soc. **69,** 141 (1947).
[12] R. H. Ferguson, F. B. Rosevear, and R. C. Stillman, Ind. Eng. Chem. **35,** 1005 (1943).
[13] K. W. Gardiner, M. J. Buerger, and L. B. Smith, J. Phys. Chem. **49,** 417 (1945).
[14] J. W. McBain, third report on colloid chemistry and its general and industrial applications (Br. Assn. Adv. Sci.) p. 2 to 31 (1920); also numerous papers in J. Chem. Soc., J. Am. Chem. Soc., and Ind. Eng. Chem.
[15] J. W. McBain, O. E. A. Bolduan, and S. Ross, J. Am. Chem. Soc. **65,** 1873 (1943).
[16] J. W. McBain, A. DeBretteville, Jr., and S. Ross, J. Chem. Phys. **11,** 179 (1943).
[17] J. W. McBain, and S. Ross, Oil & Soap **21,** 97 (1944); J. Am. Chem. Soc. **68,** 296, 547 (1946).
[18] P. A. Thiessen and E. Ehrlich, Z. physik. Chem. **165A,** 464 (1933).
[19] P. A. Thiessen and J. Stauff, Z. physik. Chem. **176A,** 397 (1936).
[20] R. D. Vold and R. Clemens, private communication.
[21] R. D. Vold, J. D. Grandine, II, and M. J. Vold, J. Coll. Sci. **3,** 339 (1948).
[22] R. D. Vold and G. S. Hattiangdi, Ind. & Eng. Chem. Publication pending.
[23] G. Hattiangdi and M. Swerdlow, J. Research NBS **42,** 343 (1949) RP1973; G. Hattiangdi, W. W. Walton, and J. I. Hoffman, J. Research NBS **42,** 361 (1949) RP1974.

WASHINGTON, December 10, 1948.

UNIVERSITY OF MICHIGAN LIBRARIES

U. S. Department of Commerce
National Bureau of Standards

Research Paper RP1973
Volume 42, April 1949

Part of the Journal of Research of the National Bureau of Standards

Characterization of Alkali Soaps by Electron Microscopy

By Gopal S. Hattiangdi[1] and Max Swerdlow

The morphological differences between several closely related alkali soaps have been determined by the techniques of electron microscopy. The crystalline alkali soaps consist of an interlocked mesh of bundled fibers, whereas the liquid-crystalline soaps exhibit a flagellar and/or featureless phase. The micellar groupings for the individual soaps are unique, and a scheme based upon the electron micrographs is suggested for their characterization. The structures of lithium, sodium, and potassium palmitates are closely related. The laurate, palmitate, and stearate of sodium also exhibit homologous structures.

The results of these morphological investigations offer a rapid and accurate means of identification and have been successfully applied to the problem of characterizing commercial soaps of unknown composition.

I. Introduction

When alkali soaps are heated, desiccated, hydrated, or ground mechanically, they pass through a remarkable series of forms, each constituting a definite stable phase existing over a definite range of temperature and/or composition. Attempts have been made to characterize these phases by means of X-ray diffraction patterns, but the data reported in the literature are rather anomalous. Buerger, Smith, Ryer, and Spike [1][2] believe that sodium soaps exist in seven distinct crystalline phases (κ, ζ, μ, ϵ, δ, α, and η); in addition, they suggest several others (α', α'', η', η'', etc.), which are closely related to these seven. Ferguson, Rosevear, and Stillman [3] report only four solid soap phases (α, β, δ, and ω), their omega phase corresponding to Buerger's kappa and eta phases and their beta, to Buerger's epsilon and zeta phases. Also, Ferguson's omega phase is believed [3] to be identical to the gamma phase reported several years earlier by deBrettеville and McBain [2]. Added to this rather confusing use of different designations for the same phase is the large amount of somewhat conflicting data reported by these investigators, a general idea of which is presented elsewhere [4].

The electron microscope, with its high resolving power, has been used with considerable success in recent years to study a variety of colloidal systems. The curd fibers of sodium laurate have been investigated by Marton, McBain, and Vold [5] with the aid of an electron microscope, and have been shown to consist of a mass of fibers that are thin ribbons whose widths are reported to be integral multiples of approximately twice the length of the soap molecule.

The present investigation is of an exploratory nature. It is designed to reveal morphological differences between eight pure alkali soaps representing different homologous cations and anions, and to characterize some commercial soaps of unknown composition.

II. Materials Used

The soaps investigated were the palmitates of lithium, sodium, potassium, rubidium, and cesium, and sodium laurate, sodium stearate, and sodium oleate. All the palmitates were prepared by neutralizing a solution of palmitic acid in

[1] Guest worker, Section of Surface Chemistry.

[2] Figures in brackets indicate the literature references at the end of this paper.

95-percent ethyl alcohol with an alcoholic solution of the corresponding alkali hydroxide and drying the product to constant weight at 105° C. The sodium soaps were prepared by neutralizing a solution of the fatty acid in 95-percent ethyl alcohol with sodium ethylate; sodium laurate and sodium stearate were dried to constant weight at 105° C, and sodium oleate was dried under reduced pressure at 40° C. The constants of the fatty acids used are given in the following tabulation:

Acid	Equivalent weight	Iodine number	Melting point
			°C
Lauric (Eastman Kodak Company's best quality)	202.6	0.05	45.0
Palmitic (Eastman Kodak Company's best quality)	257.0	.0	62.2
Stearic (Kahlbaum, Schering's pure quality)	284.3	.0	69.0
Oleic (British Drug Houses' pure quality)	288.3	85.8	-----

Two toilet soaps (T3 and T8), one manufactured in the United States and the other in India, and samples of washing (W5) and shaving (S5) soaps (both manufactured in India) were the same as those used for the X-ray diffraction studies [4]. They were obtained from the retail market and were examined without any purification. Chemical analysis disclosed that the cation was sodium in all of the four soaps.

III. Experimental Procedure

The soaps were dispersed in anhydrous *n*-butyl alcohol by milling with a mullite mortar and pestle for 5 minutes in an air conditioned room at 24°C and 60-percent relative humidity. The suspension was cast on Formvar (polyvinyl formal) plastic films supported by 200-mesh stainless steel specimen screens. Upon drying, the specimens consist primarily of the undissolved soaps, since their solubility in *n*-butyl alcohol is very low.

Since metallic shadowing adds contrast as well as a three-dimensional aspect to the surface details, a very thin coating of evaporated chromium was deposited obliquely (at an angle whose tangent equals 5 cm/20 cm) upon the soap specimens. This was achieved in a manner similar to that of Williams and Wyckoff [8] by slowly evaporating 100 mg of pure (electrolytically deposited) chromium metal with a current of 30 amp at 15 v in about 10 min at a pressure of 10^{-5} mm of Hg. The chromium was outgassed for about 20 min with 10 to 20 amp of current through the tungsten-wire basket. During the deposition of the metal, elevations and depressions on the surface of the soap specimen cast shadows characteristic of its contour; where no metal is condensed, transmission of the incident beam is maximum, and where thick elevations occur, electron scattering is maximum and little or no electrons are transmitted. More details concerning the technique of metallic shadowing used here are reported elsewhere [7].

The shadowed specimens of the soaps were examined and photographed with an RCA—EMU (50 kv) electron microscope. The sampling plan included at least eight separate specimens for each soap. Representative micrographs of characteristic areas for the individual soaps are presented in figures 2 to 13, the linear magnification in each case being denoted below each reproduction. Negative prints are shown in the figures. For proper interpretation of the surface features and structures, they may be viewed as though the soap formations were obliquely illuminated.

IV. Results and Discussion

One of the most characteristic features of the soaps when viewed through the electron microscope is that many of them exhibit an interlocked mesh of fiber bundles of varying diameters and different degrees of twist but with a general tendency toward retaining both a criss-cross and a parallel structure (fig. 7, A). The diameters of the fibers are dependent not only upon the nature of the soap but also upon the concentration and rate of crystallization, inasmuch as denser areas of the same soap specimen exhibit stouter fibers than those found in regions of lower concentration. Although any measurement and subsequent interpretation of the ultimate fiber widths in terms of absolute units seems questionable, a qualitative comparison of dimensions and structures between soaps is reasonable. The growth of the fibers in parallel rows at right angles to each branch, either in the same or in different planes, is interesting and is probably related to

the monoclinic angle (the angle of tilt of the hydrocarbon chains, β). When $\beta=90°$, preferred orientation of the lateral branches is a maximum. The packing of the hydrocarbon parts of the soap molecules can be achieved in several ways. One possible manner, constructed from known values for the bond distances, bond angles, and atomic radii [6], is shown in figure 1, in which the packing of the soap molecules in the fiber is restricted to a lateral association of the hydrocarbon chains.

Another outstanding fact revealed by the electron microscope is that each soap exhibits unique and distinct features, such as a curdy mass, an octopean mass, filamentous, hairy, frond-like, and sheaf-like formations. The presence of these formations as well as the increase or decrease in their degree of crystallinity, internal and external structure, etc., are dependent upon the position of the soap in the cationic or anionic series. That these formations are characteristic and reproducible is shown consistently by the presence of approximately the same number, size, and shape of such formations in different specimens of the same soap prepared under identical conditions. These are probably due to a type of structural unit, such as a micellar grouping, within the soap fibers and are probably related either to the mosaic structure of the surface of crystals or to the crystal of the individual phases. Before any correlation of statistical significance can be made with regard to external morphology and molecular arrangements, further studies are necessary. Whatever the interpretation, these patterns serve as excellent guides for a quick characterization of the alkali soaps notwithstanding possible artifacts.

1. The Alkali Palmitates

Lithium palmitate is characterized by thick curdy clumps. Whether present singly or joined together with one or more of such clumps, they always exhibit a tendency for the curd to grow out in a frond-like formation that is usually opaque to the electron beam and lacks fine structure (fig. 2,A,B, and C). The primary pattern for sodium palmitate is revealed in the less dense areas as a very fine network of interlaced fibers that show a perceptible periodic structure (fig. 3,C). On this background are developed mounds similar to those for lithium palmitate but with fine spicular fibers fanning out from them (fig. 3,B). In the less concentrated regions, these mounds have the configuration of the fan palm (fig. 3,A). The resemblance of the sheaf-like appearance found in figures 2,C and 3,A is noteworthy. Potassium palmitate, like sodium palmitate, appears basically crystalline (fig. 4,B and C), and the fibers show a spiral periodicity that is not exhibited by lithium palmitate. Furthermore, the fibers tend to pack laterally with their periodic structure in register (fig. 4,B). In addition to this highly crystalline state, this soap exhibits a featureless liquid-like phase (fig. 4,A). In contrast to the somewhat analogous behavior of lithium, sodium, and potassium palmitates, rubidium and cesium palmitates show almost entirely different habits. Rubidium palmitate is characterized by a liquid-like phase from which small spheroidal particles seem to separate (fig. 5,B), the larger aggregates being present as terraced mounds of irregular shape (fig. 5,A and C). Cesium palmitate also exhibits a liquid-like phase that is present in the form of amorphous ribbon-like films (fig. 6,A). Figure 6,B and C show thin long fibers, which probably have a greater degree of crystallinity, developing from an agglomerated mass of this liquid phase.

In summation, it might be said that of the five homologous alkali palmitates, lithium, sodium, and potassium exhibit a somewhat similar appearance, whereas rubidium and cesium are distinctly different. The first three soaps are differentiated by the mounds of curd-like material from which fibers grow. The degree of crystallinity, orientation, and periodicity of these fibers are least for lithium palmitate and most for potassium palmitate. Rubidium and cesium palmitates have a predominant liquid-like phase unlike the other three soaps, which exhibit a linear network of interlaced fibers. Rubidium palmitate is characterized by very small terraced mounds of eccentric shapes, whereas cesium palmitate exhibits agglomerated masses, from which thin long fibers grow out in all directions.

2. The Sodium Soaps

Sodium laurate has a basic structure of curd-like fibers intermeshed in a more or less regular parallel formation (fig. 7,A). The resemblance between the unshadowed specimen (fig. 7,B) and that published by Marton, McBain, and Vold [5] is very interesting because the soap structures seem to be independent of the two different methods of

specimen preparation and of the ionic or monionic nature of the solvents used. In the less concentrated areas, the bundled fibers appear to be flattened out into a sheaf-like pattern (fig. 7,C). There also appears a thorny protrusion in these fibers. Sodium palmitate exhibits finer fibers, and sodium stearate has the finest (fig. 8,A), but both these soaps have a parallel bundling similar to that for the laurate. Sodium stearate has extremely fine fibers developed in dendritic forms (fig. 8,C). By contrast, the basic structure for sodium oleate consists of a very stout fibrous network, the less concentrated areas showing a fine swirled flagellar formation (fig. 9,A). From this predominant phase large micellar groupings develop with an octopean structure—a semicrystalline mound in the center and curling fiber bundles of varying diameters emanating in all directions (fig. 9,B).

In summation, it might be said that the sodium soaps of the saturated fatty acids exhibit a homologous behavior, characterized by a meshwork of interwoven fibers laid out in a regular linear formation and a sheaf-like bundling of the finer fibers (fig. 8,B, 3,A, and 7,C). The fineness of the sheaf-like formations varies for the sodium soaps in the order: laurate < palmitate < stearate. Sodium oleate exhibits a very different behavior, characterized by a lack of linearity and is probably due to the essentially liquid-crystalline nature of this soap.

The increase in the periodic spacings of the soap fibers with increasing molecular weight of the soap (LiP < NaP < KP and NaL < NaP < NaStr) suggests their possible correlation. This is brought out in the tabulation below, in which data are presented for the periodicity for the alkali soap fibers as found in the original electron micrographs.

Soap	Molecular weight	Approximate periodicity
		A
Sodium palmitate	278. 3	500
Potassium palmitate	294. 4	675
Sodium stearate	306. 3	750

The periodic structure that results from a type of stress imposed upon the growth of the soap fibers is exhibited by those soaps that are crystalline in nature and are salts of the saturated fatty acids. Other factors that have an important bearing on the amorphous and/or crystalline nature of the soaps are the degree of hydration, composition, temperature, pressure, extent of mechanical treatment, and rate of precipitation. Assuming that all these factors are similar for the various soaps, it seems reasonable to conclude that for the soaps with the same *anion*, the strain is probably caused by the heavy cation attached to the fatty acid radical; and for the soaps with the same *cation*, the strain is brought about by the inertia of the heavy hydrocarbon chains (fig. 1).

3. Application to Commercial Soaps

Electron micrographs of the samples of two toilet soaps exhibit a network of fine interlaced fibers (figs. 10, B and 11, C); numerous mounds of curd-like material from which fine fibers showing traces of periodic structure grow out (figs. 10, A and 11, A); and a swirled flagellar formation (figs. 10, C and 11, B). The first two characteristics are typical of sodium palmitate and the third of sodium oleate. Toilet soaps are usually made from oils of high palmitate-oleate content. Analysis by X-ray diffraction cannot definitely identify the components of the binary system, since only an average value for the two long spacings and overlapping peaks for the short spacings are obtained [4]. On the other hand, observations by electron microscopy are in excellent agreement with chemical analysis, and in such cases prove to be not only more rapid but more accurate than X-ray diffraction or other methods of analysis.

The washing (laundry) soap (fig. 12) is characterized by an essentially liquid-like phase from which aggregates of indefinite shape and little fine structure separate. The extremely primitive state of these aggregates and the absence of any appreciable number of fiber or flagellar formations makes identification of this soap uncertain, although the possible existence of sodium palmitate is indicated. X-ray diffraction data [4] show that the long-spacing value for this soap does not correspond to that for any single pure sodium soap.

The shaving soap consists of a very fine network of interlaced fibers, which show a periodicity of about 600 A (fig. 13, C), and curd-like mounds from which fine short fibers emanate (fig. 13, A and B). The first may be expected from a mixture of sodium palmitate and sodium stearate, and

the second from sodium palmitate alone. X-ray diffraction data [4], however, indicate the presence of several phases of sodium plamitate and do not reveal the presence of any other type of soap.

The authors are very grateful to Robert D. Vold for some of the soap samples, to James W. McBain and Howard F. McMurdie for their critical comments on the interpretation of this study, and to Esther Golovato for her very valuable assistance in processing the many electron micrographs.

V. References

[1] M. J. Buerger, L. B. Smith, F. V. Ryer, and J. E. Spike, Jr., The crystalline phases of soap, Proc. Nat. Acad. Sci. **31**, 226 (1945).

[2] A. deBretteville, Jr. and J. W. McBain, X-ray evidence for a third polymorphic form of sodium stearate, Science **96**, 470 (1942); X-ray diffraction investigation of sodium stearate from room temperature to the melting point, J. Chem. Phys. **11**, 426 (1943).

[3] R. H. Ferguson, F. B. Rosevear, and R. C. Stillman, Solid soap phases, Ind. Eng. Chem. **35**, 1005 (1943).

[4] G. S. Hattiangdi, Characterization of some commercial soaps by X-ray diffraction, J. Research NBS **42**, (1949) RP1972; G. S. Hattiangdi, W. W. Walton, and J. I. Hoffman, Some physical-chemical properties of aqueous solutions of soaps and soapless deturgents, J. Research NBS **42** (1949) RP1974.

[5] L. Marton, J. W. McBain, and R. D. Vold, An electron microscope study of curd fibers of sodium laurate, J. Am. Chem. Soc. **63**, 1990 (1941).

[6] L. Pauling, The nature of the chemical bond (Cornell University Press, Ithaca, N. Y., 1940).

[7] M. Swerdlow and G. S. Seeman, A method for the electron microscopy of wool, J. Research NBS **41**, 231 (1948) RP1921; Textile Res. J. **18**, 536 (1948).

[8] R. C. Williams and R. W. G. Wyckoff, Applications of metallic shadow-casting to microscopy, J. Applied Phys. **17**, 23) (1946).

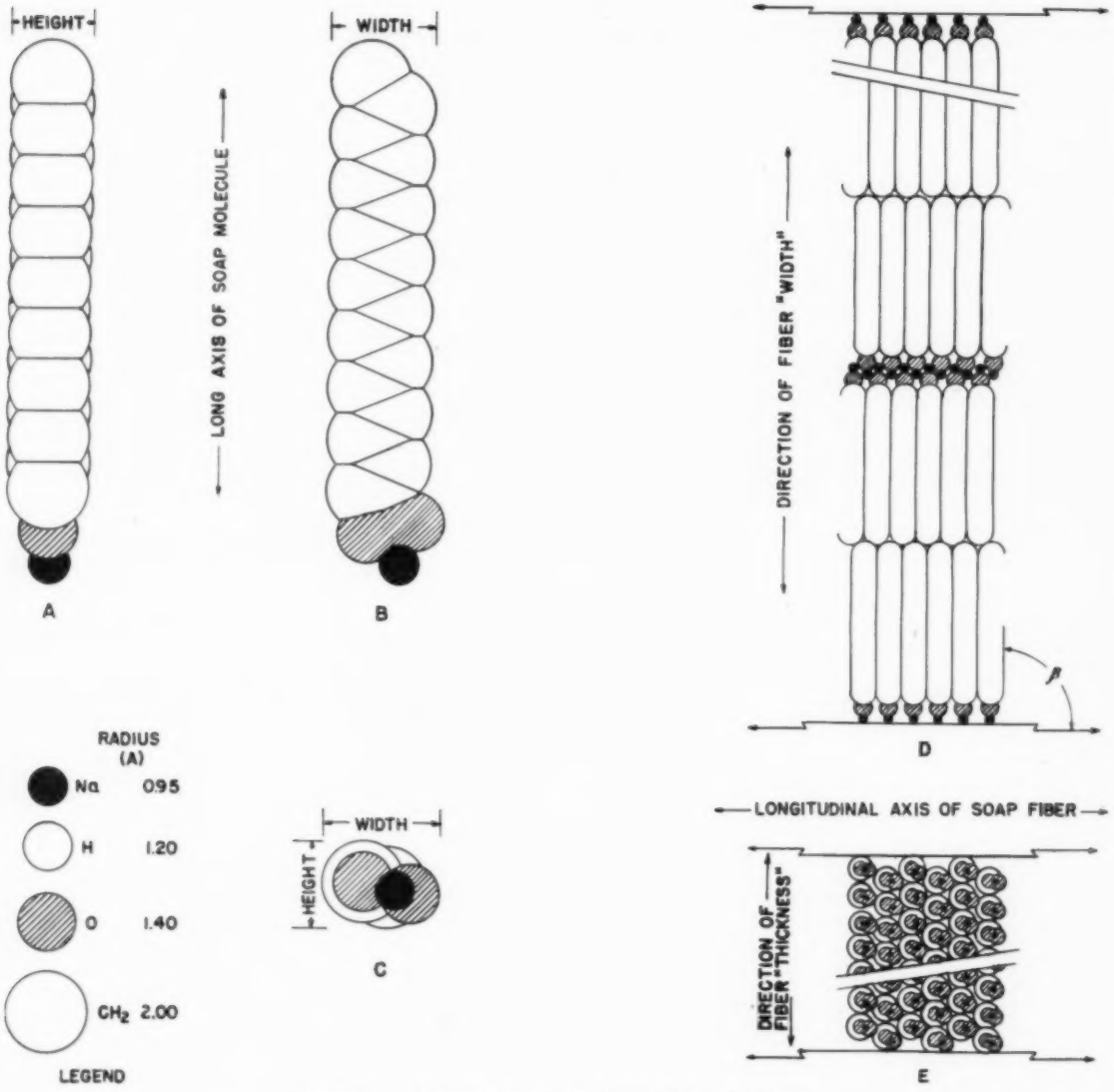

FIGURE 1. *Schematic representation of molecular packing*

This shows the soap (sodium stearate) molecule as viewed from different directions. Views D and E are drawn to approximately one-third the scale indicated for views A, B, and C. A, viewed in a direction perpendicular to the long axis of the molecule but lying in the plane of the hydrocarbon chain; B, perpendicular to both the long axis of the molecule and the plane of the carbon atoms in the chain; C, parallel to the long axis of the molecule as viewed from the carboxylate end; D, sodium stearate molecules (probably 10 or more in number) packed laterally end to end to form a linear chain, thus contributing to the "width" of the fiber. The orientation is not necessarily perpendicular as shown, but tilted at an angle, β, which varies from soap to soap; E, the packing of molecules viewed along a direction parallel to both the long axis of the molecules and the plane of the carbon atoms in the chain (corresponding to view C). Such a packing in the plane of the carbon atoms takes place almost indefinitely and contributes to the "length" of the fiber. The "height", or "thickness", of the fibers is dependent upon the number of soap molecules packed in a direction perpendicular to the plane of the carbon atoms but parallel to the long axis of the soap molecules.

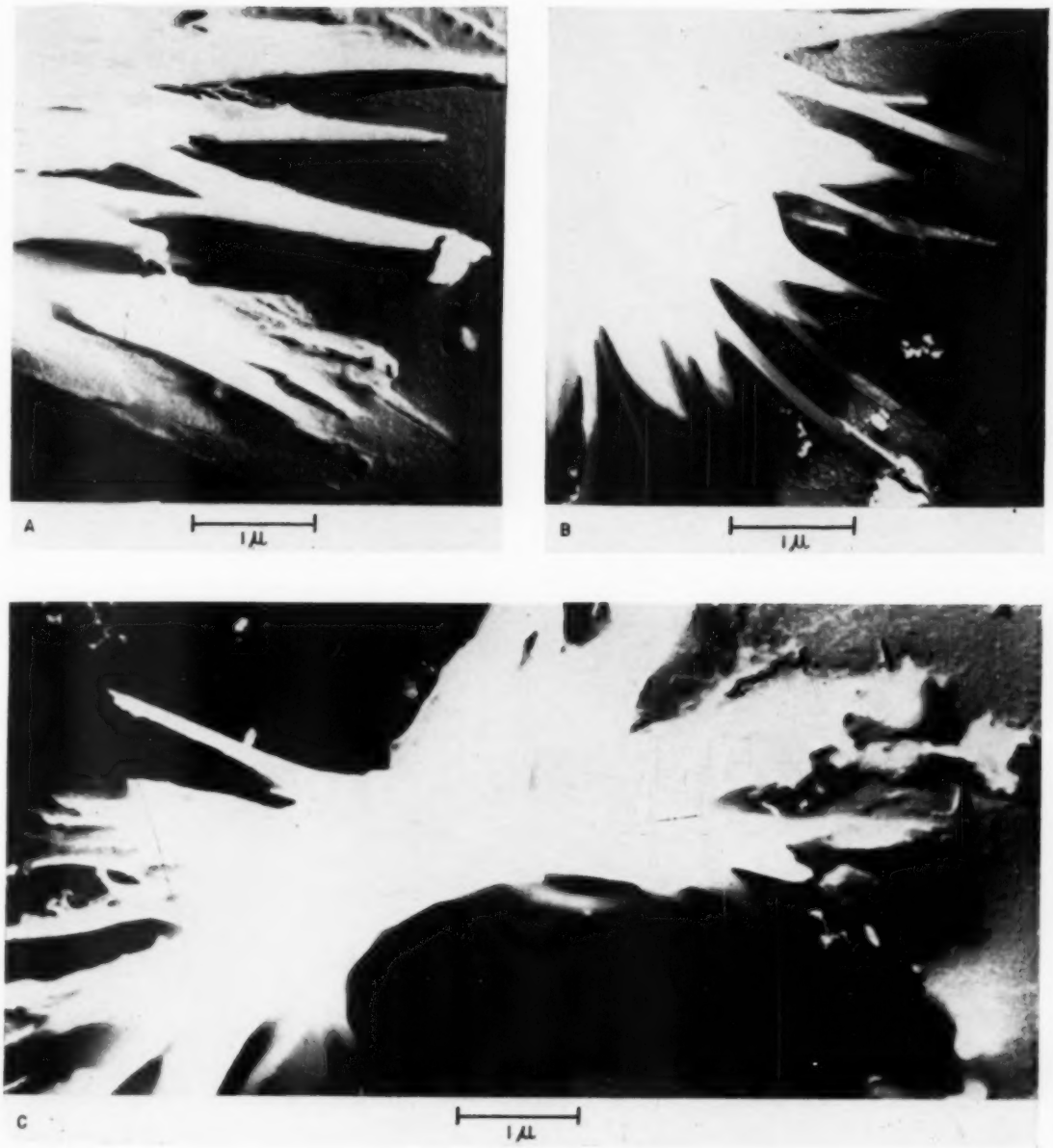

FIGURE 2. *Lithium palmitate*

	Total magnification	Electronic	Optical
A	19,000	9,500	2.0
B	19,000	9,500	2.0
C	18,700	5,200	3.6

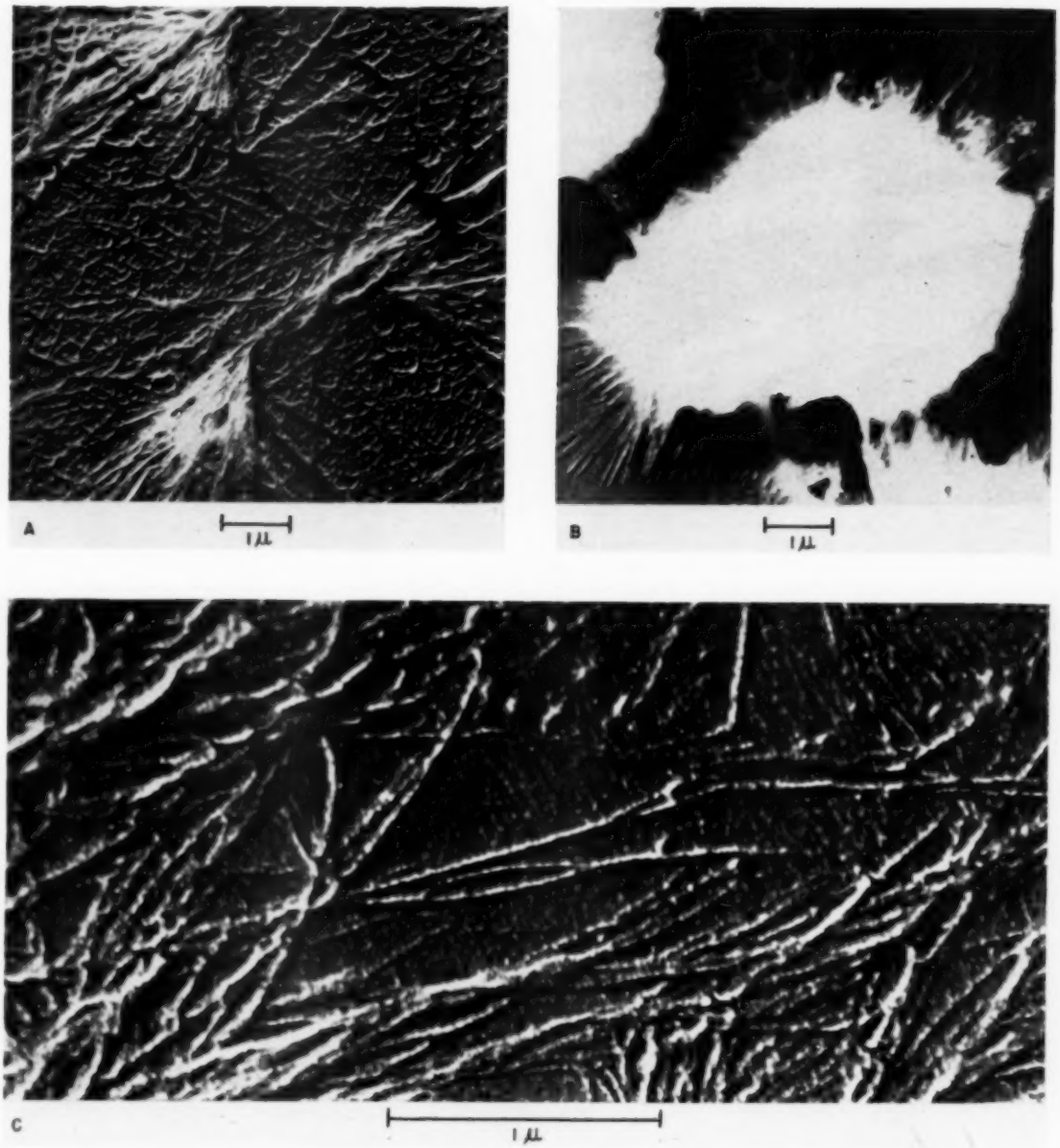

FIGURE 3. *Sodium palmitate*

	Total magnification	Electronic	Optical
A	10, 400	5, 200	2.0
B	10, 400	5, 200	2.0
C	42, 800	9, 500	4.5

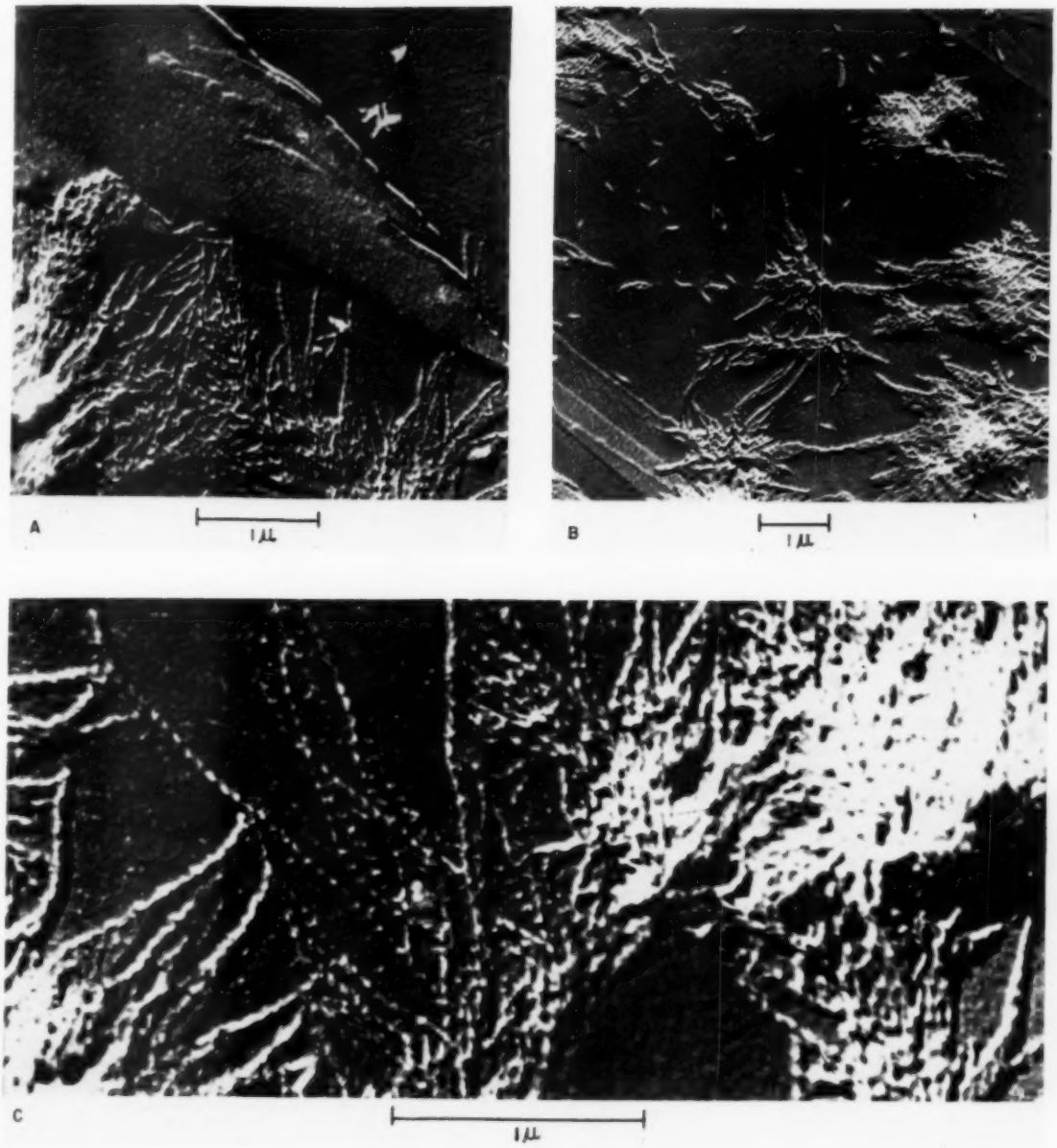

FIGURE 4. *Potassium palmitate*

	Total magnification	Electronic	Optical
A	19,000	9,500	2.0
B	10,400	5,200	2.0
C	39,900	9,500	4.2

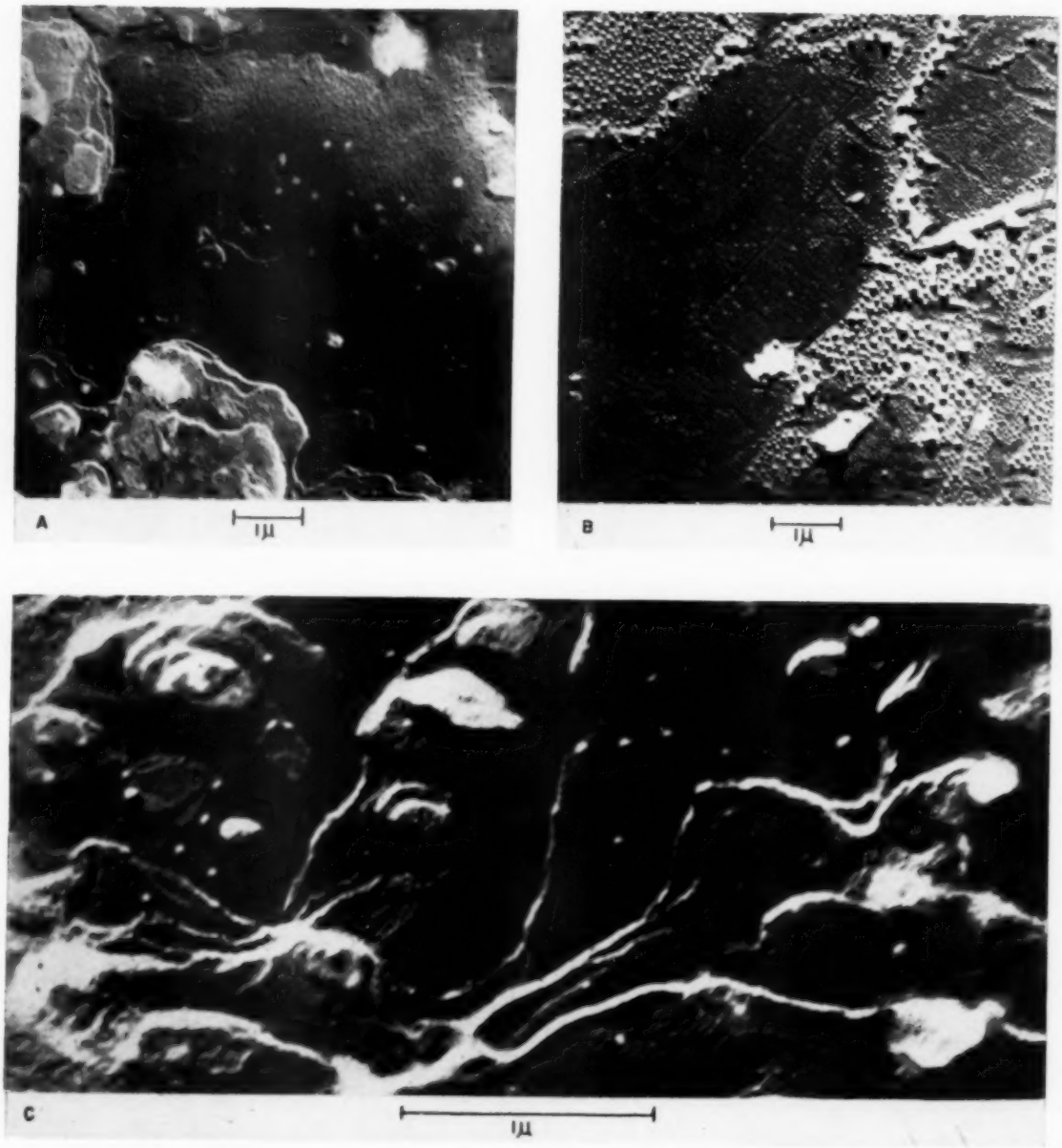

FIGURE 5. *Rubidium palmitate*

	Total magnification	Electronic	Optical
A	10, 400	5, 200	2.0
B	10, 400	5, 200	2.0
C	35, 200	9, 500	3.7

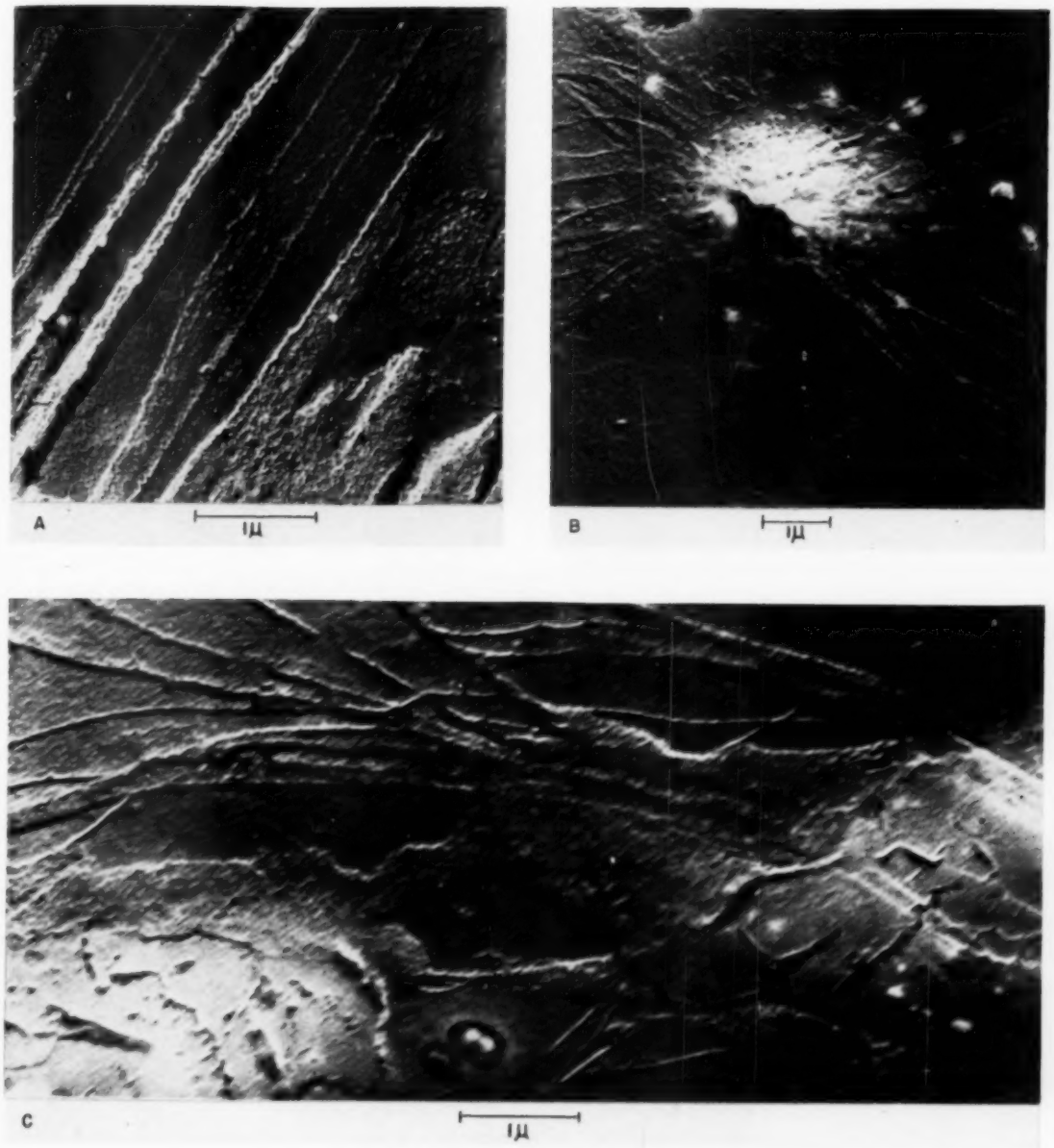

FIGURE 6. *Cesium palmitate*

	Total magnification	Electronic	Optical
A	19,000	9,500	2.0
B	10,400	5,200	2.0
C	18,700	5,200	3.6

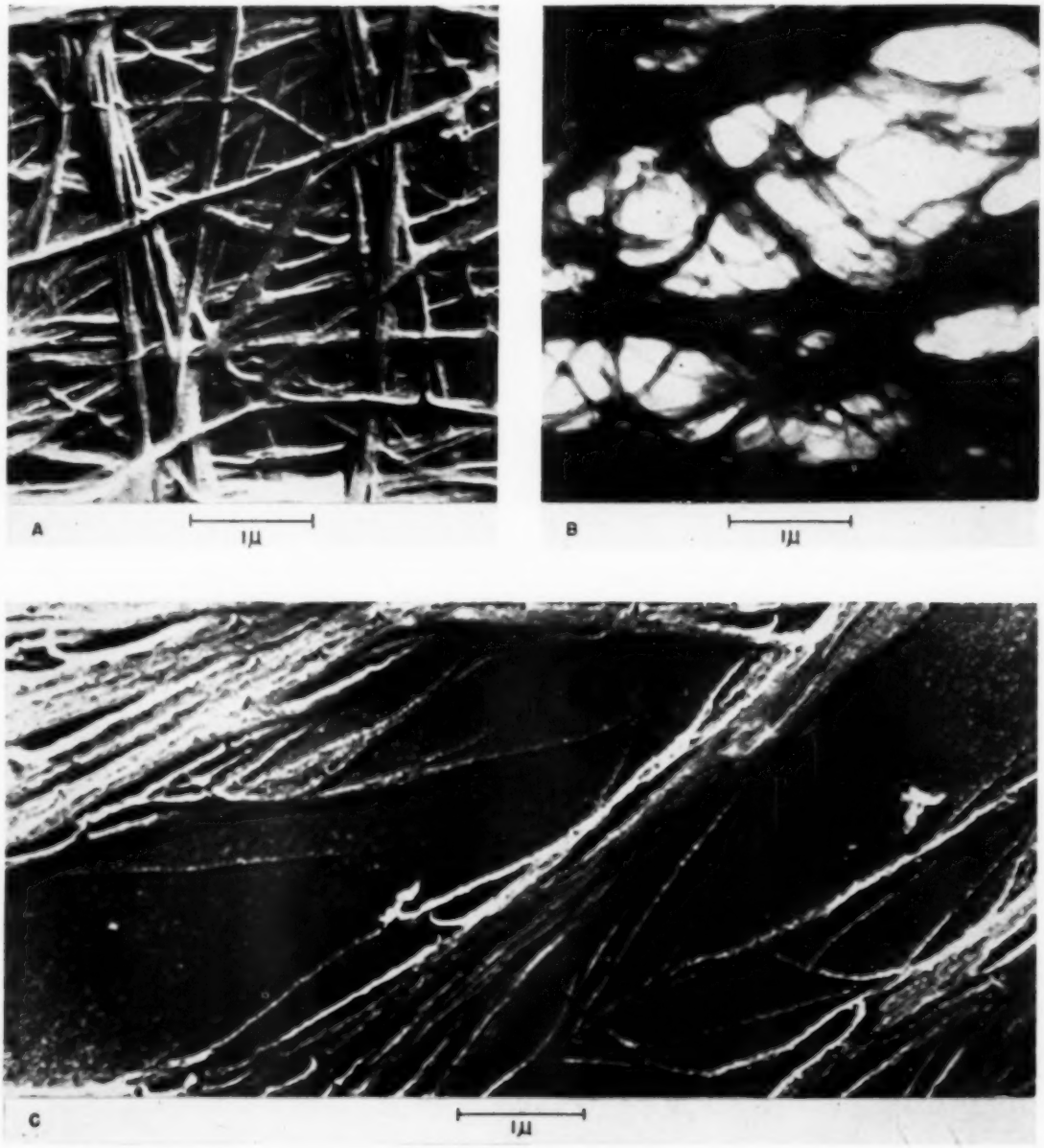

FIGURE 7. *Sodium laurate*

	Total magnification	Electronic	Optical
A	19,000	9,500	2.0
B	19,000	9,500	2.0
C	19,800	5,200	3.8

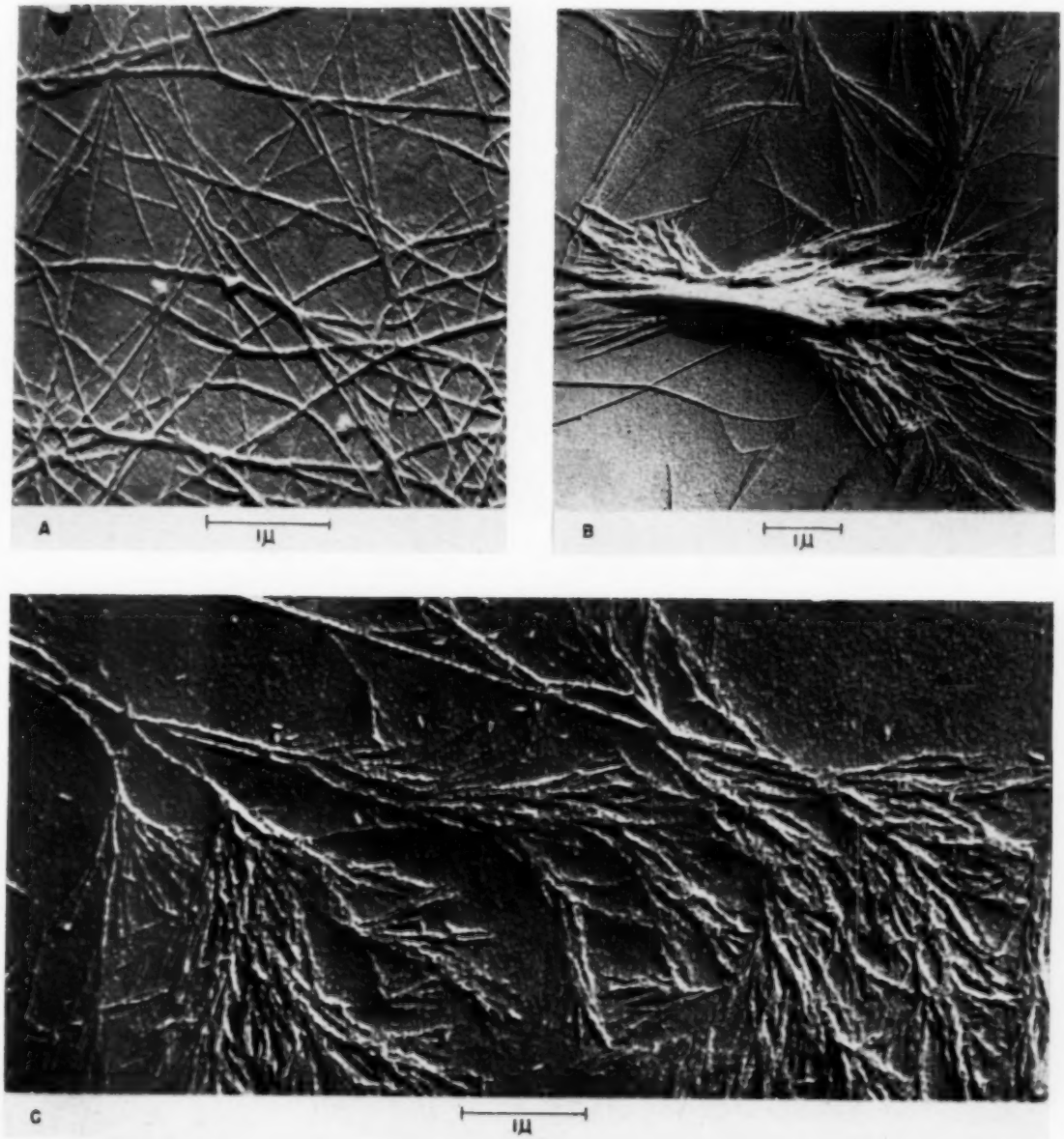

FIGURE 8. *Sodium stearate*

	Total magnification	Electronic	Optical
A	19,000	9,500	2.0
B	12,000	6,000	2.0
C	19,200	5,200	3.7

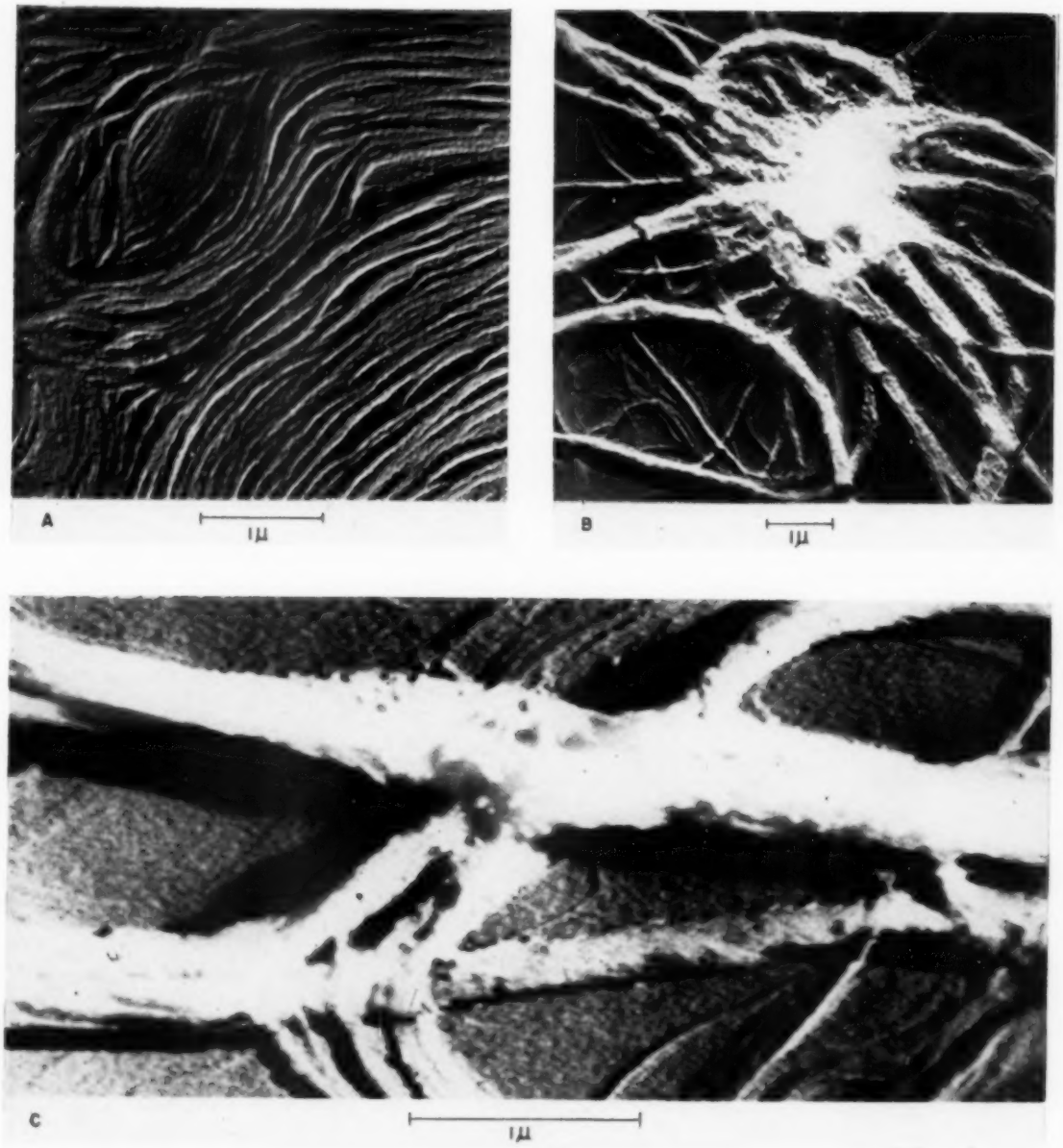

FIGURE 9. *Sodium oleate*

	Total magnification	Electronic	Optical
A	19,000	9,500	2.0
B	10,400	5,200	2.0
C	38,100	9,500	3.8

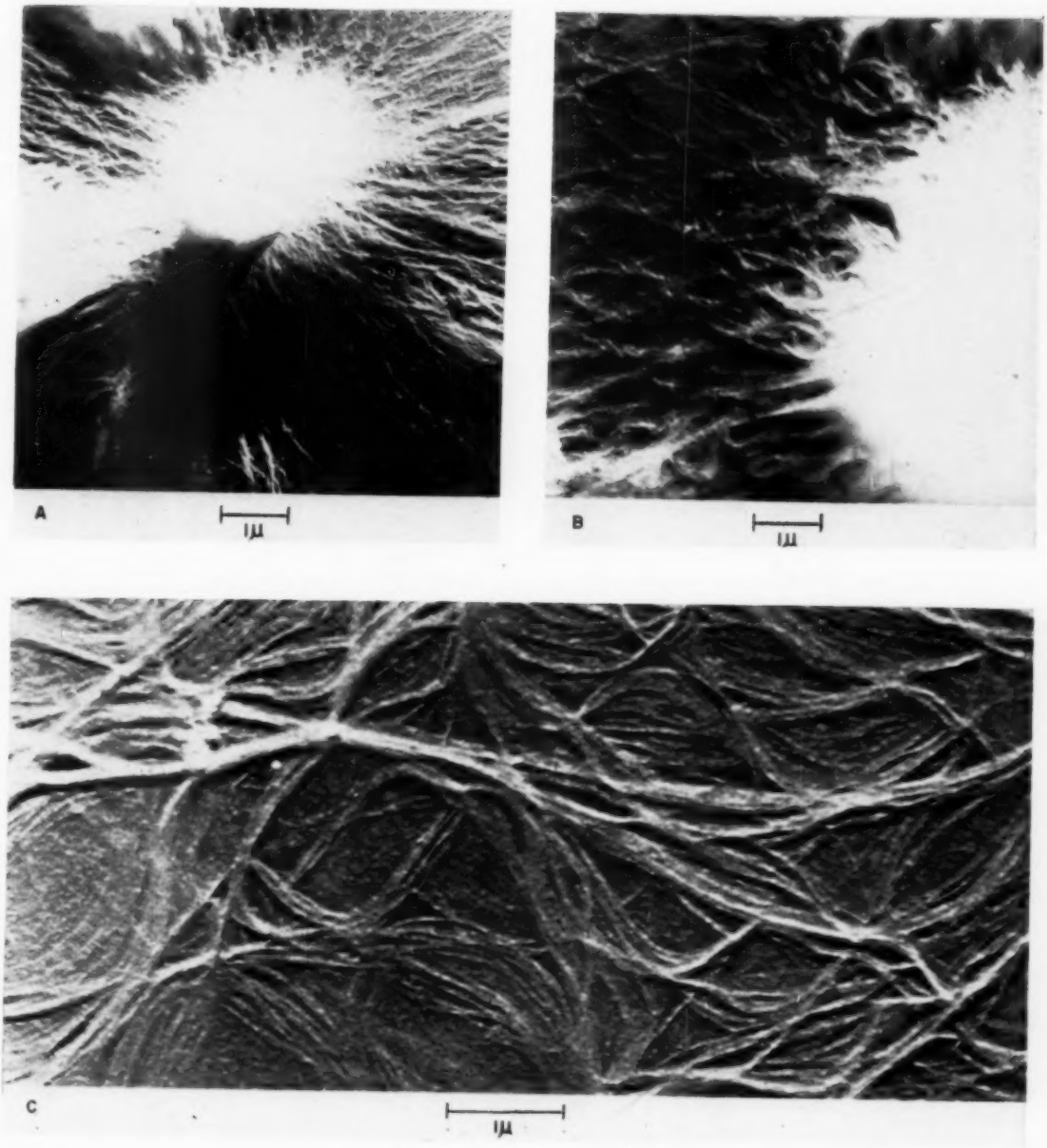

FIGURE 10. *T3 toilet soap (USA)*

	Total magnification	Electronic	Optical
A	10,400	5,200	2.0
B	10,400	5,200	2.0
C	18,700	5,200	3.6

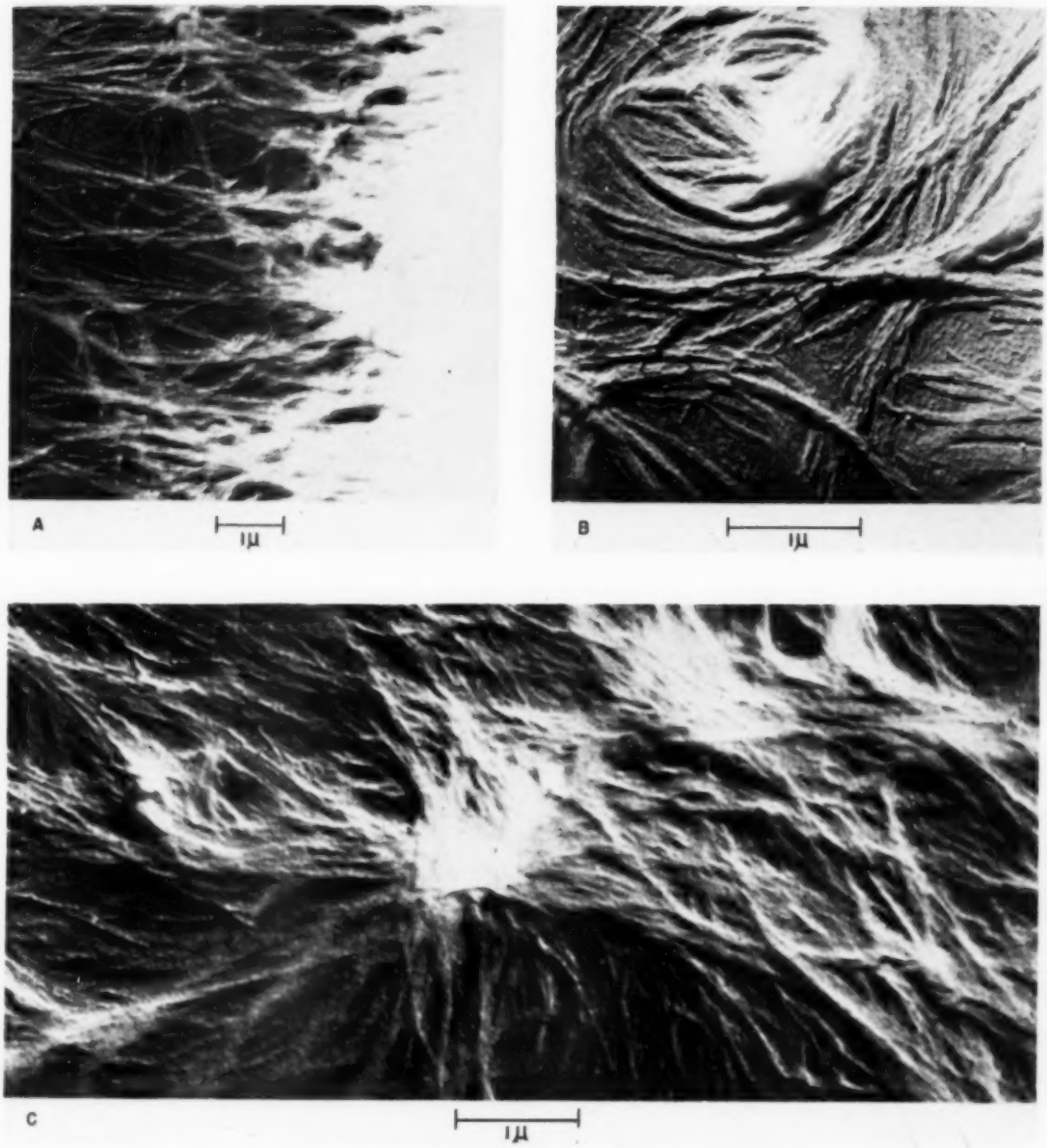

FIGURE 11. *TS toilet soap (India)*

	Total magnification	Electronic	Optical
A	10,400	5,200	2.0
B	21,000	10,500	2.0
C	19,200	5,200	3.7

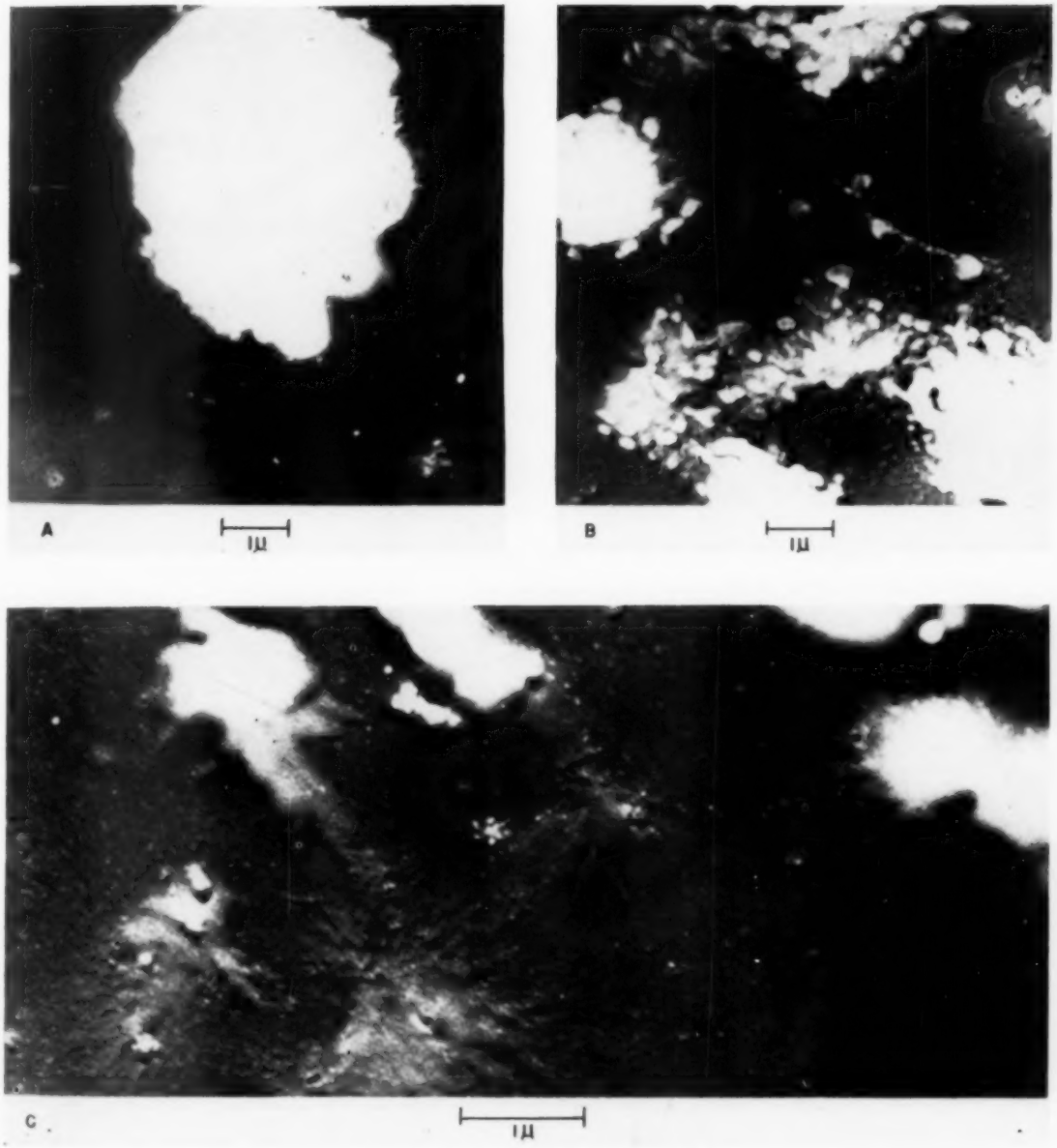

FIGURE 12. *W5 washing soap (India)*

	Total magnification	Electronic	Optical
A	10, 400	5, 200	2.0
B	10, 400	5, 200	2.0
C	19, 200	5, 200	3.7

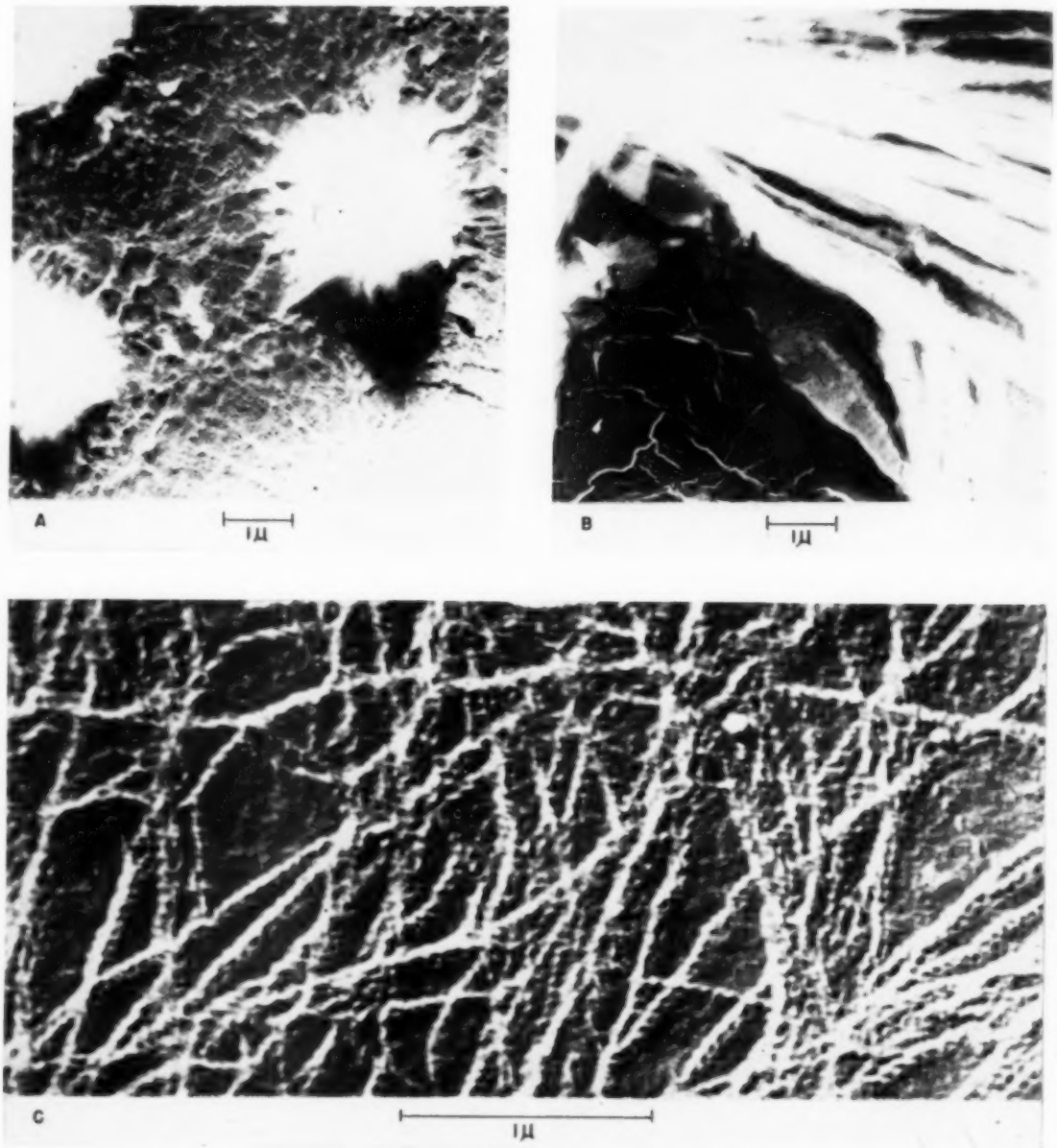

FIGURE 13. *S5 shaving soap (India)*

	Total magnification	Electronic	Optical
A	10, 400	5, 200	2.0
B	10, 400	5, 200	2.0
C	38, 900	10, 500	3.7

U. S. Department of Commerce
National Bureau of Standards

Research Paper RP1974
Volume 42, April 1949

Part of the Journal of Research of the National Bureau of Standards

Some Physical Chemical Properties of Aqueous Solutions of Soaps and Soapless Detergents

By Gopal S. Hattiangdi,[1] William W. Walton, and James I. Hoffman

A study has been made of the effect of concentration on the surface tension, electrical conductance, pH, opacity, and foam formation of aqueous solutions of 30 typical commercial soaps and 6 popular soapless detergents. The soaps included the following types: Toilet, "medicated," glycerin, coco, washing (laundry), and shaving soaps. The results are explained on the basis of the colloidal nature of the solutions and the soap phases that have been found in the solid soaps by studies of X-ray diffraction and electron microscopy. The significance of the results in terms of micelle formation and the relationship between micelles and detergent action are discussed.

I. Introduction

Running water was the earliest "detergent" used, the cleansing being caused mainly by mechanical action and partly by solvent action. The relatively superior washing action of aqueous solutions, suspensions, and pastes of various herbs, plants, and nuts was quickly realized, to be followed a few centuries thereafter by the manufacture and use of saponified oils and fats (soap). In more recent times, synthetic soapless detergents are being commonly used by the housewife for laundering, dish-washing, and cleansing in general. Whether it is the ancient herb, the more recent soap, or the modern soapless synthetic compound, the cleansing action in all cases is based upon the same principle—the replacement of the undesired dirt by a detergent, leaving the dirt in a suspended and protected state so that it is easily removed by running water.

The criteria used in purchasing soaps and soapless washing compounds are usually their appearance and texture, the quantity of suds they produce, and, with some critical housewives, the action of the compound on the skin and hands. There are, however, no universally accepted physical-chemical standards to which soaps are referred with regard to their washing power. Some pertinent experimental methods suggest themselves if the prerequisites for efficient washing are critically reviewed and analyzed.

In trying to wash a greasy dish or a dirty fabric, a superior wetting or surface-active agent is needed. After the greasy dirt is removed from the surface of the dish or fabric, the dirt particles must be suspended in the aqueous medium. This can be achieved by compensating the charge around the particles. When the charge is neutralized, both the uncharged dirt particles and the clean surface of the dish or fabric must be protected with an adsorbed film of the detergent so that the removal of the dirt with running water may be facilitated. The use of an efficient detergent also enhances the degree of solubilization of the insoluble dirt, owing to its sorption by, or inclusion inside, the colloidal particles of the detergent. The factual data on these factors may be obtained by making direct measurements of surface tension, interfacial tension, carbon number, gold number, and dye number.

Other factors, which may be considered significant by the housewife, are the quantity of suds produced (properties of foams), the irritation to the skin and hands (control of pH), and the clarity of the solution (opacity of turbidity).

The literature is profuse with physical-chemical data for aqueous solutions of pure alkali soaps, stress being laid in most of these investigations on

[1] Guest worker, Section of Surface Chemistry.

826086—49——3

the colloid chemical viewpoint. Krafft and Stern [4][2] suggest that soaps must be in solution in order to exhibit appreciable detergent action. McBain [6] has shown conclusively that the detergent action of aqueous soap solutions is due to their colloidal nature, and that this action is influenced by the chemical constitution of the detergent only insofar as this affects their behavior as colloids. Investigations conducted during the past 10 years have shown, however, that sodium soaps of the saturated fatty acids display probably three alternative crystal forms, as well as a sequence of about 5 or 10 stable mesomorphic forms, each having different and unique physical-chemical properties [9].

The purpose of this paper is to present data for several physical-chemical properties of aqueous solutions of numerous commercial soaps and soapless detergent materials, and to correlate these with the structure and phase nature of the solid soaps as revealed by investigations with X-ray diffraction [2] and electron microscopy [3], and to interpret the significance of the results in terms of fundamental colloid chemical hypotheses.

II. Materials Used

Thirty typical commercial soaps (toilet, "medicated," glycerin, coco, washing (laundry), and shaving soaps) and six popular synthetic soapless detergents were investigated. The commercial soaps were the same as those used in previous investigations [2, 3]. Of the soapless detergents, two (D1 and D5) are reported by their manufacturers to be nonalkaline compounds, one (D6) as containing "a special ingredient that dissolves grease on contact," and one (D2) as a new kind of soap. The active principles of the soapless detergents D1, D3, D4, and D5 are probably a fatty alcohol sulfate, an alkyl-aryl sulfonate plus an alcohol sulfate, a sulfated monoglyceride of coconut oil, and an alkyl-aryl sulfonate, respectively.

III. Experimental Techniques

Aqueous solutions corresponding to 10, 5, 2.5, 1.25, 0.625, 0.313, 0.156, and 0.078 percent, by weight, of the soap or soapless detergent were prepared by dissolving the appropriate amount of the soap (or soapless detergent) in hot (80° to 100° C) distilled water. The solution was then cooled, transferred to a 250-ml volumetric flask, and fresh cold distilled water added until the solution reached the standard mark.

1. Surface Tension

A du Nouy tensiometer was used for making surface-tension measurements. The platinum ring had a circumference of 6.014 cm and a ratio of R/r equal to 53.5. The instrument was calibrated against known standard weights and also against conductivity water.

2. Electrical Conductance

The electrical conductance was measured with a dip-type conductivity cell, with a cell constant of 0.8307, and a conductivity bridge manufactured by the Solar Manufacturing Corporation, New York (model–RC1; 20 watts; 100 to 125 volts; 50 to 60 cycles). The null point was detected with the help of a magic-eye, which flickered when the switch multiplier was turned from one position to another, indicating that the null point occurred in that region. The multiplier was then kept steady and the resistance dial moved until the green portion of the magic-eye receded to a maximum. This was the null point. In the absence of accurate knowledge of the exact equivalent weights of the commercial soaps and soapless detergents, values for the specific conductance rather than the equivalent conductivity have been calculated and are presented in this paper. However, the data in figure 2 were calculated by the equation

$$\text{weight conductance}=\frac{1{,}000\times K}{C},$$

where K equals specific conductance, and C equals weight of soap or soapless detergent in grams per liter. This was done to obtain curves similar to those that would be obtained if equivalent conductance were plotted.

3. pH

The pH of the various soap and soapless detergent solutions was measured with a glass-electrode pH meter. The instrument was standardized against standard solutions of Borax (pH equals 9.18 at 25° C for a 0.01-molar solution).

[2] Figures in brackets indicate the literature references at the end of this paper.

4. Opacity

The opacity of the various solutions was measured with a Klett-Summerson photoelectric colorimeter. A projection type of electric lamp (100 watts; 110 volts) fitted with a green filter (540 millimicrons) was used as the source of light, and the current produced by the photocells was measured by means of a suspension wire type of galvanometer. The opacity of the system, that is the reciprocal of the intensity of transmitted light, was measured in terms of the divisions on the potentiometer slide-wire that are necessary to nullify the potential applied to the galvanometer.

5. Foaming

The rate of growth of foam was determined by measuring the height to which the foam rises under a standard bubbling rate. The bubbler was prepared as follows. A glass tube, ⅛ in. in diameter and 18 in. long, was sealed at one end with small pieces of copper wire (0.01 mm diameter) fused into it. When the end of the tube had cooled it was dipped into nitric acid, which dissolved the copper wire and left 20 fine holes of uniform diameter. The open end of the tube was then connected to an air-pressure valve via a flow regulator, and the bubbler was dipped into a 1,000-ml measuring cylinder containing 200 ml of the solution to be tested. The time was noted on a stop watch.

IV. Results and Discussion

Data for aqueous solutions of some typical soaps and soapless detergents are presented in figures 1 to 4, in which the surface tension, weight conductance, pH, and opacity of the various solutions are plotted with respect to concentration. Data for all the soaps and soapless detergent solutions at a concentration of 2.5 percent are presented in tables 1 and 2, since such a tabulation permits quick comparison and evaluation.

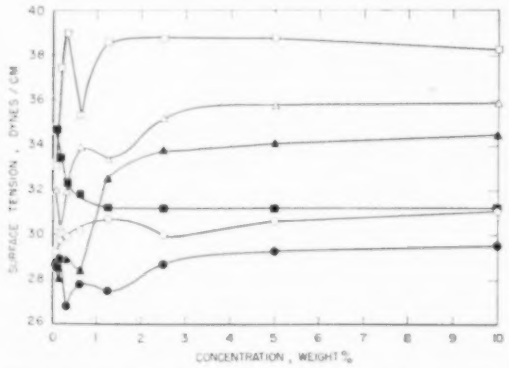

FIGURE 1. *Variation of surface tension with concentration.*

○ T3 toilet soap; ● C1 coco soap; △ G2 glycerin soap; ▲ W5 washing soap; □ S5 shaving soap; ■ D5 soapless detergent.

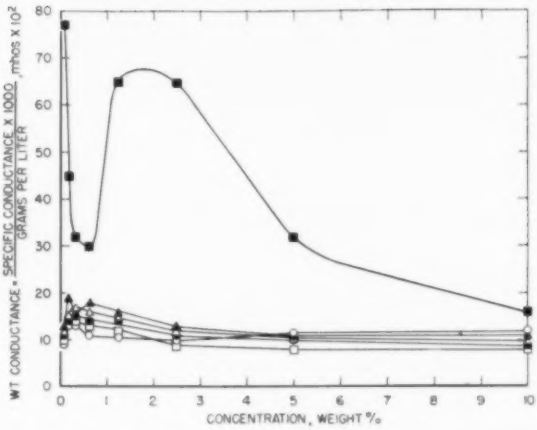

FIGURE 2. *Variation of specific conductance with concentration.*

○ T3 toilet soap; ● C1 coco soap; △ G2 glycerin soap; ▲ W5 washing soap; □ S5 shaving soap; ■ D5 soapless detergent.

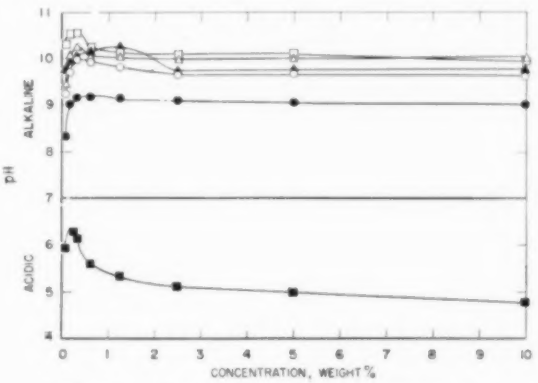

FIGURE 3. *Variation of* pH *with concentration*

○ T3 toilet soap; ● C1 coco soap; △ G2 glycerin soap; ▲ W5 washing soap; □ S5 shaving soap; ■ D5 soapless detergent.

1. Surface Tension

The curves obtained by plotting surface tension with respect to concentration are very similar for the various toilet soaps but differ somewhat from those for the coco, glycerin, washing, and shaving

TABLE 1. *Some physical-chemical properties of 2.5 percent aqueous soap solutions*

Soap	Specific conductance	Surface tension	pH	Opacity	Rate of growth of foam
	mhos x 10^6	*Dynes/cm*		*Klett scale divisions*	*Time in seconds per 100-division rise*
Toilet:					
T1	25.96	31.4	10.18	600	17
T2	27.70	31.5	9.93	284	19
T3	25.10	30.0	9.66	420	18
T4	29.67	31.7	10.10	455	19
T5	23.34	34.0	10.18	218	18
T6	26.37	31.6	10.18	310	19
T7	23.73	33.4	10.00	750	19
T8	32.21	31.7	10.04	163	19
T9	21.58	32.5	10.02	650	19
T10	31.35	30.8	9.95	82	20
T11	30.21	31.9	10.22	245	20
T12	29.67	33.1	10.05	480	19
Coco:					
C1	28.65	28.7	9.23	2	19
C2	25.96	28.2	9.11	2	19
Glycerin:					
G1	30.77	33.5	9.93	200	19
G2	31.35	35.2	10.07	170	19
"Medicated":					
M1	27.24	33.1	10.20	105	23
M2	27.70	33.0	10.10	140	20
M3	27.24	32.6	9.92	350	25
Washing (laundry):					
W1	30.77	29.7	9.80	60	20
W2	51.93	36.1	10.41	47	19
W3	50.35	33.6	10.42	80	20
W4	53.60	37.0	10.42	23	22
W5	30.77	33.8	9.73	21	18
Shaving:					
S1	29.67	34.0	10.10	900	20
S2	28.16	31.2	9.75	475	22
S3	28.16	37.2	10.19	425	22
S4	29.15	31.1	10.00	750	20
S5	24.43	38.8	10.05	530	19
S6	29.15	32.8	10.16	850	20

soaps. Solutions of the toilet soaps are characterized by a very low value of surface tension at small concentrations (about 0.1 to 0.2 %), which increases to a maximum value around 1.25 percent of soap content. The surface tension then decreases slowly to a minimum value, around 2.5 percent of soap, which either remains constant or increases very slowly as the soap content is increased. The curves thus show two minima, around 0.1 to 0.2 percent and 2.5 percent of soap.

The solutions of coco, glycerin, washing, and shaving soaps are characterized by the surface tension passing through a minimum value in very dilute solutions (about 0.2 to 0.3 % of soap), and then following a somewhat irregular and indefinite path up to about 1.25 percent. The value of surface tension then increases somewhat to reach a maximum, which is either retained or decreases slightly as the concentration of the soap is increased. In contrast to the data for solutions of the toilet soaps, solutions of this group of soaps do not show a second minimum around 2.5-percent concentration.

In either case, the minima in the region of lower concentration are due to the surface film being saturated with a single layer of soap molecules, whereas the minima in the region of higher concentration indicate the formation of soap micelles with single or multiple charges. The steady value of surface tension obtained beyond a concentra-

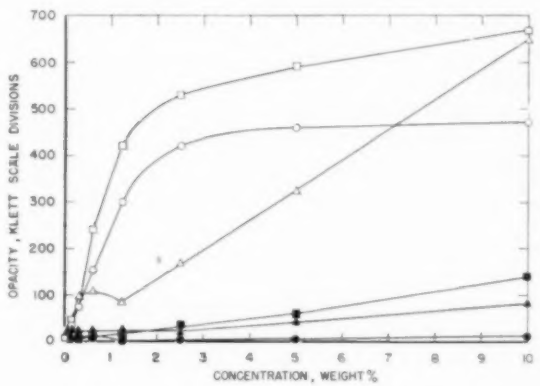

FIGURE 4. *Variation of opacity with concentration.*

○ T3 toilet soap; ● C1 coco soap; △ G2 glycerin soap; ▲ W5 washing soap; □ S5 shaving soap; ■ D5 soapless detergent.

TABLE 2. *Some physical-chemical properties of 2.5-percent aqueous soapless detergent solutions*

Detergent	Specific conductance	Surface tension	pH	Opacity	Rate of growth of foam
	mhos x 10^6	*Dynes/cm*		*Klett scale divisions*	*Time in seconds per 100-division rise*
D1	138.50	29.5	7.51	1	21
D2	48.88	31.8	9.68	375	21
D3	138.51	28.2	9.29	120	21
D4	184.60	30.3	6.10	5	20
D5	166.20	31.4	5.13	63	20
D6	61.55	33.5	10.70	185	24

tion of about 2.5 to 4 percent of soap indicates that both the surface and the interior of the system are saturated with respect to the charged micelles. The exhibition of two regions of minimum surface tension for solutions of the toilet soaps and of only one such region for solutions of other types of soaps is probably to be explained as being caused by the presence of many sizes and kinds of colloidal particles in the former and of a constant particle size in the latter.

The solutions of the soapless detergents are characterized by a continuously decreasing value of surface tension with increasing concentration, an almost constant value being reached after about 1.25 percent. The shape and nature of the curves for the solutions of the soapless detergents are thus very different from those for the soap solutions. It seems reasonable to conclude from these data that the concentrations at which monolayers and ionic micelles are formed are much lower for the soapless detergent solutions than those for the soaps. In terms of washing action, this may be interpreted as indicating that at lower concentrations the soapless detergents are better surface-active cleansing agents than the soaps

2. Electrical Conductance

In the absence of data regarding exact equivalent weights of the soaps and soapless detergents, values of the specific conductance rather than of equivalent or molar conducitivity have been presented in tables 1 and 2, and values of the weight conductance were plotted in figure 2 (see p. 363). The curves in figure 2 show that the conductance for the various soap solutions rises rather sharply in dilute solutions to a maximum around 0.25 percent and then decreases to about 2.5 percent, beyond which an almost constant value is obtained. The decrease in conductivity is due to the replacement of ions by colloidal particles which, although conducting, have a lower equivalent conductivity than the ions from which they are formed. The variations in the regions of maxima for the different soap solutions is probably caused by the presence of many sizes and kinds of colloidal particles in equilibrium with one another and to the shifting of the equilibrium position with concentration and soap type.

Whereas soap solutions exhibit a high electrical conductance in dilute solutions and low and decreasing values with increasing concentration, solutions of the soapless detergents are characterized by very high values of conductance, which decrease rapidly up to 0.5 percent, then increase up to about 2 percent and finally decrease slowly with increasing concentration. The formation of colloidal particles thus appears to take place at very low concentrations in solutions of the soapless detergents, and the relatively high charge carried by them tends to make them better cleansing agents than commercial soaps in solutions of similar low concentrations.

3. pH

The pH-concentration curves in figure 3 show that the values of pH for the soap solutions increase very sharply at low concentrations up to a maximum around 0.2 percent, followed by an equally sharp decrease and a minimum between 1 to 2.5 percent. A further increase in the concentration of the soap does not appreciably change the pH value.

Table 1 shows that the values of pH average about 10 for solutions of different soaps at a concentration of 2.5 percent. The presence of excess alkali in aqueous soap solutions favors the formation of ionic micelles [6] and helps to clarify the solutions by driving back hydrolysis and simultaneously increases the viscosity of the system. The relatively high alkalinity of the various soap solutions is caused by their readiness to hydrolyze in water and also by the free (unreacted) alkali in the commercial products. In either case, the alkali has an irritating effect upon the skin.

The solutions of the soapless detergents may be either acidic or alkaline, depending upon the nature of the major constituent of the products. As with the alkaline soap solutions, irritation to the skin may be caused by these alkaline or acidic solutions, and likewise solutions of these soapless detergents would seem to be best used in greater dilution.

4. Opacity

The opacity-concentration curves for the various soap-water systems are shown in figure 4 and indicate that the solutions at lower concentrations are clear and transparent. With increasing concentration the solutions become at first cloudy and translucent, and then dense and opaque at

higher concentrations. It is presumptuous to attribute the turbidity of the soap solutions to their colloidal nature alone, because perfectly transparent solutions of various colloidal materials and translucent to opaque systems of crystalloidal substances are obtainable. Also, the insoluble acid soap may sediment out almost entirely on standing, leaving the bulk of the soap in a clear transparent solution, or it may remain partly or wholly suspended in particles whose dimensions range all the way from coarse suspensions down to the smallest resolvable particles.

In concentrated as well as dilute solutions, the opacity of the coco and glycerin soaps is substantially low. The former made from coconut oil, have a high laurate-myristate content; the opacity of solutions of soaps of the lower fatty acids is lower than that for corresponding solutions of soaps of the higher fatty acids. The high transparency of the glycerin soap solutions probably results from the presence of glycerin and sugars that are adsorbed on the surface of the soap particles and suitably change the index of refraction.

Solutions of the soapless detergents exhibit a very high transparency at both low and high concentrations. The initial low values of opacity occur in regions of concentration in which there is low surface tension and relatively high electrical conductance, and is probably due to the formation of monolayers and primary aggregates of the detergent molecules. The slight increase in opacity that starts around 1.25-percent concentration corresponds to the region in which the surface tension reaches a constant value, and the weight conductance levels off and then decreases. This is probably to be ascribed to the formation of secondary aggregates and ionic micelles.

5. Foaming

Measurements of the height to which the foam rises when a standard bubbling rate is employed indicate that there is no appreciable change in the rate of growth of foam with variations in the concentration of a given soap or soapless detergent. However, the rate is probably slightly slower in dilute solutions and somewhat faster in concentrated solutions.

The first signs of foam formation are shown in solutions containing approximately 0.0035 percent of soap, but at this extremely low concentration, the foam is very unstable and breaks down as soon as it is formed. Relatively stable foam is produced beyond about 0.007 percent. The formation of foam in these extremely dilute soap solutions shows that the stabilizing action of adsorption layers attains its maximum at surface concentrations much below the saturation of the surface layer (about 0.1 to 0.2%). This stabilization arises not only by a mere enhancement of the mechanical properties of the surface layer, but also by a certain degree of mobility of the stabilizing molecules necessary for the rapid bridging of ruptures in the surface layers.

The foam produced from solutions containing 0.078 to 10 percent of soap or of soapless detergent is very stable and remains almost unchanged for an hour or more if the system is not disturbed by mechanical or thermal agitation. The requirements for a stable foam, enabling the bubbles to withstand mechanical shocks, are a lowering of the boundary tension by adsorption and suitable mechanical properties of the adsorbed stabilizing film. It is worth while remembering, however, that the power of foaming is not always or entirely to be ascribed to low surface tension. For instance, saponin solutions, whose surface tensions are only slightly less than that for water, have a very great power of foaming on account of the formation of a solid or highly viscous film of an adsorbed material on the surface. It should be very worth while to examine the decay of foam under standard conditions of agitation and the stability of single bubbles liberated beneath the liquid surface, in the case of both the commercial soap and soapless detergent solutions.

6. Correlation with Data on the Phase Nature and Structure of the Solid Soaps

X-ray diffraction studies of commercial soaps have shown [2] that the toilet and "medicated" soaps consist essentially of beta sodium palmitate and small amounts of omega sodium oleate, the coco soaps consist primarily of omega sodium laurate and sodium myristate, the shaving soaps consist essentially of two or more distinct phases (alpha, and/or beta, omega, and delta) of sodium palmitate, and the constituents of the glycerin and washing soaps are rather indefinite, the latter being probably in the omega phase. Electron microscopic investigations [3] also indicate that sodium palmitate may be in the washing soaps.

With a view to obtaining some information regarding the general physical-chemical properties of the solid soaps and their phase nature, some qualitative experiments were conducted on the hardness of the soaps, their solubility, and their reaction to water. In general, it was found that:

The hardness of the soaps, based on the resistance offered to the fine edge of a steel spatula on application of a 100-g load, decreases in the following order: Toilet, "medicated", washing, shaving.

The solubility of the coco, glycerin, and "medicated" soaps in warm water is the greatest of the groups and decreases in the order: coco, glycerin, medicated. The shaving soaps are more soluble than the toilet soaps and give transparent to translucent solutions on cooling, whereas the solutions of the toilet soaps set to opaque gels or curds. The solubility of all the five types of soaps is, however, relatively low in cold water and in hard water.

The percentage of soap rubbed off the cake (bar), when used in water against a laboratory towel, decreases in the following order: Shaving, toilet, washing.

On standing with water, the toilet and shaving soaps swell and disintegrate, whereas the washing soaps crack somewhat with little or no swelling.

Data in tables 1 and 2 show that the values of most physical-chemical properties are distinctly different for solutions of soaps as against those of the soapless detergents. Aside from this, the most striking behavior is perhaps the ability of the soapless detergents to dissolve rapidly and work in cold as well as in hard water. A considerable part of the soap used in household applications is probably employed to soften hard water in order to make the additional soap effective. On the contrary, the soapless detergents usually work equally efficiently in hard and in soft water, none being wasted in the task of softening the water.

7. Micelles and Their Applications in Cleansing Action

There is some difference of opinion as to the origin, manner of formation, structure, size, etc. of the colloidal aggregates termed loosely as "micelles". McBain [7] postulates at least two types of micelles (ionic and lamellar), whereas Hartley [1] postulates only one, namely, the ionic micelle. Solutions of different colloidal electrolytes exhibit different phenomena with varying concentrations, and this behavior can be explained only if one assumes the existence of more than one type of micelle. It is the general belief that the ionic micelle in soap solutions, which is of significance in the present investigations, consists of a loose spherical aggregate of the paraffin chain ions with the polar groups oriented toward the aqueous phase. Recent investigations by Mattoon, Stearns, and Harkins [5] have shown that aqueous solutions of soaps and soapless detergents give a Bragg spacing that is independent of concentration and that is equal approximately to the double length of the molecule. They have designated this as the micelle thickness, their conception of a micelle being cylindrical, rather than spherical or lamellar.

The evidence for the existence of ionic micelles in solutions of commercial soaps and soapless detergents is based primarily on data on electrical conductance and surface tension. The former show the formation of micelles by the rapid decrease in conductivity with increasing concentration—the ionic micelles have a lower conductivity than the ions. Surface-tension data indicate the formation of monolayers of soap molecules on the surface of the solutions at very high dilutions and the formation of colloidal aggregates (ionic micelles) at slightly higher concentrations. Electrical conductance and surface-tension data for the solutions of the soapless detergents indicate that micelle formation reaches a very high value at relatively high dilutions.

The mechanism by which solutions of soaps and soapless detergents dissolve relatively insoluble substances, such as grease and dirt, can be explained simply in terms of either concept of the ionic micelle and the action of mixed monolayers: (a) the hydrocarbons in the dirt are dissolved in the interior of the micelle; (b) the polar compounds in the dirt are removed by adsorption on the surface of the micelle, with the hydrocarbon part inside the micelle and the polar groups in the aqueous phase; and (c) compounds that are soluble in water but insoluble in hydrocarbons are taken up by the polar group of the micelle and thus act as peptizing agents.

Since the degree of solubilization is related to the number and size of the micelles present [8], it seems reasonable to conclude that greater solubilization and hence more efficient cleansing may

be achieved by using soaps in concentrations ranging from 2.5 to 4 percent and soapless detergents in less concentrated solutions (about 1.25% or less).

V. References

[1] G. S. Hartley, Trans. Faraday Soc. **31,** 183 (1935); Colloidal electrolytes—a general discussion held by the Faraday Society, 1935; Aqueous solutions of paraffin-chain salts (Herman, Paris, 1936).

[2] G. S. Hattiangdi, J. Research NBS **42,** 331 (1949 RP1972.

[3] G. S. Hattiangdi and M. Swerdlow, J. Research NBS **42,** 343 (1949) RP1973.

[4] F. Krafft and A. Stern, Ber. deut. chem. Ges. **27,** 1747 (1894); **32,** 1584 (1899).

[5] R. W. Mattoon, R. S. Stearns, and W. D. Harkins, J. Chem. Phys. **16,** 644 (1948).

[6] J. W. McBain, Third report on colloid chemistry and its general and industrial applications, British Association for the Advancement of Science, p. 2 to 31 (1920).

[7] J. W. NcBain, J. Phys. Chem. **43,** 671 (1939); Nature **145,** 702 (1940).

[8] J. W. McBain, Advances in colloid science **1,** 99 (Interscience Publishers, Inc., New York, N. Y., 1942).

[9] R. D. Vold and M. J. Vold, Colloid chemistry **5,** 266 (edited by J. Alexander, Reinhold Publishers Corporation, New York, N. Y., 1945).

Washington, January 18, 1949.

U. S. Department of Commerce
National Bureau of Standards

Research Paper RP1975
Volume 42, April 1949

Part of the Journal of Research of the National Bureau of Standards

Doubly Charged Ion Spectra in Mass Spectra of Hydrocarbons

By Fred L. Mohler, Evelyn G. Bloom, Edmund J. Wells, Jr., Jonathan H. Lengel,[1] and C. Edward Wise

A compilation of doubly charged ions in the mass spectra of 148 hydrocarbons has been made, based on mass spectra published in the American Petroleum Institute Catalog of Mass Spectral Data. In hydrocarbons with three, four, or five carbon atoms, the most probable double ionization process involves loss of all but two or three hydrogen atoms without breaking carbon bonds. Unsaturated molecules give larger doubly charged ion peaks than saturated molecules, and ions with an even number of hydrogen atoms tend to be more abundant than those with an odd number. In saturated hydrocarbons with six or more carbon atoms, double ionization with breaking of carbon bonds is most probable, but in benzenes and highly unsaturated molecules, double ionization without loss of carbon atoms is probable. These heavier molecules show distinctive differences depending on molecular structure.

The ratio of ion current at 70 volts to that at 50 volts ionizing voltage is an indication of the appearance potential of the ion. It increases as the number of hydrogen atoms removed increases, and the results indicate that hydrogen atoms are removed in pairs to give H_2.

I. Introduction

The mass spectra of hydrocarbons and other polyatomic molecules in general show some small peaks that arise from doubly charged ions. Ions with a double charge are characterized by an apparent mass equal to half the molecular weight of the ion. If the molecular weight is an odd number, the doubly charged ion will be distinguished by half-integer values; if it is an even number, then it will often happen that the apparent mass of the doubly charged ion is coincident with the mass peak of a singly charged ion. For this reason the data on the occurrence of doubly charged ions are necessarily incomplete.

The application of the mass spectrometer to chemical analysis has resulted in the careful measurement of mass spectra of at least 200 hydrocarbons; and these spectra afford a vast amount of data on the existence of doubly charged ions, but no attempt has previously been made to collect and correlate these data. The Catalog of Mass Spectral Data of the American Petroleum Institute [1] [2] has been the source of data used in this compilation, and the tables contributed by the Mass Spectrometry Section of the National Bureau of Standards have been used except in cases noted in the text. There are distinct advantages in using data of one laboratory insofar as possible, for there are minor differences between laboratories arising from instrumental differences and different methods of operation. In three cases, ethane [2], ethylene [3], and benzene [4], appearance potentials of some doubly charged ions have been published. For most molecules all that is known is the relative intensity of the doubly charged ions at one or two ionizing voltages.

[1] Now at Naval Powder Factory, Indian Head, Md.

[2] Figures in brackets indicate the literature references at the end of this paper.

826086—49——4

II. Experimental Procedure

Mass spectra have been measured with a 180° Consolidated mass spectrometer following recommended procedures [5]. The instrument is equipped with automatic electron current control, and the ionization chamber is thermostatically maintained at 245° C. The compounds used are in most cases the pure NBS Standard Samples.

The Catalog of Mass Spectral Data [1] gives intensities of mass peaks relative to the maximum peak taken as 100. The limit of this instrument is about 0.01 percent of the maximum deflection, and as spectra are always obtained with a pressure sufficient to give a nearly full scale deflection at the maximum, the lower limit remains about the same in all spectra. Peaks of doubly charged ions rarely exceed 1 percent of the maximum, and most of the peaks are less than 0.1 percent. The reproducibility on these small peaks is about 10 percent of the peak height, or 0.01 percent of the maximum for peaks less than 0.1 percent.

The tables in the catalog give relative intensities with ionizing voltages of both 50 and 70 volts. This paper tabulates values at 70 volts and includes some data on the ratio of ion current at 70 volts to that at 50 volts. The relative intensity at 70 volts is greater than at 50 volts and often much greater. The API Catalog gives spectra from several laboratories for many of the compounds, and in general there is good agreement on these small doubly charged ion peaks in all cases where they are reported.

III. Results

1. C_2 Hydrocarbons and Methane

No doubly charged ions in the mass range 6 to 8 are observed in methane. Table 1 lists the doubly charged ions in $CH_3.CH_3$, $CH_2{=}CH_2$ and $CH{\equiv}CH$. The doubly charged ions all contain two carbon atoms, and those ions of even molecular weight are coincident with the singly charged ions CH^+, CH_2^+ and CH_3^+. However, in two cases there is a basis for estimating the intensity of doubly charged ions of even molecular weight. Kusch, Hustrulid, and Tate [3] report a small peak in ethylene at mass 14½ from the ion $C^{12}C^{13}H_4^{++}$. The $C_2^{12}H_4^{++}$ peak will be about 50 times as large as the 14½ peak. They used a mass spectrometer of greater sensitivity than the Consolidated instrument. Similarly, in acetylene a peak has been observed at 13½ from the ion $C^{12}C^{13}H_2^{++}$, and the $C_2^{12}H_2^{++}$ peak is computed from this. The distinctive differences between the three C_2 compounds are of a type not found in the heavier hydrocarbons.

TABLE 1. *Doubly charged ions of C_2 hydrocarbons*

Relative intensities in percentage of maximum peak in spectrum

Compound	C_2H	C_2H_2	C_2H_3	C_2H_4	C_2H_5
Ethane	.....	.....	0.07	.....	0.70
Ethylene	[1] 0.007	.....	.42	[1] 0.3	.....
Acetylene	.....	[2] 3.9	.....	.....	.....

[1] Kusch, Hustrulid, and Tate, Phys. Rev. **52**, 843 (1937). The value for $C_2H_4^{++}$ is an estimate based on a small peak at 14½ from $C^{12}C^{13}H_4^{++}$.
[2] The value for $C_2H_2^{++}$ is based on a peak at 13½ from $C^{12}C^{13}H_2^{++}$.

2. C_3 Hydrocarbons

Table 2 lists doubly charged ions found in the five hydrocarbons $CH_3.CH_2.CH_3$, $CH_2.CH_2.CH_2$, $CH_2{=}CH{-}CH_3$, $CH_2{=}C{=}CH_2$, and $CH_3{-}C{\equiv}CH$. All observed doubly charged ions contain three carbon atoms, and the apparent masses fall in a mass range 19 to 21 containing no singly charged ions. Delfosse and Bleakney [6] have previously published data on doubly charged ions in propane, propylene, and propadiene at 100-volts ionizing voltage.

TABLE 2. *Doubly charged ions of C_3 hydrocarbons*

Relative intensities in percentage of maximum peak in spectrum

Compound	C_3H_2	C_3H_3	C_3H_4	C_3H_5	C_3H_6
Propane	1.10	0.61	1.12	0.26	0.02
Cyclopropane	3.33	1.44	2.40	.73	.02
Propylene	3.23	1.96	2.35	.67	.04
Propadiene [1]	2.79	3.20	3.61	.....	.....
Propyne [1]	3.23	2.34	0.80	.....	.....

[1] From unpublished mass spectra at a 50-volt ionizing potential.

With one exception, the relative intensity of the ions $C_3H_2^{++}$, $C_3H_3^{++}$ and $C_3H_4^{++}$ are similar in the five molecules in contrast to some distinctive differences in the spectra of the singly charged ions. Propyne differs from the others in that the $C_3H_4^{++}$ peak is small, and this is of interest because otherwise the mass spectra of propyne and propadiene are nearly identical.

3. C_4 Hydrocarbons

Table 3 lists the doubly charged ions in ten C_4 hydrocarbons. $C_2H_n^+$ ions of mass 25 to 29 mask doubly charged C_4 ions of even molecular weight, but in 1,3-butadiene a small peak at 27½ from $C^{13}C_3^{12}H_6^{++}$ permits a rough estimate of the intensity of the $C_4^{12}H_6^{++}$ peak.

TABLE 3. *Doubly charged ions of C_4 hydrocarbons*

Relative intensities in percentage of maximum peak in spectrum

Compound	C_2H_2	C_2H_3	C_2H_4	C_4H	C_4H_3	C_4H_5	C_4H_6	C_4H_7
n-Butane	0.04	0.01	0.02	.....	0.36	0.08	.....	0.05
i-Butane	.05	.02	.04	.....	.21	.02	.....	.....
1-Butene	.06	.03	.02	.....	1.06	.17	.....	.06
cis-2-Butene	.02	.01	.01	.....	1.55	.27	.....	.17
trans-2-Butene	.....	.....	.....	.....	1.65	.29	.....	.27
i-Butene	.06	.03	.03	.....	0.95	.09	.....	.....
1,2-Butadiene	.03	.02	.....	.....	4.07	.60	.....	.....
1,3-Butadiene	.09	.02	.....	.....	3.99	.48	[1] 1.60	.....
1-Butyne	.06	.05	.....	.03	3.62	.20	.....	.....
2-Butyne	.....	.....	.....	.01	3.25	.46	.....	.....

[1] Estimated from a small peak of $C^{13}C_3^{12}H_6^{++}$.

The relative intensities are roughly similar in all these spectra, and there is no evident relation between the intensity distribution in the mass spectra of doubly charged and singly charged ions. $C_4H_3^{++}$ is in every case the largest peak, and the height is least in C_4H_{10} isomers, greater in the C_4H_8 isomers, and largest in C_4H_6 molecules. There is a small but real difference between the *cis*- and *trans*-2-butene (the singly charged ion spectra are very similar).

4. C_5 Hydrocarbons

Table 4 lists doubly charged ions of 12 C_5 hydrocarbons. It includes all C_5H_{12} and C_5H_{10} isomers except some rare cyclics but only two of the many C_5H_8 isomers. As in the case of C_4 and C_3 hydrocarbons, the relative intensities in all these spectra are similar. $C_5H_2^{++}$ is the largest doubly charged peak and it is smallest in C_5H_{12} isomers, larger in C_5H_{10} isomers, and largest in the C_5H_8 isomers. Ions with three or four carbon atoms give small peaks often near the threshold for observation. Ions with an even number of hydrogen atoms tend to be more abundant than those with an odd number. This is probably a fairly general rule for doubly charged ions, partially concealed by the fact that there is often masking of ions with a double charge and an even number of H atoms.

TABLE 4. *Doubly charged ions of C_5 hydrocarbons*

Relative intensities in percent of maximum peak in spectrum

Compound	C_2H_2	C_2H_3	C_2H_4	C_4H_2	C_5H	C_5H_2	C_5H_3	C_5H_4	C_5H_5	C_5H_6	C_5H_7	C_5H_8	C_5H_9
n-Pentane	.....	.....	.....	0.04	.....	0.33	0.08	0.13	0.05	0.07	0.02	.....	.....
i-Pentane	.....	.....	.....	.06	.....	.27	.05	.09	.02	.03	.....	.....	.....
Neopentane	.....	.....	.....	.04	.....	.09	.02	.04	.01	.....	.....	.....	.....
Cyclopentane	.....	.....	.....	.....	0.01	.84	.19	.44	.16	.24	.05	0.01	.....
1-Pentene	0.02	0.01	0.01	.03	.01	1.03	.24	.34	.21	.22	.10	.04	0.02
cis-2-Pentene	.....	.....	.....	.06	.03	1.23	.37	.53	.25	.22	.09	.08	.02
trans-2-Pentene [1]	.01	.....	.01	.06	.01	1.52	.37	.53	.26	.24	.10	.09	.03
2-me-1-Butene	.....	.....	.....	.06	.01	.90	.21	.29	.15	.13	.06	.04	.01
3-me-1-Butene [1]	.....	.....	.....	.10	.01	.55	.14	.15	.08	.06	.04	.....	.....
2-me-2-Butene	.01	.....	.01	.04	.02	1.15	.25	.39	.17	.29	.07	.12	.02
Cyclopentene	.03	.02	.01	.02	.05	2.43	.64	1.00	.70	.74	.35	.13	.....
2-me-1,3-Butadiene [2]	.03	.01	.01	.15	.10	4.31	1.07	1.07	.80	.85	.30	.41	.....

[1] These also have a small peak at $C_4H_3^{++}$.

[2] Also has a peak $C_3^{++}0.08$.

5. C_6 Hydrocarbons

Table 5 lists 23 C_6 hydrocarbons including all C_6H_{14} isomers and most of the common C_6H_{12} isomers but only two C_6H_{10} molecules. Doubly charged C_6 ions with an even number of hydrogen atoms are masked by singly charged ions. These spectra in contrast to C_5, C_4, and C_3 molecules show considerable variations and do not follow the rule that double ionization without loss of a carbon atom is most probable. C_6 doubly charged ions are missing in C_6H_{14} isomers and are relatively weak in the olefins. The intensity distribution

TABLE 5. *Doubly charged ions of* C_6 *hydrocarbons*

Relative intensities in percentage of maximum peak in spectrum

Compound	C_4H_2	C_5H_2	C_5H_3	C_5H_4	C_5H_5	C_5H_6	C_5H_7	C_5H_8	C_5H_9	C_6H_3	C_6H_5	C_6H_7	C_6H_9
n-Hexane	0.02	0.07	0.02	0.06	0.03	0.05	0.02	0.01	....	....	....	....	....
2-me-Pentane	.02	.08	.02	.05	.03	.06	.03	.02	0.02	....	....	....	....
3-me-Pentane	.02	.08	.03	.06	.03	.03	....	....	....	....	....	....	....
2,2-me$_2$-Butane	.02	.03	.03	.07	.02	.03	.03	.03	.01	....	....	....	....
2,3-me$_2$-Butane	.01	.06	.01	.04	.02	.02	.02	.02	....	....	....	....	....
Cyclohexane	.03	.06	....	.06	.02	.04	....	....	....	....	0.01	0.07	0.03
me-Cyclopentane	....	.12	.02	.08	.06	.07	.03	....	....	....	....	.02	....
1-Hexene	.01	.15	.04	.09	.05	.03	.02	....	....	.06	....	....	....
cis-2-Hexene	.02	.20	.04	.12	.02	.02	.01	....	....	.05	....	.02	....
trans-2-Hexene	.02	.14	.04	.10	.02	.02	.01	....	....	.05	....	.01	....
trans-3-Hexene	.02	.28	.09	.14	.11	.24	.15	.02	.42	.09	.01	.04	.03
3-me-1-Pentene	.02	.18	.05	.10	.07	.04	.02	....	....	....	....	....	....
4-me-1-Pentene	....	.17	.05	.18	.13	.17	.13	.03	.07	.01	....	....	....
2-me-2-Pentene	.02	.19	.05	.09	.05	.03	.02	....	....	.03	....	.05	.05
3-me-*cis*-2-Pentene	.01	.14	.04	.12	.04	.03	.01	....	....	.02	....	.04	.02
3-me-*trans*-2-Pentene	.01	.19	.04	.10	.04	.03	.02	....	....	.03	....	.05	.03
4-me-cis-2-Pentene	....	.32	.09	.16	.11	.09	.07	.02	.02	.01	....	....	....
4-me-*trans*-2-Pentene	....	.29	.09	.17	.12	.09	.07	.02	.02	.01	....	....	....
2-eth-1-Butene	.04	.23	.05	.10	.04	.04	.03	....	.02	.03	....	.03	....
3,3-me$_2$-1-Butene	.02	.18	.06	.07	.06	.02	.04	....	....	....	....	....	....
2,3-me$_2$-2-Butene	....	.17	.05	.07	.02	.02	....	....	....	.01	....	.01	.08
Cyclohexene	.03	.11	.02	.05	.02	....	....	....	....	.25	.11	.53	.09
1,5-Hexadiene [1]	.03	.14	.04	.05	.03	....	....	....	....	.07	.02	.05	....

[1] This also has peaks $C_4H_3^{++}$0.03, $C_5H_2^{++}$0.02, $C_5H_4^{++}$0.02, $C_5H_5^{++}$0.01.

TABLE 6. *Doubly charged ions of* C_7 *hydrocarbons*

Relative intensities in percentage of maximum peak in spectrum

Compound	C_5H_2	C_5H_3	C_5H_4	C_5H_5	C_5H_6	C_5H_7	C_5H_8	C_5H_9	C_5H_{10}	C_6H_7	C_6H_9	C_7H_6	C_7H_7	C_7H_8	C_7H_9	C_7H_{10}
n-Heptane	0.03	....	0.02	....	0.02	....	....	....	....	....	....	....	....	0.02	....	....
2-me-Hexane	.02	....	.02	....	.02	....	....	....	....	....	0.02	....	....	.01	....	....
3-me-Hexane	.03	....	.03	....	.02	....	....	....	....	....	....	....	....	.01	....	....
3-eth-Pentane	.02	....	....	....	....	....	....	....	....	....	....	....	....	.01	....	....
2,2-me$_2$-Pentane	.02	0.01	.03	0.01	.02	....	....	....	....	....	.07	....	....	....	....	....
2,3-me$_2$-Pentane	.02	....	.04	....	.01	....	....	....	....	....	....	....	....	....	....	....
2,4-me$_2$-Pentane	.05	....	.02	.01	.09	0.05	0.05	0.09	0.06	....	.02	....	....	.01	....	....
3,3-me$_2$-Pentane	.03	.01	.02	....	....	....	....	....	....	....	....	....	....	....	....	....
2,2,3-me$_3$-Butane	.02	....	.03	....	.02	....	....	....	....	....	.03	....	....	....	....	....
me-Cyclohexane [1]	.03	....	.03	....	.04	....	.04	....	.03	0.05	....	0.20	0.06	.26	0.02	0.10
eth-Cyclopentane	.08	.01	.02	....	.02	....	.01	....	....	.01	.02	.16	.05	.19	.02	.02
1,1-me$_2$-Cyclopentane	.04	....	.02	....	.01	....	.01	....	....	.18	.12	.14	.03	.19	.01	.02
cis-1,2-me$_2$-Cyclopentane	.07	.01	.03	....	.01	....	.01	....	....	.03	.02	.16	.05	.21	.03	.02
trans-1,2-me$_2$-Cyclopentane	.06	....	.05	....	....	....	.02	....	....	.02	.02	.14	.04	.21	.03	.02
cis-1,3-me$_2$-Cyclopentane	.07	....	.04	....	.03	....	.08	....	.07	.08	.13	.17	.04	.21	.02	.04
trans-1,3-me$_2$-Cyclopentane	.07	....	.04	....	.04	....	.09	....	.11	.07	.12	.16	.05	.23	.03	.04
1-Heptene	.10	....	....	....	....	....	....	....	....	....	....	.07	.02	.05	....	....
4,4-me$_2$-1-Pentene [2]	.04	....	.02	.03	....	....	....	....	....	.10	.16	.02	....	.02	....	....
2,3,3-me$_3$-1-Butene [2]	.05	....	.02	....	....	....	....	....	....	.11	.10	.05	....	.04	....	....

[1] Also gives peaks $C_7H_3^{++}$0.02, $C_7H_{11}^{++}$0.01.

[2] Also give small peaks at $C_4H_{11}^{++}$

among the C_5 ions is frequently much like that in the C_5 hydrocarbons, though the intensity is less. *Trans*-3-hexene is an exception, for here $C_5H_9^{++}$ is the largest peak, and this peak is small or absent in all other C_6 hydrocarbons. The benzene spectrum is given in table 9.

6. C_7 Hydrocarbons

Table 6 lists doubly charged ions of 19 C_7 hydrocarbons. Ions $C_7H_2^{++}$ and $C_7H_4^{++}$ would be masked by singly charged ions in C_7H_{16} and C_7H_{14} isomers. The nine C_7H_{16} isomers give a variety of mass spectra of doubly charged ions with C_5 ions the most prominent, except in one case, 2,2-dimethylpentane, which has a maximum peak at $C_6H_9^{++}$. The only other C_7 with a maximum at this peak is 4,4-dimethyl-1-pentene. This is a structurally similar molecule, except that it contains a double bond. The cyclics all give quite similar doubly charged ion spectra with $C_7H_8^{++}$ the maximum peak. Table 9 gives the spectrum of methylbenzene.

7. C_8 Hydrocarbons

Table 7 lists doubly charged ion spectra of 15 C_8H_{18} isomers, 22 cyclic and olefin C_8H_{16}

TABLE 7. *Doubly charged ions of C_8 hydrocarbons*

Relative intensities in percentage of maximum peak in spectrum

Compound	C_3H_2	C_3H_4	C_3H_6	C_4H_6	C_5H_{10}	C_6H_7	C_6H_9	C_6H_{11}	C_7H_5	C_7H_{16}	C_7H_7	C_7H_8	C_7H_9	C_7H_{10}	C_7H_{11}	C_7H_{12}	C_7H_{13}
n-Octane												0.02					
2-me-Heptane	0.01	0.01										.06	0.01	0.04		0.03	
3-me-Heptane	.02	.01										.03		.01			
4-me-Heptane	.02	.02										.02					
2,2-me$_2$-Hexane										0.03		.05		.04		.04	
2,3-me$_2$-Hexane	.01	.01										.03					
2,4-me$_2$-Hexane	.01						0.01					.04		.01			
2,5-me$_2$-Hexane							.13	0.03				.08		.05		.05	
3,3-me$_2$-Hexane	.01	.01										.02					
3,4-me$_2$-Hexane	.01	.01										.02					
2,2,3-me$_3$-Pentane										.03		.03					
2,2,4-me$_3$-Pentane	.01	.01				0.01	.14	.07		.03		.04		.03		.03	0.01
2,3,3-me$_3$-Pentane	.01											.03					
2,3,4-me$_3$-Pentane							.02					.04					
2,2,3,3-me$_4$-Butane							.02			.03		.02					
1-Octene												.03					
trans-4-Octene										.16		.03					
2,4,4-me$_3$-1-Pentene						.02				.07	.04	.21	.04	.08	0.03	.01	.30
2,4,4-me$_3$-2-Pentene						.08			0.02	.29	.11	.68	.12	.17	.10	.01	.22
Cycloheranes:																	
1,1-me$_2$						.01				.23	.07	.37	.11	.08	.03	.03	.04
cis-1,2-me$_2$										.21	.05	.25	.04	.04	.01		
trans-1,2-me$_2$										.20	.05	.20	.02	.02			
cis-1,4-me$_2$						.02	.03			.21	.06	.26	.05	.05			
trans-1,4-me$_2$						.01	.02		.01	.17	.05	.22	.04	.04	.01	.01	
cis-1,3-me$_2$						.02	.01			.14	.08	.14	.05	.05		.02	
trans-1,3-me$_2$						.02	.01			.21	.10	.27	.06	.05			
ethyl	.03	.01	0.01							.10	.03	.08	.03	.03			
Cyclopentanes:																	
n-Propyl	.03	.02								.11	.04	.11	.01				
i-Propyl	.02	.01								.20	.09	.30	.07	.04	.01		
1-me-1-eth	.02	.03								.13	.05	.13	.02	.01			.02
cis-1-me-2-eth	.02									.16	.05	.16	.02	.03			
1,1,2-me$_3$	.02	.02								.22	.09	.29	.08	.04	.03		
1,1,3-me$_3$	.01	.02	.02			.05	.04		.02	.30	.15	.53	.16	.10	.09	.04	.24
cis, cis, cis-1,2,3-me$_3$	.01	.01	.01							.12	.05	.16	.02	.02			
cis, trans, cis-1,2,3-me$_3$	.02	.02	.01							.16	.07	.22	.03	.03			
cis, trans, cis-1,2,4-me$_3$	.01	.01	.01	.01	0.04					.12	.04	.14	.03				
cis, cis, trans-1,2,4-me$_3$	.01	.01	.01	.01	.04					.09	.05	.13	.03	.01			
4-Vinyl-1-cyclohexene [1]	.04								.03	.25	.29	.11	.10				

[1] Also gives peaks $C_7H_2^{++}$0.18, $C_7H_3^{++}$0.02, $C_7H_4^{++}$0.07, $C_8H_3^{++}$0.04, $C_8H_5^{++}$0.01, $C_8H_7^{++}$0.09, $C_8H_9^{++}$0.20, $C_8H_{11}^{++}$0.01.

TABLE 8. *Doubly charged ions of C_9 hydrocarbons*

Relative intensities in percentage of maximum peak in spectrum

Compound	C_7H_6	C_7H_7	C_7H_8	C_7H_9	C_7H_{10}	C_7H_{11}	C_7H_{12}	C_7H_{13}	C_7H_{14}	C_8H_9	C_8H_{11}
n-Nonane	.....	.....	0.03	.....	0.01	.....	.....	.....	.....	.....	.....
2,2,3-me$_2$-Hexane	0.04	.....	.03	.....	.....	.....	.....	.....	.....	.....	.....
2,2,4-me$_2$-Hexane	.03	.....	.04	.....	.04	.....	0.04	.....	0.02	.....	.....
2,2,5-me$_2$-Hexane	.07	0.01	.15	0.02	.20	0.04	.33	0.14	.25	.....	.....
2,3,3-me$_2$-Hexane	.....	.....	.02	.....	.....	.....	.....	.....	.....	.....	.....
2,3,5-me$_2$-Hexane	.....	.....	.06	.01	.03	.....	.02	.....	.....	.....	.....
2,4,4-me$_2$-Hexane	.....	.....	.06	.....	.04	.....	.04	.....	.....	.....	.....
3,3,4-me$_2$-Hexane	.....	.01	.01	.....	.....	.....	.....	.....	.....	.....	.....
3,3-eth$_2$-Pentane	.....	.....	.....	.....	.....	.....	.....	.....	.....	.....	.....
2,2,3,3-me$_4$-Pentane	.....	.....	.04	.....	.03	.....	.03	.....	.....	.....	.....
2,2,3,4-me$_4$-Pentane	.04	.01	.09	.05	.03	.06	.03	.02	.....	.....	.....
2,2,4,4-me$_4$-Pentane	.04	.01	.24	.03	.24	.05	.32	.52	.28	.....	.....
2,3,3,4-me$_4$-Pentane	.....	.....	.03	.....	.....	.....	.....	.....	.....	.....	.....
Cyclopentanes											
n-Butyl	.05	.....	.08	.....	.02	.....	.02	.....	.....	.....	.....
i-Butyl[1]	.13	.03	.15	.01	.09	.....	.03	.....	.....	.....	.....
Cyclohexanes											
n-Propyl	.05	.....	.05	.....	.02	.....	.....	.....	.....	.....	.....
i-Propyl	.09	.03	.14	.03	.06	.01	05	.....	.....	.....	.....
1,1,3-me$_3$	.14	.09	.27	.17	.15	.05	.08	.....	.....	0.03	0.03
1-Nonene	.04	.....	.03	.....	.....	.....	.....	.....	.....	.....	.....

[1] This also has a peak of 0.02 at $C_8H_2^{++}$.

isomers, and 1 C_8H_{12} molecule. C_8 ions with an even number of hydrogen atoms would be masked by singly charged ions. Three C_8H_{18} isomers not included in the table give no observable doubly charged ions. These are the three octanes that have ethyl side chains; 3-ethylhexane, 2-methyl-3-ethylpentane and 3-methyl-3-ethylpentane. Most of the C_8H_{18} molecules give small doubly charged peaks, and in 12 cases the maximum peak is $C_7H_8^{++}$. The largest peaks and the greatest number of peaks are in 2,2,4-trimethylpentane. Among the C_8H_{16} cyclics, the most abundant doubly charged ions are in 1,1,3-trimethylcyclopentane and of the four olefins 2,4,4-trimethyl-2-pentene has the largest peaks. These three compounds have a structural similarity that is partially concealed by the rules used for numbering the side chains. The C_8H_{12} molecule, 4-ethenyl-1-cyclohexene, shows many peaks not found in any other molecules in this table. The occurrence of C_9 ions ranging from $C_8H_3^{++}$ to $C_8H_{11}^{++}$ is significant. The ions $C_7H_2^{++}$ and $C_7H_4^{++}$ would be masked in most of the other compounds in table 7. The spectrum resembles somewhat the alkyl benzenes of table 9.

8. C_9 Hydrocarbons

Table 8 lists doubly charged ions of 13 C_9H_{20} isomers and six C_9H_{18} isomers (cyclics and one olefin). One nonane, 3,3-diethylpentane, shows no doubly charged ions. In the octanes it was also found that isomers with ethyl side chains give no doubly charged peaks. With one exception the doubly charged ions of these molecules are C_7 ions. The exception is 1,1,3-trimethylcyclohexane with two small peaks at $C_8H_9^{++}$ and $C_8H_{11}^{++}$. This molecule gives the most intense doubly charged spectrum of the five cyclics listed. It was found that 1,1,3-trimethylcyclopentane gave the largest peaks of any of the C_8H_{16} cyclics listed in table 7. A following section gives evidence that peaks at 96, 97, and 98 are $C_7H_{12}^{++}$, $C_7H_{13}^{++}$, and $C_7H_{14}^{++}$; and not C_8^{++}, C_8H^{++}, and $C_8H_2^{++}$.

It is of interest that *n*-butyl-cyclopentane and *n*-propylcyclohexane have similar spectra and that the *iso*-butyl and *iso*-propyl are also similar to each other and different from the other cyclics.

In general the doubly charged spectra of C_9 hydrocarbons are much like those of C_8 hydrocarbons. $C_7H_8^{++}$ is the maximum peak in most cases with only two striking exceptions.

TABLE 9. *Doubly charged ions of benzene and alkyl benzenes*

Relative intensities in percentage of maximum peak in spectrum

Compound	C_6H	C_6H_2	C_6H_3	C_6H_6	C_7H	C_7H_2	C_7H_3	C_7H_4	C_7H_5	C_7H_6	C_7H_7	C_7H_8	C_8H_3	C_8H_5	C_8H_7	C_8H_9	C_8H_{10}
Benzene [1]	0.05	1.15	0.35	[2] 3.0	.....	.....	.....	.....	.....	.....	.....	.....	.....	.....	.....	.....	.....
Me-Benzene [3]	.....	.04	.....	.....	0.13	1.73	0.42	0.97	0.49	4.87	2.35	3.45	.....	.....	.....	.....	.....
Eth-Benzene	.....	.04	.02	.....	.....	.10	.02	.05	.05	.05	.20	.02	0.05	0.08	0.32	0.24	.....
1,2-me$_2$-benzene	.....	.04	.....	.....	.....	.15	.05	.08	.05	.05	.28	.03	.06	.11	.73	.66	[4] 0.2
1,3-me$_2$-benzene	.....	.03	.01	.....	.....	.16	.05	.07	.05	.04	.21	.01	.10	.12	.78	.77	[4] 2
1,4-me$_2$-benzene	.....	.....	.....	.....	.....	.06	.....	.15	.04	.02	.22	.02	.....	.07	.61	.52	[4] 5

[1] Also has peaks at $C_4H_2^{++}$ 0.03 and $C_5H_2^{++}$ 0.05.
[2] Based on a peak of 0.20 at 39.5 from $C^{13}C_5^{12}H_6^{++}$.
[3] Also has peaks at $C_5H_2^{++}$ 0.17, $C_5H_3^{++}$ 0.02, and $C_5H_4^{++}$ 0.11.
[4] Based on a peak at 53.5 from $C^{13}C_7^{12}H_{16}^{++}$.

9. Benzene and Alkyl Benzenes

Table 9 gives doubly charged ions of some aromatics. These have been listed in a separate table for convenience of tabulation, because they include many ions not found in other hydrocarbons. The peak heights are larger than in other C_6, C_7, and C_8 hydrocarbons.

Benzene has a very large $C_6H_6^{++}$ peak and only one small C_5 peak in contrast to most of the spectra in table 5. Cyclohexene is the only compound in table 5 that has large C_6 peaks.

Methylbenzene resembles qualitatively the C_7H_{14} cyclics (table 6) except for differences definitely related to the fact that there are 8 H atoms instead of 14. $C_7H_2^{++}$ and $C_7H_4^{++}$ would be masked by singly charged peaks in the cyclics.

The C_8H_{10} aromatics give spectra quite unlike any of the C_8 molecules of table 7 except the C_8H_{12} molecule, 4-ethenyl-1-cyclohexene. It differs from this in having C_8 ion peaks that are larger than the C_7 peaks. The estimate of $C_8H_{10}^{++}$ is based on very small isotope peaks and is quite uncertain. The fact that $C_7H_8^{++}$ is small or missing here in contrast to other C_8 molecules undoubtedly is a consequence of the fact that dissociation by removal of CH_3 gives $C_7H_7^{++}$, whereas multiple dissociation or rearrangement is required to give $C_7H_8^{++}$.

10. Hydrocarbons with 10 or More Carbon Atoms

There is little published data on these heavier hydrocarbons. *n*-Decane, $C_{10}H_{22}$, gives only two small peaks, $C_5H_2^{++}0.02$ and $C_5H_4^{++}0.02$.

1-Decene, $C_{10}H_{20}$, shows only one doubly charged ion, $C_7H_8^{++}0.03$. This is also the only ion in 1-octene, whereas l-nonene gave this ion and $C_7H_6^{++}$.

The four butylcyclohexanes give doubly charged spectra like the C_9H_{18} cyclics, except that the peaks are smaller. All the ions have seven carbon atoms.

The Atlantic Refining Co. has published mass spectra [7] of the three diisopropylbenzenes ($C_{12}H_{18}$) at an ionizing voltage of 50 volts. These include the heaviest doubly charged ions recorded to date. The three spectra are similar, and 1,3-diisopropylbenzene gives the following peaks: $C_9H_7^{++}0.37$, $C_9H_9^{++}0.08$, $C_9H_{11}^{++}0.05$, $C_{10}H_7^{++}0.75$, $C_{10}H_9^{++}1.25$, $C_{10}H_{11}^{++}2.79$, $C_{10}H_{13}^{++}0.53$, and $C_{11}H_{15}^{++}0.65$.

IV. Ratio of Peaks at 70- and 50-Volt Ionizing Voltage

The API tables gives mass spectra obtained with ionizing voltages of 50 and 70 volts and, in general, the doubly charged peaks are considerably larger at the higher voltage. The value of the ratio of the currents at 70 and 50 volts, $i(70)/i(50)$, is of interest, as it gives at least qualitative evidence as to the appearance potential of the ion.

A plot of ion current as a function of ionizing voltage rises at first almost linearly from the appearance potential but gradually becomes concave to the axis of abscissas approaching a flat maximum value at roughly 30 volts above the threshold. Ionizing voltages of 50 and 70 volts fall near the flat maximum for the more probable single ionization processes, and the ratio $i(70)/i(50)$ is nearly unity. However, if the appearance potential is high, then the ratio will be much greater than unity and approach infinity as the appearance potential approaches 50 volts.

There are a few direct measurements of appearance potentials of doubly charged ions and these

are correlated with the observed values of $i(70)/i(50)$ in table 10. There is a rather large experimental uncertainty in the ratio amounting to at least 10 percent, and one can only conclude that a value of 1.2 to 1.3 corresponds to a potential between 30 and 36 volts and 1.4 to roughly 40 volts. Above 40 volts the ratio will increase rapidly with increasing appearance potential.

TABLE 10. *Correlation of appearance potential and the ration of ion currents at 70 and 50 volts*

Compound	Reference	Ion	Appearance potential	$i(70)/i(50)$
C_2H_6	[2]	$C_2H_5^{++}$	32	1.25
C_2H_4	[3]	$C_2H_4^{++}$	36	1.3
C_6H_6	[4]	$C_6H_6^{++}$	27	1.0
C_6H_6	.....	$C_6H_5^{++}$	30.4	1.2
C_6H_6	.....	$C_6H_5^{++}$	39.8	1.4

Observed values of the ratio $i(70)/i(50)$ for the more abundant doubly charged ions in hydrocarbons with two to five carbon atoms and for benzene are listed in table 11. It is found that the ratios for the same ions in different isomers are nearly equal. In general, the range of values indicated is no greater than the experimental uncertainty. This is true even when the isomers are chemically different, as in the case of cyclics and olefins. The table is arranged to show that the ratio increases as the number of hydrogen atoms removed increases, and that ionization processes involving removal of equal numbers of hydrogen atoms from different molecules give the same ratio within the range of experimental uncertainty. There is not a progressive decrease in the ratio as the number of H atoms removed becomes less, but the ratio remains nearly the same for removing 7H and 8H and similarly for 5H and 6H, 3H, and 4H and for 1H and 2H.

Interpretation of ratios in terms of appearance potentials.—The interpretation of this is fairly obvious. Studies of appearance potentials of singly charged ions show that frequently but not always, the hydrogen atoms are removed in pairs to form H_2. Thus Delfosse and Bleakney [6] find that in propane, $C_3H_5^+$ is produced by the transition $C_3H_8 \rightarrow C_3H_5^+ + H_2 + H$ requiring 14 volts. The process $C_3H_8 \rightarrow C_3H_4^+ + 2H_2$ occurs at 14.7 volts, and $C_3H_8 \rightarrow C_3H_3^+ + 2H_2 + H$ requires 15.7 volts. As it requires about three electron volts

TABLE 11.—*Ratio of peaks at 70- and 50-volt ionizing voltag*

Ionization process	$i(70)/i(50)$	Remarks
$C_5H_{12} \rightarrow C_5H_2^{++} + 10H$	4.5 to 6.8	3 isomers.
$C_5H_{10} \rightarrow C_5H_2^{++} + 8H$	2.8 to 3.7	7 isomers, mean 3.5.
$C_4H_{10} \rightarrow C_4H_3^{++} + 7H$	2.2 and 3.5	2 isomers.
$C_3H_8 \rightarrow C_3H_2^{++} + 6H$	2.0	Propane.
$C_5H_8 \rightarrow C_5H_2^{++} + 6H$	2.2 and 2.45	2 isomers.
$C_5H_{10} \rightarrow C_5H_4^{++} + 6H$	1.6 to 1.9	7 isomers, mean 1.7.
$C_3H_8 \rightarrow C_3H_3^{++} + 5H$	1.9	Propane.
$C_4H_8 \rightarrow C_4H_2^{++} + 5H$	1.85 to 1.88	4 isomers.
$C_4H_{10} \rightarrow C_4H_3^{++} + 5H$	2.0	2 isomers.
$C_5H_8 \rightarrow C_5H_3^{++} + 5H$	1.7 and 1.9	2 isomers.
$C_3H_6 \rightarrow C_3H_2^{++} + 4H$	1.43 and 1.48	2 isomers.
$C_3H_8 \rightarrow C_3H_4^{++} + 4H$	1.5	Propane.
$C_4H_8 \rightarrow C_4H_4^{++} + 4H$	1.3 and 1.4	2 isomers.
$C_5H_{10} \rightarrow C_5H_6^{++} + 4H$	1.1 to 1.5	7 isomers, mean 1.2.
$C_3H_6 \rightarrow C_3H_3^{++} + 3H$	1.4	2 isomers.
$C_4H_8 \rightarrow C_4H_5^{++} + 3H$	1.42 to 1.46	4 isomers, mean 1.44.
$C_5H_8 \rightarrow C_5H_5^{++} + 3H$	1.2 and 1.35	2 isomers.
$C_6H_6 \rightarrow C_6H_3^{++} + 3H$	1.4	Benzene, appearance potential 39.8 volts.
$C_4H_8 \rightarrow C_4H_6^{++} + 2H$	1.3	2 isomers.
$C_5H_8 \rightarrow C_5H_6^{++} + 2H$	1.0 and 1.2	2 isomers.
$C_5H_{10} \rightarrow C_5H_8^{++} + 2H$	1.1 to 1.3	3 isomers, mean 1.2.
$C_2H_4 \rightarrow C_2H_3^{++} + H$	1.3	Ethylene, appearance potential 36 volts.
$C_2H_6 \rightarrow C_2H_5^{++} + H$	1.25	Ethane, appearance, potential 32 volts.
$C_3H_8 \rightarrow C_3H_5^{++} + H$	1.3 and 1.2	2 isomers.
$C_4H_8 \rightarrow C_4H_7^{++} + H$	1.2 to 1.4	4 isomers, mean 1.3.
$C_5H_8 \rightarrow C_5H_7^{++} + H$	1.1 and 1.25	2 isomers.
$C_6H_6 \rightarrow C_6H_5^{++} + H$	1.2	Benzene, appearance potential 30.4 volts.
$C_5H_8 \rightarrow C_5H_8^{++}$	1.1	Isoprene.
$C_6H_6 \rightarrow C_6H_6^{++}$	1.0	Benzene, appearance potential 27 volts.

to remove each H atom from a hydrocarbon and the energy of recombination $2H \rightarrow H_2$ is 4.5 electron volts, it makes a large difference whether the pairs are removed as H_2 or 2H. As the different radicals have different ionization potentials and may have excess kinetic energy, the appearance potentials cannot be computed from these considerations alone. However, the results of table 11 would indicate that dissociation into H_2 usually occurs in double-ionization processes. That is, it requires about the same work to remove $4H_2$ and $3H_2+H$, $3H_2$ and $2H_2+H$, $2H_2$ and H_2+H.

From comparison with the few instances in which the appearance potential is known, it appears that all double ionization processes involving removal of H or H_2 require 30° to 36 volts. Processes involving removal of H_2+H or $2H_2$ require

roughly 40 volts. Processes involving removal of $2H_2+H$ and $3H_2$ must fall in a narrow voltage range above 40 volts, whereas removal of $5H_2$ must require nearly 50 volts.

Molecules with more than five carbon atoms give values of $i(70)/i(50)$ somewhat less than those listed in table 11 for removal of a given number of H atoms. Thus in seven C_7H_{14} cyclics in the process $C_7H_{14} \rightarrow C_7H_6^{++}+8H$, the ratio ranges from 1.3 to 1.5 as compared with 3.5 given in table 11. In the same isomers $C_7H_{14} \rightarrow C_7H_8^{++}+6H$ gives a mean ratio of 1.2, as compared with the mean 1.8 for the values in table 11 for loss of 6H.

In table 7 three of the C_8H_{16} isomers give large doubly charged peaks of mass 97. This could be either C_8H^{++} or $C_7H_{13}^{++}$. The ratio $i(70)/i(50)$ is 1.15 to 1.17, indicating a low appearance potential, and for this reason the ion has been ascribed to $C_7H_{13}^{++}$. Removing 15 H atoms would require a very high appearance potential. Similarly 2,2,4,4-tetramethylpentane in table 8 gives ions of masses 96, 97, and 98. The ratios are in the range 1.13 to 1.18, and the ions have been ascribed to $C_7H_{12}^{++}$, $C_7H_{13}^{++}$, and $C_7H_{14}^{++}$.

V. Summary and Discussion

The doubly charged ion spectra of hydrocarbons with three, four, or five carbon atoms follow some simple rules that can be summarized as follows:

1. In the most probable ionization processes carbon bonds are not broken, but all except two, three, or four hydrogen atoms are removed.

2. The relative intensity distribution is similar in all hydrocarbons with the same number of carbon atoms.

3. The magnitude of the peaks is least for saturated molecules, greater for monoolefins and alkylcyclics and greatest for diolefins and cycloolefins.

4. Ion peaks tend to alternate in intensity with larger values for ions with an even number of H atoms.

These rules are in contrast to the case of singly charged ions. For these the most probable ionization processes frequently involve breaking carbon bonds, the spectra depend considerably on the structure of the molecule and are quite different for paraffins, olefins, and diolefins. Ions with an odd number of H atoms tend to be more abundant.

Doubly charged ion spectra of molecules with six or more carbon atoms are quite different from the lighter hydrocarbons. The most probable ionization processes involve breaking of carbon bonds in all these except the alkylbenzenes and the C_7 cyclics. Structural differences and the degree of saturation give large differences in the spectra. $C_3H_2^{++}$ is often the maximum peak in C_6 hydrocarbons and in C_7 paraffins. In other C_7 hydrocarbons and in C_8 and C_9 hydrocarbons, $C_7H_8^{++}$ is often the maximum peak. Rules 3 and 4 remain true, in general, with minor exceptions.

A qualitative consideration of the ionization process gives a partial explanation of some of the properties of doubly charged ion spectra. The least potential required to doubly ionize a large molecule would involve removal of two electrons from two atoms near each end of the molecule. (The Coulomb law of attraction makes the work required to remove the second electron least if it is removed from an atom as far away as possible from the first ion). The resulting ion with a charge near each end is subject to large disruptive forces, and probably a frequent result of double ionization is that the molecule ion dissociates into two singly charged ions. In general this process will be indistinguishable from single ionization processes, but Stevenson and Hipple [8] point out that the appearance potential of CH_3^+ in the two butane isomers indicates that it comes from the process

$$C_4H_{10} \rightarrow C_3H_7^+ + CH_3^+ + 2e.$$

If, however, a molecule loses most of its hydrogen atoms in the dissociation process, then the bonds between carbon atoms become double bonds and the bonding force is greatly increased. Evidently it is then sufficient to overcome the disruptive force of the double charge.

The intensity rules for doubly charged ions in molecules with three to five carbon atoms can be explained on the hypotheses that all but two to four H atoms must be removed to give stable ions, and that the probability of this ionization process decreases as the appearance potential increases. With unsaturated molecules and cyclics the number of H atoms to be removed is less, and the intensity increases. As hydrogen atoms tend to be removed in pairs to give H_2, ions with an even number of H atoms are commonly more abundant than ions with an odd number.

From table 11 it is seen that removing 10 H atoms from C_5H_{12} to give $C_5H_2^{++}$ requires nearly 50 volts. One reason why different ionization processes are involved in molecules with six or more carbon atoms is because the work required to remove all but two H atoms exceeds the ionizing voltage. In the C_6H_{14} isomers, $C_5H_2^{++}$ is again the largest peak. This can be obtained by the least energy by removing CH_4 and four H_2 molecules. The fact that $C_5H_2^{++}$, $C_5H_4^{++}$, and $C_5H_6^{++}$ are larger than the peaks with an odd number of H atoms, supports the view that loss of CH_4 and H_2 molecules actually occurs. In singly charged ion spectra, peaks with an odd number of H atoms are larger, and it is known that the more probable ionization processes involve dissociation with loss of CH_3 and other radicals with an odd number of H atoms. (Ionization with dissociation into CH_4 is known to occur but is less probable [8]).

In C_6 hydrocarbons doubly charged ions with six carbon atoms are found in C_6H_{12} isomers, and these ions are the most abundant ions in cyclohexene, C_6H_{10}, and in benzene, C_6H_6. C_6 ions become more abundant as the number of H atoms decreases. This is also true of C_7 ions in the C_7 hydrocarbons. In C_8 hydrocarbons there are no doubly charged C_8 ions in C_8H_{18} and C_8H_{16} isomers. They are strong in 4-ethenyl-1-cyclohexene, C_8H_{12}, and predominant in the C_8H_{10} alkylbenzenes.

In hydrocarbons with seven or more carbon atoms the ion $C_7H_8^{++}$ is commonly the most abundant ion. The empirical fact that such an ion is stable is another factor that makes the doubly charged ions of the heavier hydrocarbons differ from the lighter ones. Also in the heavier hydrocarbons certain configurations of carbon atoms seem to favor doubly charged ions such as the 2,2,4-trimethyl arrangement in C_8 hydrocarbons. Other configurations, such as ethyl side chains in the octanes, give no doubly charged ions. This introduces striking individual differences among isomers that are not found in the lighter hydrocarbons. Individual differences, depending on structure, are the rule in singly charged ion spectra.

VI. Conclusion

The study of doubly charged ion spectra is of interest in that it gives additional evidence as to the ionization process. Doubly charged ion peaks are, however, not very useful in the practical application of most spectra to chemical analysis, although it is essential to know the complete spectrum of every pure compound analysed. In the case of propadiene and propyne there is a striking difference in the doubly charged ions that affords the best basis for distinguishing the compounds. In nearly every other case the peaks are too small to be used in analysis.

VII. References

[1] Catalog of mass spectral data, American Petroleum Institute, Project 44, National Bureau of Standards.

[2] J. A. Hipple, Jr., Phys. Rev. **53,** 530 (1938).

[3] P. Kusch, A. Hustrulid, and John T. Tate, Phys. Rev. **52,** 843 (1937).

[4] A. Hustrulid, P. Kusch, and John T. Tate, Phys. Rev. **54,** 1037 (1938).

[5] American Petroleum Institute catalog of mass spectral data, description sheet 1.

[6] J. Delfosse and Walker Bleakney, Phys. Rev. **56,** 256 (1939).

[7] American Petroleum Institute catalog of mass spectral data, tables 57, 58, and 59 (Atlantic Refining Co., Philadelphia, Pa.)

[8] D. P. Stevenson and J. A. Hipple, J. Am. Chem. Soc. **64,** 1588 (1942).

Washington, October 29, 1948

U. S. Department of Commerce
National Bureau of Standards

Research Paper RP1976
Volume 42, April 1949

Part of the Journal of Research of the National Bureau of Standards

Heats, Equilibrium Constants, and Free Energies of Formation of Cyclopentene and Cyclohexene[1]

By Morton B. Epstein,[2] Kenneth S. Pitzer,[3] and Frederick D. Rossini [4]

For cyclopentene and cyclohexene, values are presented for the following thermodynamic properties to 1,500° K: heat-content function, free-energy function, entropy, heat content, heat capacity, heat of formation from the elements, free energy of formation from the elements, and logarithm of the equilibrium constant of formation from the elements. Equilibrium constants are given in graphical form for some reactions of isomerization, dehydrogenation, and disproportionation.

As part of the work of the American Petroleum Institute Research Project 44 at the National Bureau of Standards and the University of California, values have been compiled for the thermodynamic properties in the gaseous state to 1,500° K of the heat-content function, free-energy function, entropy, heat content, heat capacity, heat of formation, free energy of formation, and logarithm of the equilibrium constant of formation for cyclopentene and cyclohexene. Calculations have also been made of the free energies and equilibrium constants of a number of reactions involving isomerization, dehydrogenation, and disproportionation of these compounds.

The values of the constants used in the present calculations are as follows [1,2][5]: The calorie is the conventional thermochemical calorie defined as 4.1840 absolute joules; the absolute temperature of the ice point is 273.16 ±0.010° K; the gas constant is 1.98719 ±0.00013 cal/deg mole.

For cyclopentene and cyclohexene, the values of the heat-content function, free-energy function, and heat capacity were taken from reference [3]. As usual, the value of the entropy is given by the value of the heat-content function less the value of the free-energy function, and the heat content is obtained by multiplying the value of the heat-content function by the temperature.

The resulting values of the thermodynamic functions are given in table 1, which includes values of the following properties from 0° to 1,500° K: heat-content function, free-energy function, entropy, heat content, and heat capacity.

Values of the standard heat of formation at 25° C of gaseous cyclopentene and cyclohexene, from carbon (solid, graphite) and hydrogen (gaseous), were calculated from the values for the standard heat of formation for the liquid state calculated by Prosen, Yenchius, and Rossini [4] from experimental values for the heats of combustion, together with values for the standard heat of vaporization calculated by Wagman and Rossini [6] from vapor pressure data of Forziati and Rossini [7]. The values for the standard heat of formation from the elements, at 25° C, $\Delta Hf°$, from reference [4] are as follows: Cyclopentene (liquid), 1.16 ±0.16 kcal/mole; cyclohexene (liquid), −9.70 ± 0.19 kcal/mole. The values for the standard heat of vaporization at 25° C, $\Delta He°$, from reference [6], are as follows: cyclopentene, 6.71 ±0.07 kcal/mole; cyclohexene, 8.00 ±0.08 kcal/mole.

[1] This investigation was performed as a part of the work of the American Petroleum Institute Research Project 44 at the National Bureau of Standards and the University of California.

[2] Research Associate on the American Petroleum Institute Research Project 44 at the National Bureau of Standards.

[3] Associate Director of the American Petroleum Institute Research Project 44 at the University of California, Berkeley, Cal.

[4] Director of the American Petroleum Institute Research Project 44 at the National Bureau of Standards.

[5] Figures in brackets indicate the literature references at the end of this paper.

TABLE 1.—*Values of the thermodynamic functions, for the ideal gas state, to 1,500° K, for cyclopentene and cyclohexene*

Compound (gas)	Formula	Temperature in °K: 0	200	298.16	300	400	500	600	700	800	900	1,000	1,100	1,200	1,300	1,400	1,500
Heat-content function, $(H^\circ - H_0^\circ)/T$, in cal/deg mole																	
Cyclopentene	C_5H_8	0	9.97	11.63	11.65	14.12	16.98	19.90	22.71	25.36	27.82	30.09	32.19	34.13	35.92	37.57	39.10
Cyclohexene	C_6H_{10}	0	10.75	13.98	14.05	18.04	22.20	26.20	29.93	33.35	36.47	39.33	41.94	44.34	46.53	48.55	50.42
Free-energy function, $(F^\circ - F_0^\circ)/T$, in cal/deg mole																	
Cyclopentene	C_5H_8	0	−53.37	−57.62	−57.69	−61.37	−64.82	−68.18	−71.46	−74.67	−77.80	−80.85	−83.81	−86.70	−89.50	−92.23	−94.87
Cyclohexene	C_6H_{10}	0	−55.43	−60.29	−60.38	−64.96	−69.43	−73.84	−78.16	−82.38	−86.49	−90.48	−94.36	−98.12	−101.75	−105.27	−108.68
Entropy, S°, in cal/deg mole																	
Cyclopentene	C_5H_8	0	63.43	69.23	69.34	75.49	81.80	88.08	94.17	100.03	105.62	110.94	116.00	120.83	125.42	129.80	133.97
Cyclohexene	C_6H_{10}	0	66.18	74.27	74.43	83.00	91.63	100.04	108.09	115.73	122.96	129.81	136.30	142.46	148.28	153.82	159.10
Heat content, $(H^\circ - H_0^\circ)$, in cal/mole																	
Cyclopentene	C_5H_8	0	1,994	3,462	3,495	5,648	8,490	11,940	15,900	20,290	25,040	30,090	35,410	40,960	46,700	52,600	58,650
Cyclohexene	C_6H_{10}	0	2,150	4,168	4,215	7,216	11,100	15,720	20,950	26,680	32,820	39,330	46,130	53,210	60,490	67,970	75,630
Heat capacity, C_p°, in cal/deg mole																	
Cyclopentene	C_5H_8	0	12.33	17.95	18.08	25.08	31.62	37.19	41.86	45.78	49.11	51.94	54.37	56.45	58.24	59.79	61.13
Cyclohexene	C_6H_{10}	0	16.32	25.10	25.28	34.64	42.78	49.45	54.92	59.49	63.34	66.62	69.43	71.85	73.92	75.72	77.27
Heat of formation, ΔHf°, in kcal/mole																	
Cyclopentene	C_5H_8	7.05	3.14	1.16	1.12	−0.74	−2.28	−3.51	−4.49	−5.22	−5.75	−6.09	−6.29	−6.35	−6.35	−6.27	−6.15
Cyclohexene	C_6H_{10}	−2.24	−7.44	−9.70	−9.74	−11.69	−13.21	−14.35	−15.18	−15.74	−16.07	−16.19	−16.14	−15.95	−15.70	−15.36	−14.96
Free energy of formation, ΔFf° in kcal/mole																	
Cyclopentene	C_5H_8	7.05	.....	19.77	19.89	26.43	33.41	40.66	48.11	55.66	63.31	71.01	78.73	86.46	94.20	101.9	109.6
Cyclohexene	C_6H_{10}	−2.24	.....	17.12	17.28	26.60	36.36	46.38	56.58	66.86	77.22	87.60	97.96	108.3	118.7	129.0	139.3
Logarithm of equilibrium constant of formation, $\log_{10} Kf$																	
Cyclopentene	C_5H_8	∞	.....	−14.491	−14.487	−14.439	−14.602	−14.811	−15.019	−15.206	−15.374	−15.519	−15.642	−15.746	−15.837	−15.909	−15.975
Cyclohexene	C_6H_{10}	∞	.....	−12.548	−12.592	−14.533	−15.892	−16.895	−17.664	−18.266	−18.750	−19.143	−19.462	−19.727	−19.951	−20.136	−20.294

The method of calculating values of the standard heat of formation, the standard free energy of formation, and the logarithm of the equilibrium constant of formation for the different temperatures in the range 0° to 1,500° K is the same as that described in section IV, 1 of reference [5].

The resulting values for the formation of the given hydrocarbon in the gaseous state, from the elements carbon (solid, graphite) and hydrogen (gaseous), each in its thermodynamic standard reference state, are included in table 1, which gives values of the following properties to 1,500° K: heat of formation, free energy of formation, and logarithm of the equilibrium constant of formation.

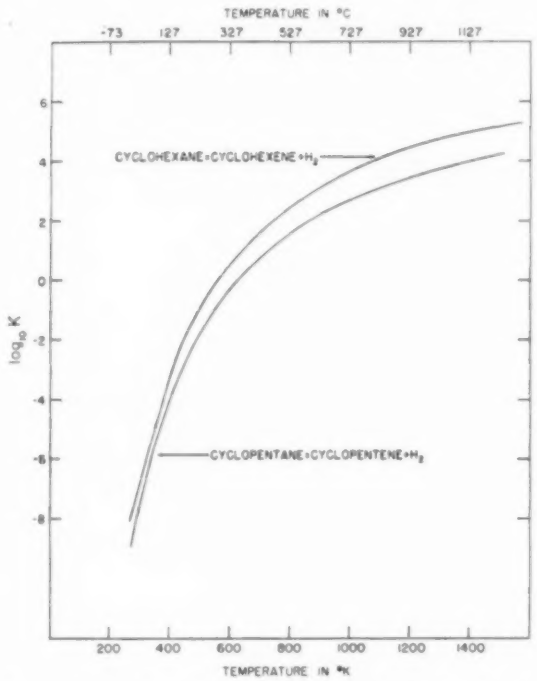

FIGURE 1. *Dehydrogenation of cycloparaffins to cycloolefins.*

The curves give the logarithm of the equilibrium constant as a function of temperature for the following reactions in the gaseous state:

C_5H_{10} (gas, cyclopentane) = C_5H_8 (gas, cyclopentene) + H_2 (gas).

C_6H_{12} (gas, cyclohexane) = C_6H_{10} (gas, cyclohexene) + H_2 (gas).

In figure 1 are plotted, as a function of temperature, values of the logarithm of the equilibrium constant for the reactions of dehydrogenation of cyclopentane to cyclopentene and of cyclohexane to cyclohexene.

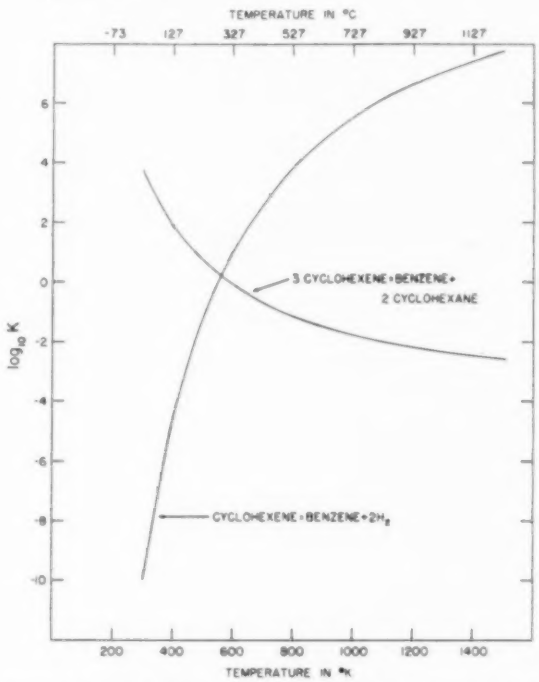

FIGURE 2. *Dehydrogenation of cyclohexene to benzene and disproportionation of cyclohexene to benzene and cyclohexane.*

The curves give the logarithm of the equilibrium constant as a function of temperature for the following reactions in the gaseous state:

C_6H_{10} (gas, cyclohexene) = C_6H_6 (gas, benzene) + $2H_2$ (gas).

$3C_6H_{10}$ (gas, cyclohexene) = C_6H_6 (gas, benzene) + $2C_6H_{12}$ (gas, cyclohexane).

In figure 2 are plotted, as a function of temperature, values of the logarithm of the equilibrium constant for the dehydrogenation of cyclohexene to benzene and for the disproportionation of cyclohexene to cyclohexane and benzene.

In figure 3 are plotted, as a function of temperature, values of the logarithm of the equilibrium

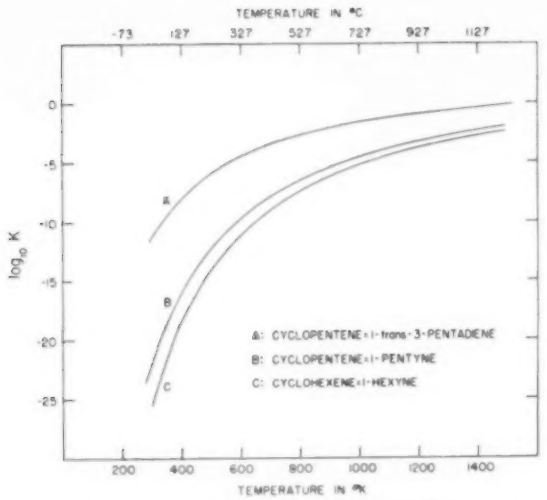

FIGURE 3. *Isomerization of cycloolefins to diolefins and to acetylenes.*

The curves give the logarithm of the equilibrium constant as a function of temperature for the following reactions in the gaseous state:

(A) C_5H_8 (gas, cyclopentene) = C_5H_8 (gas, 1-*trans*-3-pentadiene).

(B) C_5H_8 (gas, cyclopentene) = C_5H_8 (gas, 1-pentyne).

(C) C_6H_{10} (gas, cyclohexene) = C_6H_{10} (gas, 1-hexyne).

constant for the isomerization of cyclopentene to 1-pentyne, of cyclopentene to 1-*trans*-3-pentadiene, and of cyclohexene to 1-hexyne.

References

[1] Selected values of chemical thermodynamic properties (December 31, 1947). National Bureau of Standards.

[2] Selected values of properties of hydrocarbons. Table α. (December 31, 1947). American Petroleum Institute Research Project 44, National Bureau of Standards.

[3] C. W. Beckett, N. K. Freeman, and K. S. Pitzer, J. Am. Chem. Soc. **70,** 4227 (1948).

[4] E. J. Prosen, F. Yenchius, and F. D. Rossini, National Bureau of Standards. Unpublished.

[5] D. D. Wagman, J. E. Kilpatrick, W. J. Taylor, K. S. Pitzer, and F. D. Rossini, J. Research NBS **34,** 143 (1945) RP1634.

[6] D. D. Wagman and F. D. Rossini, National Bureau of Standards. Unpublished.

[7] A. F. Forziati and F. D. Rossini, National Bureau of Standards. Unpublished.

WASHINGTON, January 11, 1949.

U. S. Department of Commerce
National Bureau of Standards

Research Paper RP1977
Volume 42, April 1949

Part of the Journal of Research of the National Bureau of Standards

Preparation of Calcium Melibionate[1]

By William W. Walton and Horace S. Isbell

It has been found possible to prepare the comparatively rare salt, calcium melibionate, in any desired quantity by electrolytic oxidation of a crude solution of melibiose. The melibiose solution, prepared from commercial raffinose, is subjected to electrolytic oxidation in the presence of calcium carbonate and calcium bromide, and the calcium melibionate is crystallized directly from the electrolyte. The optical rotation of a 2-percent aqueous solution of calcium melibionate, expressed on the anhydrous basis, was found to be $[\alpha]_D^{20}+106.2°$, which disagrees with the value, $[\alpha]_D^{17}+88.6°$, reported in the literature. Calcium melibionate forms a basic calcium salt, $Ca(C_{12}H_{21}O_{12})_2.4CaO$. This is analogous to the basic calcium salts of lactobionic and maltobionic acids.

I. Introduction and Discussion

The need for calcium melibionate in connection with a study of the glycosyl derivatives of ascorbic acid led to an investigation of methods available for its preparation. Neuberg, Scott, and Lachmann [1] [2] prepared calcium melibionate by oxidizing melibiose with bromine, removing the excess bromine with a stream of air, neutralizing with calcium carbonate, and separating the calcium melibionate from the accompanying calcium bromide by repeated crystallization from ethanol.

Levene and Wintersteiner [2] treated a solution of raffinose with baker's yeast and malt sprouts to obtain a crude solution of melibiose. This solution was purified by treatment with basic lead acetate, hydrogen sulfide, and a decolorizing carbon, and the melibiose in solution was oxidized with iodine in the presence of barium iodide and barium hydroxide. A lengthy purification of the melibionic acid involved the use of lead carbonate, sulfuric acid, silver sulfate, hydrogen sulfide, and barium hydroxide. The calcium salt was obtained by neutralization of the melibionic acid with calcium carbonate and crystallization from water by the addition of methanol.

Levene and Jorpes [3] obtained crystalline melibiose from raffinose and then oxidized the melibiose with bromine in the presence of barium benzoate [4]. They purified the melibionic acid by successive treatment with silver carbonate, hydrogen sulfide, sulfuric acid, and barium hydroxide, and finally by extraction of benzoic acid with chloroform. The solution of melibionic acid was boiled with calcium carbonate; the resulting calcium melibionate was precipitated by adding methanol and was recrystallized by dissolving in water and adding methanol.

The laborious purification steps required in all of these methods of preparation made desirable a simpler method for the preparation of calcium melibionate. Isbell and Frush [5] have developed a convenient method for the preparation of aldonic acids from aldoses by electrolytic oxidation. In the case of glucose, crude solutions can be oxidized and the acid separated directly from the electrolyte as the calcium salt. It seemed possible that calcium melibionate might be prepared by this method directly from the liquor that remained after hydrolysis of raffinose and fermentation of the resulting fructose.

Application of the electrolytic method to the preparation of calcium melibionate from melibiose and calcium carbonate gave a product that crystallized directly from the electrolyte as the reaction proceeded. The crystals were easily separated by filtration. By returning the mother liquor to the

[1] The subject matter reported in this paper was abstracted from a thesis submitted by William W. Walton, of this Bureau, in June 1947 to the Faculty of the Graduate School of the University of Maryland, represented by Dr. Nathan L. Drake, in partial fulfillment of the requirements for the degree of Doctor of Philosophy. (See also J. Research NBS **41**, 119 (1948) RP1910.)

[2] Figures in brackets indicate the literature references at the end of this paper.

electrolytic cell with additional melibiose and calcium carbonate, the salt can be prepared in a continuous process similar to that used for the production of calcium gluconate [6]. The relatively small quantities of the salt required for the present study, however, were obtained in several separate preparations. The crude product was readily recrystallized from hot water.

Crystalline calcium melibionate is reported in the literature to contain from 11 to 15 percent of water. The product prepared by electrolytic oxidation varied in water content from 6.6 to 13.9 percent, and it was found that air-dried material lost or gained weight from day to day, apparently from changes in the relative humidity. An anhydrous sample gained more than 10 percent in weight when stored in a vacuum oven at 50° C but was restored to its anhydrous condition when dried in vacuum over anhydrous magnesium perchlorate at room temperature. The specific rotation, $[\alpha]_D^{20}$, of the pure salt in 2-percent aqueous solution was found to be +106.2°, expressed on an anhydrous basis. The specific rotation is recorded in the literature as +88.6° at a temperature of 17° C. Unfortunately, the wavelength of the light used is not given in the original publication [1], but the constant is quoted in various handbooks [7, 8] as $[\alpha]_D^{17}$.

Inasmuch as basic calcium salts are useful for the separation and purification of a number of sugar acids [9], it seemed desirable to ascertain whether melibionic acid also forms such a salt. The basic calcium salts of the monobasic acids derived from monosaccharides are of the type $Ca(anion)_2.2CaO$. Two acids derived from disaccharides, lactobionic acid, and maltobionic acid, however, have yielded basic calcium salts having the formula $Ca(anion)_2.4CaO$. A basic calcium salt of melibionic acid has now been prepared and found to have the composition $Ca(C_{12}H_{21}O_{12})_2.4CaO$, which corresponds to the basic salts prepared from lactobionic and maltobionic acids. The new substance is difficultly soluble and useful for the preparation and purification of melibionic acid.

II. Experimental Details

1. Preparation of a Solution of Melibiose

Six hundred grams of raffinose (purity 99.08 % based on optical rotation), equivalent to 1 mole of pure raffinose, was dissolved in 3.6 liters of water containing 60 ml of nutrient solution.[3] Four drops of a 1:1 aqueous acetic acid solution was added to bring the pH of the solution to 4.5. The optical rotation of the solution was found to be 90.3° S (2-dm tube). Twenty milliliters of invertase solution [4] was added, and the mixture was allowed to stand at room temperature for 24 hr. The observed rotation, based on the volume before the addition of the invertase solution, was 47.8° S (2-dm tube). This value indicates that the sugar had been converted to melibiose and fructose to the extent of 97.4 percent.

To remove the fructose, two cakes of baker's yeast were added, and the solution was allowed to ferment for 3 days at room temperature. The optical rotation at the end of this period was 70.5° S (2-dm tube). For complete hydrolysis and destruction of the fructose, the calculated rotation should be 70.7° S. The rotation obtained indicates that the conversion of the raffinose to melibiose and removal of the fructose was substantially quantitative.

The solution was heated to boiling to destroy the yeast, and clarified by the addition of 30 ml of a decolorizing carbon, and filtration. The filtrate was concentrated under reduced pressure to 1.8 liters and used directly for the preparation of calcium melibionate.

2. Preparation of Calcium Melibionate

The solution of melibiose obtained from 600 g of raffinose was transferred to a 3-liter beaker, and 32 g of calcium bromide and 55 g of calcium carbonate were added. Two graphite electrodes, 22 mm in diameter, were immersed to a depth of 12 cm, and the solution was stirred mechanically while a current of 1 ampere at 10.8 v was passed through. The electrolysis was stopped when titration of an aliquot with iodine [10] indicated that 97.3 percent of the melibiose had been oxidized. The current efficiency was 82.9 percent. Higher current efficiencies were obtained for lower percentages of oxidation.

The solution was heated to dissolve the portion of the calcium melibionate that had crystallized, and the hot solution was filtered. The filtrate was concentrated under reduced pressure to a volume

[3] The nutrient solution was made by dissolving 2.5 g of NH_4NO_3, 0.3 g of KH_2PO_4, and 2.5 g of $MgSO_4.7\ H_2O$ in 1 liter of water.

[4] The invertase solution is a commercial product made by Difco Laboratories, Detroit, Mich.

of about 800 ml and allowed to cool to room temperature. The calcium melibionate that crystallized from the solution was collected on a Büchner funnel and washed with three 25-ml portions of cold water. Three hundred and twenty-five grams of crystalline calcium melibionate, calculated on the anhydrous basis, was obtained. The filtrate was concentrated under reduced pressure to 100 ml, and 75 ml of methanol was added. An additional crop of 40 g of calcium melibionate, calculated on the anhydrous basis, was obtained. The total yield of crude product was 365 g or 96.7 percent. Larger quantities of raffinose were used in a number of preparations without any difficulty.

For analysis, the crude material was recrystallized several times from hot water, and finally was air-dried. The water content of the material was determined by drying samples to constant weight at room temperature over anhydrous magnesium perchlorate, and the results reported below are expressed on the anhydrous basis.

Analysis: Calculated for anhydrous $Ca(C_{12}H_{21}O_{12})_2Ca$, 5.31; C, 38.2; H, 5.6. Found: Ca, 5.33; C, 38.2; H, 5.7. $[\alpha]_D^{20} = +106.2°$ (water, c=2).

3. Preparation of Basic Calcium Melibionate, $Ca(C_{12}H_{21}O_{12})_2.4CaO$

Ten grams of calcium melibionate was dissolved in 200 ml of water, and the solution was cooled to 0° C. A suspension of 3.5 g of calcium oxide in 200 ml of water at 0° C. was added, and the mixture was shaken for several minutes. It was then filtered into a flask through which a current of carbon-dioxide-free air was passed. The clear solution was concentrated under reduced pressure to 150 ml and finally heated for a few minutes on the steam bath to complete the precipitation of the basic salt. The salt was separated by filtration in the absence of carbon dioxide and dried at 60° C in vacuum. Analysis: Calculated for $Ca(C_{12}H_{21}O_{12})_2.4CaO$: total Ca, 20.47; CaO, 22.91. Found: total Ca, 20.45; CaO, 22.56.

The authors express their appreciation to Nancy B. Holt for the measurements of optical rotations and to Rolf A. Paulson for the determinations of carbon and hydrogen reported in this paper.

III. References

[1] C. Neuberg, L. Scott, and S. Lachmann, Biochem. Z. **24,** 162 (1910).

[2] P. A. Levene and O. Wintersteiner, J. Biol. Chem. **75,** 321 (1927).

[3] P. A. Levene and E. Jorpes, J. Biol. Chem. **86,** 403 (1930).

[4] C. S. Hudson and H. S. Isbell, BS J. Research **3,** 57 (1929) RP82.

[5] H. S. Isbell and H. L. Frush, BS J. Research **6,** 1145 (1931) RP328.

[6] H. S. Isbell, H. L. Frush, and F. J. Bates, BS J. Research **8,** 571 (1932) RP436.

[7] B. Tollens and H. Elsner, Kurzes Handbuch der Kohlenhydrate, p. 463 (Johann Ambrosius Barth, Leipzig, 1935).

[8] H. Vogel and A. Georg, Tabellen der Zucker und Ihrer Derivate, p. 604 (Julius Springer, Berlin, 1931).

[9] H. S. Isbell and H. L. Frush, BS J. Research **11,** 649 (1933) RP613.

[10] G. M. Kline and S. F. Acree, BS J. Research **5,** 1063 (1930) RP247.

Washington, December 6, 1948.

U. S. Department of Commerce
National Bureau of Standards

Research Paper RP1978
Volume 42, April 1949

Part of the Journal of Research of the National Bureau of Standards

Polarographic Limiting Currents

By John Keenan Taylor, Roberta E. Smith, and Irvin L. Cooter

A cathode-ray oscillograph and special camera were used to record instantaneous values of the current for the dropping-mercury electrode. The results show that the Ilkovic equation does not represent the current as a function of time. The relation between the average current during the life of a drop and that measured by several polarographic circuits was determined.

I. Introduction

The theory of currents limited by the rate of diffusion of an electrolyzable constituent of a solution to the electrode has been developed by others. For linear diffusion to a plane electrode, the theoretical relation between the instantaneous current, $(i_d)_t$, and time, t, is given by [1, 2, 3][1]

$$(i_d)_t = A\sqrt{\frac{D}{\pi}}nFCt^{-1/2}, \qquad (1)$$

where A is the area of the electrode, D is the diffusion constant, C is the concentration of the diffusing material in the bulk of the solution, n is the number of electrons taking part in the electrode reaction, and F is the Faraday constant. The corresponding equation for a spherical electrode of fixed radius, R, [1, 3] is

$$(i_d)_t = A\sqrt{\frac{D}{\pi}}nFCt^{-1/2} + 4\pi RnFDC. \qquad (2)$$

A similar equation for the dropping-mercury electrode [4, 5] is

$$(i_d)_t = 4\left[\frac{7}{3}\right]^{1/2}\left[\frac{3}{4d}\right]^{2/3}\pi^{-1/6}nFD^{1/2}Cm^{2/3}t^{1/6}, \qquad (3)$$

where d is the density of the mercury and m is the mass of mercury emitted by the electrode in unit time.

[1] Figures in brackets indicate the literature references at the end of this paper.

Integration over the life span of a drop of the values of $(i_d)_t$ given by eq. 3 gives the expression

$$i_d = k n D^{1/2}Cm^{2/3}t^{1/6}, \qquad (4)$$

where i_d is the average current, t is the drop time, and k expresses all of the numerical constants. Equation 4 is used widely in polarographic measurements and referred to as the Ilkovic equation.

Relations between diffusion current and time have been investigated experimentally. Laitinen and Kolthoff [3] found that eq 1 expresses the current for plane electrodes, provided care is taken to eliminate the disturbing effects of convection and adverse density gradients. However, these workers were not able to obtain the predicted behavior with spherical electrodes in aqueous solutions and only approached it in gelatin gels, where disturbances are minimized by the high viscosity of the medium.

No conclusive studies have been made of the current-time relationship for the dropping-mercury electrode.[2] Ilkovic [6] made some measurements and states that the data are represented by a parabola of approximately the sixth order. However, he does not give sufficient details of his experiments to permit a recalculation of the data. Most of the tests of the Ilkovic equation fall into

[2] Since this paper was prepared, Hugh A. McKenzie reported some work to us in which he found current-time curves that were approximately one-third order parabolas. A preliminary report of his work has been published (J. Am. Chem. Soc. **70**, 3147 (1948)). Also, we have been informed that F. L. Steghart read a paper to the Physical Methods Group of the Society of Public Analysts at London on December 12, 1947, in which he reported current-time curves which did not follow the Ilkovic equation.

two groups. The first consists in measurements or calculation of all of the parameters of the equation and comparing the diffusion current calculated with that observed [7]. The second consists in determining the constancy of the diffusion current constant, $I=i_d/Cm^{2/3}t^{1/6}$, as C, m, and t are varied [8]. All of these experiments have been performed while using highly damped apparatus for the electrical measurements, the assumption being made that average currents were measured.

The present paper reports the results of some experiments designed to determine the current-time relationship for the dropping-mercury electrode. Because of their practical interest, the relations between the average currents, and those measured by several polarographic circuits also have been determined.

II. Experimental Details

A schematic diagram of the circuits and apparatus used for measuring the polarographic diffusion currents as a function of time is shown in figure 1. In this figure, P_1 is a Leeds & Northrup portable potentiometer for supplying the voltage for the circuit, which consists of the polarographic cell and the calibrated resistance box, R_1. When the selector switch, S_1, is on the "measure" position, the voltage drop across R_1, after amplification, deflects the beam of a cathode-ray tube. A photographic record of the deflection of the beam as a function of time is made by means of the drum camera.

As the voltage across R_1 is only a few millivolts, and the voltage required on the deflection plates of the oscillograph is approximately 100 volts, an amplification factor of several thousand is required. Moreover, this amplification factor should remain constant over the range of applied voltage and during the recording time of several seconds. These requirements were met by using a direct-coupled amplifier designed at the David W. Taylor Model Basin [9]. This amplifier, which has only resistance coupling so that it can be used with aperiodic phenomena, has an amplification factor of 1,000, 2,000, or 5,000, with uniform response in the frequency range from 0 to 50,000 c/s. The output of this amplifier is connected directly to the vertical deflection plates of a Du Mont cathode-ray oscillograph, type 208. The photographic record of the deflection of the beam of the

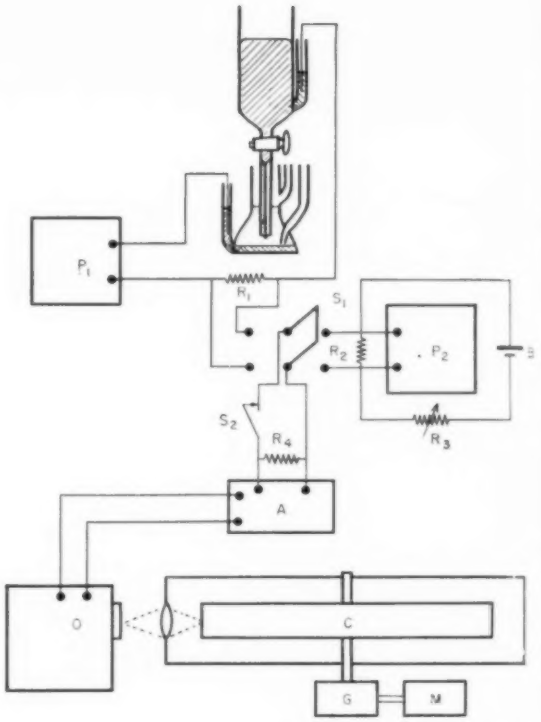

FIGURE 1. *Apparatus used for measuring limiting current.*

P_1, P_2, potentiometers; R_1, R_2, resistance boxes; R_3, current-limiting resistor; R_4, stabilizing resistor; S_1, selector switch; S_2, tapping key; B, battery, 1.5 v; A, amplifier; O, oscillograph; C, camera; G, reduction gear; M, motor.

cathode-ray tube is made by a drum camera. Essentially, this camera consists of a lens and shutter mounted in a light-tight housing enclosing a drum having a circumference of 60 in. and a rim 4 in. wide. The drum is mounted on a vertical axle and is belt-driven by a direct-current motor through reduction gears. When the drum is rotating at 2 rpm, the peripheral speed is approximately 2 in./sec. The housing can be opened to permit the mounting of a film on the drum.

For the electrodes used in these experiments, the time of each drop was approximately 3.5 sec, so that the diffusion current record for each drop extended about 7 in. on the film; this permitted records of seven or eight successive drops on each film.

In order that the recorded amplitude of the diffusion current at any point represent the true amplitude, it is necessary that the reference line for zero current remain constant during the re-

cording for each drop. Since there is a small but significant drift of the zero position of the amplifier during the 30 sec of recording, it is necessary to record a sufficient number of zero positions during this interval to establish a reliable reference line. A simple means of doing this is to incorporate a tapping key, S_2, into the input circuit of the amplifier, between R_3 and R_1. The normal position for this switch is closed, but by tapping the key the external circuit of the amplifier can be periodically opened for a short time interval. Linear interpolation between the various zero marks was used to determine the zero level corresponding to a given deflection.

The correlation of the recorded amplitude with the voltage producing the deflection was obtained by means of the calibrating circuit, consisting of a battery, B, a current-limiting resistor, R_3, and a calibrated resistance box, R_2. With selector switch, S_1, on the "calibrate" position, known voltage was applied to the amplifier by means of the calibrating circuit. By means of the current-limiting resistor, the voltage drop across R_2 was adjusted so that measurable potentials are applied to the amplifier input. These potentials were so selected that, without changing the gain controls of the amplifier, the deflection due to the calibrating voltage covered, in several steps, the maximum range of the deflection due to the polarographic current. These calibrating voltages were measured with the precision potentiometer, P_2. The deflection of the cathode-ray oscillograph beam due to these calibration voltages was recorded on the same film immediately after the recording of the polarographic current. From the magnitude of the calibrating voltages and the resulting measured deflections, a calibration curve may be obtained by plotting sensitivity (mv/cm.) with respect to the deflection in centimeters of the oscilloscope. From the calibration curve, the measured deflection due to the polarographic current, and the value of R_1 and R_4, it is possible to calculate the diffusion current.

A calibration factor for converting length measurement along the film to time was obtained by measuring the average drop rate of the electrode and dividing this by the average measured length of the current-time curve for a number of drops. This quotient, when multiplied by the measured length interval, would give the time interval. Care was taken to make the vertical axis of the oscillograph-beam deflections parallel to the axis of rotation of the drum in order to eliminate timing errors, which might otherwise occur.

The current-time records were measured on a special comparator. The comparator consisted of a heavy metal bed, 4 ft. long on which rested a traveling carriage. The carriage, driven by a screw with a graduated head, had a range of about 90 cm of longitudinal motion. Two long glass plates for holding the film, illuminated from below by a green fluorescent light, were set about 2½ in. below the carriage and parellel to it. On the carriage itself was the observing microscope, supported on a micrometer slide. The observing microscope, of magnification 4×, contained the reference cross hairs. By the use of this comparator, values of the abscissa (time) and ordinate (current) could be measured with a precision of a few microns.

The solution used for the oscillographic measurements was 3.018 millimolar in cadmium, 0.1 molar in potassium chloride, and contained 0.01 percent of gelatin to suppress maxima. A similar solution, except for the cadmium concentration, which was 2.724 millimolar, was used in all of the other work. These solutions were made with known amounts of cadmium metal and checked by analysis.

A silver wire wrapped around the dropping-mercury electrode served as the anode in all but a few cases where the mercury pool was employed. Diffusion-current measurements for cadmium were made at the potential −0.9 v with respect to the silver–silver-chloride anode. The droptime, t, of the electrode was determined at this potential as was also the flow, m, of mercury from the capillary. It was found that the value of m in the solution and at this value of the applied potential was about 4 percent smaller than when measured in air, in agreement with previous investigators [10].

Purified nitrogen was used to free all of the solutions of oxygen. The diffusion-current measurements were made in a thermostated bath at 25° C.

III. Results

A number of current-time curves were obtained in which the zero was marked on the film after the recording of current, but the slight drift of the amplifier was sufficient to preclude their use in quantitative calculations. The qualitative con-

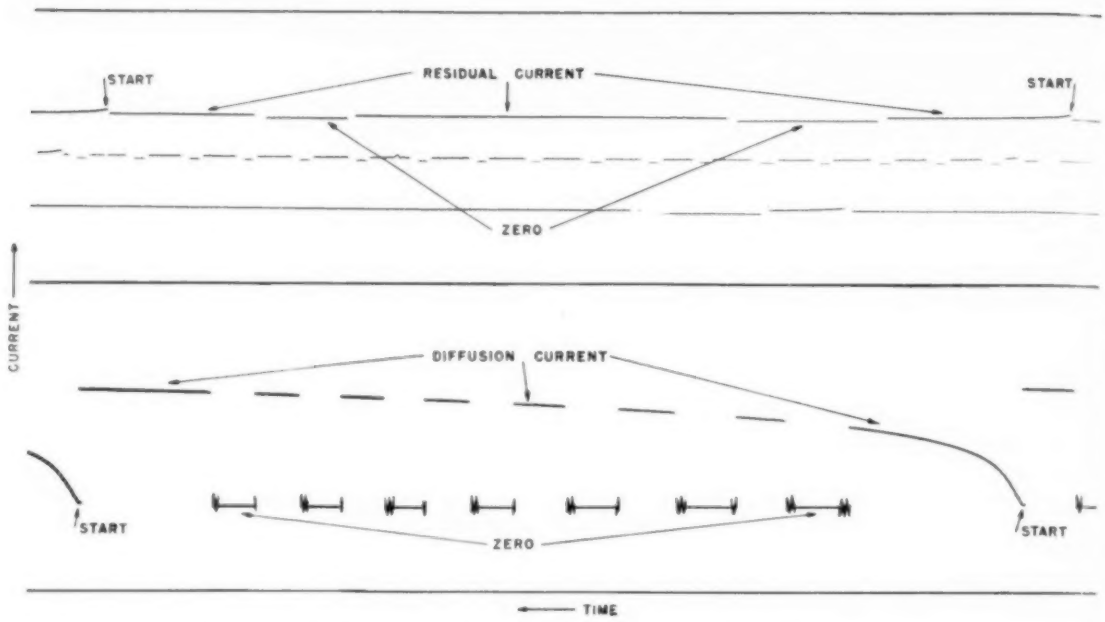

FIGURE 2. *Typical photographic records of residual current and diffusion current.*

The upper portion shows three traces for the residual current (one labeled), whereas the lower portion shows one trace of the diffusion current. The start of each new drop is indicated, and the time interval between each of such designations is about 3.5 sec.

clusions drawn from them are, however, in agreement with and support the more precise observations.

Several experiments were performed in which the zero was put on the film during the measurements of the limiting current. However, wherever a zero mark occurred, no record of the limiting current was obtained, so that some of the records were spoiled. Thus the start, or ending of a particular drop, or the portion of the curve where the current was changing most rapidly might be missing. Any of these defects was sufficient reason for discarding the measurement. As a result, only the complete records of two drops were accepted and used for quantitative interpretation. A number of the other traces were used for measurements of the value of the maximum current, however, or for the study of selected portions of the current-time curve.

A portion of the photographic record is shown in figure 2. The ordinate increases in the usual direction, but the time axis increases in the right to left direction. Three traces of the residual current are shown in the upper part of the figure. The current will be observed to start at a high value and to decrease with time, the zero trace being always below the residual current line. The polarographic limiting current is shown in the lower part of the figure. This current is not zero at the start of the drop but goes through a minimum, and then increases rapidly at first and more slowly later until the drop is disengaged from the capillary. Figures 3 and 4 are large scale plots of

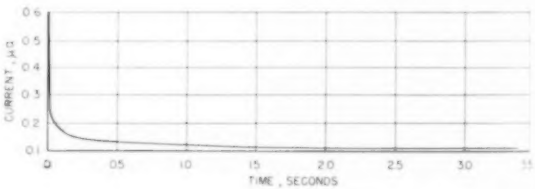

FIGURE 3. *Plot of residual current.*

the residual current and limiting current, respectively. The initial behavior of the limiting current is due to the residual current being greater than the limiting current during the very early period of drop formation. When the instantaneous value of the residual current is subtracted from the corresponding value for the limiting

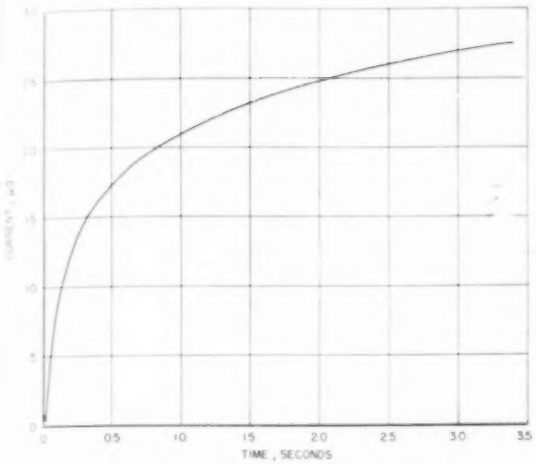

FIGURE 4. *Plot of limiting current.*

TABLE 1. *Variation of diffusion current with time for drop one*

t=3.392 sec; m=2.305 mg/sec; C=3.018 millimole/liter

Abscissa	Deflection	Time	Limiting current, i_l	Residual current, i_r	Diffusion current, i_d
Turn	*cm*	*sec*	*μa*	*μa*	*μa*
0	0.054	0	0.60	0.60	0.00
0.128	.031	0.005	.34	.29	.05
.237	.045	.009	.49	.27	.22
.363	.061	.013	.67	.25	.42
.506	.104	.018	1.14	.24	.90
.673	.179	.025	1.96	.23	1.73
1.347	.399	.049	4.40	.20	4.20
2.061	.625	.076	6.93	.19	6.74
2.828	.794	.104	8.84	.17	8.67
4.176	.989	.153	11.07	.16	10.91
5.576	1.124	.204	12.63	.15	12.48
8.076	1.291	.296	14.56	.14	14.42
12.576	1.494	.461	16.94	.13	16.81
17.306	1.634	.635	18.60	.13	18.47
23.544	1.766	.863	20.17	.12	20.05
28.312	1.845	1.038	21.11	.12	20.99
39.576	2.005	1.451	23.03	.11	22.92
54.069	2.164	2.005	24.94	.11	24.83
66.704	2.253	2.446	26.05	.11	25.94
80.086	2.325	2.937	26.92	.11	26.81
92.487	2.371	3.392	27.49	.11	27.38

current, the resulting diffusion current starts at zero within the error of the experiment.

The photographic records were measured in the manner described, and the abstracted data are given in tables 1 and 2. The first column contains the abscissa readings in turns of the lead screw of the comparator, and the second column gives

TABLE 2. *Variation of diffusion current with time for drop two*

t=3.488 sec; m=2.305 mg/sec; C=3.018 millimole/liter

Abscissa	Deflection	Time	Limiting current, i_l	Residual current, i_r	Diffusion current, i_d
Turn	*cm*	*sec*	*μa*	*μa*	*μa*
0	0.056	0	0.62	0.60	0.02
0.160	.035	0.006	.38	.27	.11
.331	.055	.012	.60	.25	.35
.548	.119	.020	1.31	.24	1.07
.728	.178	.027	1.95	.23	1.72
1.468	.440	.054	4.86	.21	4.65
1.969	.595	.072	6.59	.19	6.40
2.718	.759	.100	8.44	.18	8.26
3.968	.946	.145	10.58	.16	10.42
5.468	1.095	.200	12.29	.15	12.14
8.468	1.293	.310	14.53	.14	14.44
10.468	1.390	.384	15.72	.13	15.59
13.510	1.509	.495	17.11	.13	16.98
19.508	1.683	.719	19.18	.12	19.06
28.968	1.860	1.062	21.29	.12	21.17
40.019	2.013	1.468	23.13	.11	23.02
54.914	2.147	2.014	24.75	.11	24.64
65.716	2.246	2.410	25.96	.11	25.85
81.531	2.338	2.980	27.09	.11	26.98
95.133	2.397	3.488	27.81	.11	27.70

the corresponding deflection of the oscilloscopic spot from its zero position. The third column gives the elapsed times from the beginning of the drop, which were obtained by multiplying column one by the abscissa factor. The values for the limiting current, i_l, in column four resulted from multiplying the deflection by the corresponding sensitivity for that deflection found from the calibration curve. The residual current, computed in a like manner, was plotted on a large scale as a function of time, and values corresponding to the tabulated values of time were read and recorded in column five. Values for the diffusion current, i_d, in column six are the differences of columns four and five.

Figure 5 is a plot of the logarithm of the current with respect to the logarithm of the time. For conformance with the Ilkovic equation, the plot should be linear with a slope numerically equal to one-sixth. The plot is not linear, and a comparison with the slopes drawn in the figure shows that it never reached this value at any time during the life of the drop. This is emphasized by the mathematical treatment in which the function $i_d=kt^n$, in its logarithmic form, was adjusted to the data by the method of least squares. When the entire range of the measurements was used, the value for

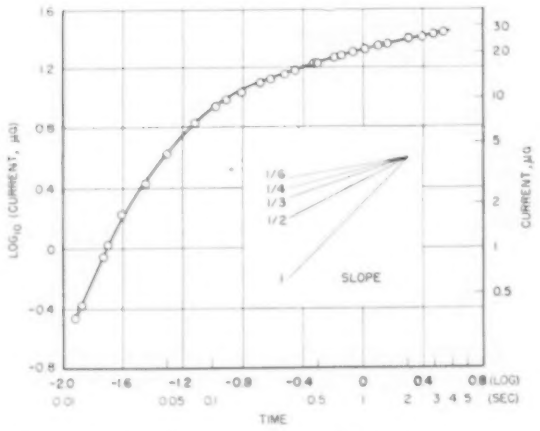

FIGURE 5. *Logarithmic plot of diffusion current with respect to time.*

exponent $n=0.82$ was obtained, but the fit was extremely poor. In the range 0.1 sec to maturity, the value, $n=0.31$, was found with an average deviation of ± 4.5 percent. For all times greater than 0.5 sec there resulted $n=0.249$, with an average deviation of ± 0.97 percent, whereas in the more limited range of 1 sec or greater, $n=0.227$, and the average deviation was ± 0.70 percent. If times greater than 2 sec are used for the calculation, the exponent became $n=0.186$, and the average deviation was ± 0.30 percent. A number of attempts were made to fit other simple equations of various types to the data, but none was found satisfactory.

The average current is of interest, since this is the quantity to be expected to be measured when using highly damped galvanometers or other measuring instruments. Accordingly, large-scale plots were made of the data for two drops, and the average current was found by graphical integration. For drops having maximum currents of 27.37 and 27.70 μa, respectively, the corresponding average currents were 22.1_7 and $22.3_0\mu$a. The ratios of the average to the maximum current were 0.81_0 and 0.80_5 in the two cases, which are to be compared with the value 0.859 (6/7) found from integration of the Ilkovic equation. Integration of the equation $i_d=kt^{0.249}$ gives 0.80_1 for the ratio, in good agreement with the graphical integration. Although this latter equation does not fit the data during the early time of drop formation, the bulk of the area under the curve occurs during the time when the fit is good, which explains the agreement of the value found by integration with that obtained by graphical means.

Calculation of the diffusion-current constant [11], I, defined by the expression $I=i_d/Cm^{2/3}t^{1/6}$ is a satisfactory means of reducing experiments done under slightly different conditions to a common basis, since this expression has been shown to hold true for widely varying characteristics of the electrode. When the maximum current is inserted in the expression, the constant $I_{max}=4.25$ is obtained whereas the average current yields the value $I=3.44$.

Less precise but confirmatory evidence for the deviation of the experimental current-time curve from that of the Ilkovic equation was obtained from measurements with a Hathaway galvanometer oscillograph, model 58 B. A chart speed of 28 mm/sec was used, and the galvanometer had a sensitivity of 0.38 μa/mm and a frequency response of 20 c/s, permitting a faithful record of the current for all but about the first 0.2-sec period of the life of the drop. The apparatus was calibrated in a manner similar to that used in the work with the cathode-ray oscillograph, and diffusion-current measurements were made on the cadmium solution already described and on a solution 3 millimolar in lead, with 1-*N* hydrochloric acid as the supporting electrolyte. From values of the maximum current and of average current obtained from graphical integration of the curves, extrapolated to zero time, diffusion-current constants were calculated. The results are given in table 3. (The extrapolation introduces no significant error in integration, since the area under this part of the curve is a small fraction of the total area.)

TABLE 3. *Diffusion-current constants from measurements with the galvanometer oscillograph*

Solution	I_{max}	I	I/I_{max}
Cadmium	4.20	3.42	0.81_0
Lead	4.81	3.86	$.80_2$

The residual current, i_r, may be considered to be composed of a faradayic current, i_f, and a condenser current, i_c. The former is the sum of the diffusion currents due to reducible impurities in the solution, whereas the latter arises as the result of charging or discharging the condenser resulting from the double layer at the mercury-solution

interface. The condenser current at any time, t, during the life of a drop should be expressed by $i_c = kt^{-1/6}$, where k represents the product of the capacity of the double layer, the difference between the applied potential and that of the electrocapillary maximum, and geometrical constants [12, 13]. Accordingly a plot of the logarithm of the residual current with respect to the logarithm of the time should be linear with slope equal to minus one-third. Such a plot is given in figure 6 and is seen to be linear, but the slope is only one-half of the theoretical value. Although pure materials were used for the supporting electrolyte and care was exercised to remove oxygen from the solutions, it is possible that there may have been some contribution of i_f to the residual current. The present experiments do not permit conclusions as to the reason for the discrepancy.

It is of interest to determine the magnitude of the current measured by various types of polarographic apparatus and to study how this depends upon the constants of the measuring instrument. The simplest apparatus is one in which a reflecting galvanometer is placed in series with the cell and the deflection read with the conventional lamp and scale. It is well known that galvanometers may be used to integrate the current. In the measurement of asymmetrical periodic phenomena with highly damped instruments or ones whose period during operation is long with respect to that of the event observed, the excursions of the galvanometer spot around an average position are small when compared with the total deflection, and the midpoint of the oscillation should approximate the average current. With relatively short-period equipment, this method is no longer adequate.

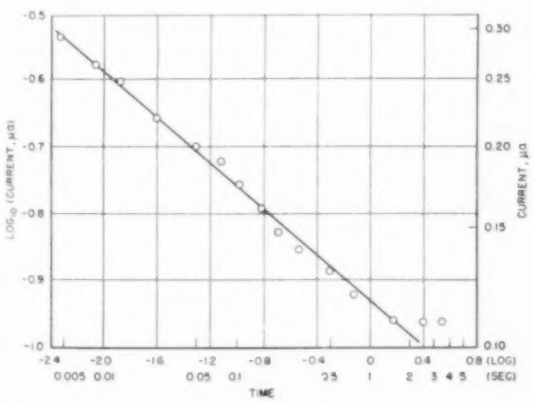

FIGURE 6. *Logarithmic plot of residual current with respect to time.*

TABLE 4. *Dependence of the diffusion current on the characteristics of the galvanometer*

In column 2, the values in italic type indicate the critical damping resistance

Galvanometer period	Damping resistance	Average deflection	Oscillation	I (average deflection)	I (integrated deflection)
sec	*Ohm*	*cm*	*cm*		
1.85	∞	5.87	5.5	2.99	3.48
	500	5.82	4.7	2.93	3.34
	200	5.65	3.9	3.02	3.39
	100	6.98	4.7	3.14	3.34
	43	5.81	2.7	3.27	3.35
	10	7.58	2.1	3.53	3.53
	5	4.35	1.1	3.45	3.45
2.0	∞	14.50	6.4	3.07	3.40
	∞	25.43	12.0	3.28	3.46
4.7	50	35.75	18.0	3.20	.....
	10	30.88	7.0	3.47	.....
	5	36.00	6.0	3.47	.....
	2	17.18	2.6	3.45	.....
	1	9.44	1.3	3.45	.....
5.0	∞	24.80	7.6	3.50	.....
	500	23.61	7.0	3.50	.....
	40	23.04	3.7	3.50	.....
	10	21.32	2.2	3.45	.....
	1	21.06	1.7	3.48	.....
6.4	*11*	22.23	3.9	3.46	.....
	5	19.21	3.0	3.41	.....
	1	25.80	3.5	3.43	.....
15.5	*21,000*	19.45	.5	3.47	.....

The results of measurements with several galvanometers are reported in table 4. Galvanometers with the periods indicated in column 1 were damped with the resistances across the terminals shown in column 2. The average deflection is shown in column 3, whereas column 4 gives the values of the corresponding total oscillations of the galvanometer spot. The diffusion-current constants of column 5 were calculated by using the midpoints of the oscillations as the average current. For the short-period galvanometers, an attempt was made to determine the variation of the galvanometer oscillation with time by observing the time when the galvanometer spot crossed selected points on the scale. The resulting data were plotted, integrated graphically, and the values in column 6 were calculated by using the average currents so obtained.

It is interesting to note that those instruments that had a period several times that of the dropping electrode or were highly damped gave essentially the same values for I when calculated from the midpoints of the galvanometer oscillations.

826086—49——5

The galvanometer of period 1.85 sec was of the enclosed spotlight type with a short scale, so that only small deflections could be observed with a corresponding low precision. The data, however, are conclusive in showing that, except for the highly damped condition, low values are obtained when the midpoints of the oscillations are used to calculate the current. If the wave form of the oscillation is known, however, the integrated current is in satisfactory agreement with that found with galvanometers of relatively long period, and with the true average current found in the studies with the oscillograph.

Diffusion currents can be determined from measurement of the potential drop across a known resistance. This potential varies throughout the life of the drop, and hence an average value is usually measured. The potentiometric balance, using as a criterion the symmetrical oscillations of the galvanometer, is influenced by the characteristics of the indicating instrument. Data illustrating this dependence are given in table 5. The spotlight galvanometer of period 1.85 sec was used and damped as indicated. The diffusion-current constant found for the highly damped experiments was 3.44, which is in excellent agreement with that found for the average current. On the basis of these and other experiments not reported, it may be concluded that the same considerations as found for the direct measurement of current apply to galvanometers used to indicate potentiometric balance.

TABLE 5. *Dependence of the diffusion current measured potentiometrically on the characteristics of the galvanometer*

Damping resistance	Limiting current	Diffusion current	I
Ohm	*μa*	*μa*	
∞	17.0	16.9	2.90
300	17.2	17.1	2.93
100	18.5	18.4	3.16
50	19.2	19.1	3.28
25	19.9	19.8	3.40
10	20.1	20.0	3.43
1	20.2	20.1	3.45

An interesting confirmation of the potentiometric experiments is given by some measurements with the Speedomax potentiometer to record the potential drop across a 200-ohm resistance in series with the cell. The apparatus used required 1 sec to complete a full-scale deflection of 25 cm and had a chart speed of 4 in./min. In the particular experiments a maximum deflection of 24 cm was obtained, and the magnitude of the oscillations was 9 cm. By using the average oscillation for determining the average current, the low value of the diffusion-current constant of 3.32 was obtained. After graphical integration of the potential-time curves, a diffusion-current constant of 3.49 was found, which is in fair agreement with the true average value, considering the precision of the measurement.

Several models of commercial polarographs were used to measure the diffusion current of the cadmium solution used in the experiments with the oscillograph. The current sensitivities of these were determined under the exact conditions of use by measuring the recorded deflection produced by a known current, the latter being determined by measuring the potential drop across a standard resistance. Corrections for residual current were made by both graphical and exact methods. With the Heyrovsky model VIII instrument the value for $I=3.42$ was found, whereas with a Sargent-Heyrovsky model XII polarograph a large number of measurements gave $I=3.43$.

A Sargent model XX instrument was also used for determining diffusion currents. This apparatus is provided with circuit elements to damp electrically the oscillations of the recorder caused by the periodic growth of the drop. The degree of damping may be varied from position 1, undamped except for the natural period of the recorder, to position 5, which introduces the maximum damping. The cadmium solution already described and a solution 3 millimolar in lead in a supporting electrolyte of 1–N hydrochloric acid were studied, and the average of a number of determinations gave the results in table 6. The constants for both solutions are somewhat higher than those found for the other types of apparatus. The circuit constants were such that even with the

TABLE 6. *Diffusion-current constants from measurements with a Sargent model XX polarograph*

Solution	Damping position				
	1	2	3	4	5
Cadmium	3.52	3.48	3.55	3.57	3.57
Lead	4.03	3.93	4.01	4.05	4.05

maximum damping, large oscillations of the recorder were observed. Lingane [14] has reported that this apparatus gives high values for diffusion current under such a condition, which may explain the results found.

Schulman Battey, and Jelatis [15] have described apparatus that incorporates a current rerecorder of low damping. An instrument of this design, now marketed under the trade name, Polaro-analyzer, was loaned to the authors for this work. The Esterline-Angus recorder used gives a full-scale deflection in about 0.5 sec. Although this is too slow to give a faithful record of the current during the early period of formation of a drop, the response is adequate to follow the current in the later stages of drop growth, when using drop times of the order of 3 sec. With the 3-millimolar cadmium solution, the value $I_{max}=4.11$ was found. By using the damping circuit with which the apparatus is equipped, the ratio of the average to the maximum current was found to be 0.82, in satisfactory agreement with the values found when using the oscillograph. It is concluded that the peak current found with this apparatus corresponds to the maximum current within a few percent.

IV. Conclusions

The results of this investigation are conclusive in showing that the Ilkovic equation does not represent the instantaneous current for the dropping-mercury electrode. The deviation is greatest at the start of drop formation but is appreciable at all times. Part of the deviation may be due to an unsymmetrical diffusion field resulting from mechanical screening by the body of the capillary. Density gradients at the surface of the electrode may exert disturbances similar to those observed by Laitinen and Kolthoff for solid spherical electrodes. Experiments are now being planned in which capillaries with substantially the same drop-rate but with different values of m will be studied. These and other investigations may yield valuable information concerning the nature of the deviations.

Although the Ilkovic equation does not represent the instantaneous current, several investigators have shown that it explains, quantitatively, the variation of the diffusion current with concentration of electrolyzable constituent and with the characteristics of the electrode, provided a sufficient concentration of suppresser of maxima is present [8] and electrodes with very small drop times are not used [16]. The conditions governing the quantitative use of diffusion-current constants have been reviewed in a previous paper [17]. To these should be added the precaution to make sure that precise values of either maximum or average current are measured by the apparatus. A preferable procedure is for each worker to determine his own values for the constants to be used. The individual idiosyncrasies of the equipment and personal errors of the observer have the least effect in this manner.

V. References

[1] F. G. Cottrell, Z. physik. Chem. **42,** 385 (1902).
[2] D. MacGillavry and E. K. Rideal, Rec. trav. chim. **56,** 1013 (1937).
[3] H. A. Laitinen and I. M. Kolthoff, J. Am. Chem. Soc. **61,** 3344 (1939).
[4] D. Ilkovic, Coll. Czechoslov. Chem. Commun. **6,** 498 (1934).
[5] I. M. Kolthoff and J. J. Lingane, Polarography, p. 362 (Interscience Pub. Inc., New York, N. Y., 1941).
[6] D. Ilkovic, Coll. Czechoslov. Chem. Commun. **8,** 31 (1936).
[7] J. J. Lingane and I. M. Kolthoff, J. Am. Chem. Soc. **61,** 825 (1939).
[8] F. Buckley and J. K. Taylor, J. Research NBS **34,** 97 (1945) RP1631.
[9] G. R. Mezger, Electronics **17,** 126, 254 (1944).
[10] J. J. Lingane and B. A. Loveridge, J. Am. Chem. Soc. **66,** 1425 (1944).
[11] J. J. Lingane, Ind. Eng. Chem., Anal. Ed. **15,** 583 (1943).
[12] J. Heyrovsky, Polarographie, p. 55 (Springer, Vienna, 1941).
[13] I. M. Kolthoff and J. J. Lingane, Polarography, p. 108 (Interscience Pub. Inc., New York, N. Y., 1941).
[14] J. J. Lingane, Ind. Eng. Chem., Anal. Ed. **18,** 734 (1946).
[15] J. H. Schulman, H. B. Battey, and D. G. Jelatis, Rev. Sci. Instr. **18,** 226 (1947).
[16] J. J. Lingane and B. A. Loveridge, J. Am. Chem. Soc. **68,** 395 (1946).
[17] J. K. Taylor, Anal. Chem. **19,** 368 (1947).

Washington, December 10, 1948.

U. S. Department of Commerce
National Bureau of Standards

Research Paper RP1979
Volume 42, April 1949

Part of the Journal of Research of the National Bureau of Standards

Stress Distribution Near Reinforced Circular Hole Loaded by Pin[1]

By Samuel Levy and Frank C. Smith

This paper presents a theoretical analysis for the stress distribution in a flat plate near a reinforced circular hole loaded by a pin, and a comparison of the theory with test results for a plate of sandwich construction. It is assumed that an auxiliary reinforcement at the edge of the hole is so rigid that no distortion of the shape of the hole occurs due to the load. The plate is reinforced in the vicinity of the hole by circular "doubler" plates. The theory and experiment are found to be in good agreement.

I. Introduction

This paper presents a theoretical analysis for the stress distribution in a flat plate near a reinforced circular hole loaded by a pin, as shown in figure 1, and a comparison of the theory with test results for a plate of sandwich construction. It is assumed that an auxiliary reinforcement at the edge of the hole is so rigid that no distortion of the shape of the hole occurs due to the load. The plate is reinforced in the vicinity of the hole by circular "doubler" plates, which increase the thickness by a factor β. The analysis proceeds from the assumption that the reinforced sheet is in a condition of plane stress. This requires the reinforcement to be symmetrical on both sides of the sheet to eliminate bending stresses, and it requires the thickness to be small compared to the other dimensions so that the stress can be considered constant across the thickness. The stress cannot be assumed constant for points a distance less than one thickness from the boundary between doubler plate and sheet.

Previous work on the problem of a plate with a circular hole loaded by a pin includes a photoelastic investigation by Coker and an empirical analysis by Bickley [1].[2] These investigations were confined to unreinforced holes.

Closely allied with the problem of the stress distribution in a flat plate near a reinforced circular hole loaded by a pin is that of an unloaded reinforced circular hole in a plate under stress. This problem has been solved approximately by Timoshenko [2], who treated the reinforcement as a curved beam of constant section. Other solutions of the unloaded hole problem based on the plane stress theory were obtained by Sezawa and Kubo [3], by Gurney [4], and by Beskin [5].

Another related problem is that of the stress distribution in a flat plate containing an elliptical region filled with material having a greater stiffness than the material in the rest of the plate. A solution to this problem was obtained by Donnell [6] by using a method that is a generalization of Inglis' solution for the elliptical hole.

In the present paper, use is made of the general plane stress solution in polar coordinates. The solution given is approximate in that it does not give zero stress on the free boundaries of the plate. However, there is reason to believe that for plates with moderately small holes, e. g., plates in which the hole reduces the section of the plate 15 percent or less, this solution gives a good approximation of the stress distribution, particularly in the neighborhood of the hole.

It was decided to check the theory by comparing computed strains with values measured in tests on a specimen of Metalite sandwich construction under concentrated load acting in the plane of the

[1] Presented before Seventh International Congress for Applied Mechanics, London, Sept. 1948.

[2] Figures in brackets indicate the literature references at the end of this paper.

plate. It was hoped that the comparison would indicate that reinforcements in this type of construction could be designed rationally on the basis of the plane stress theory.

II. Boundary Conditions

The analysis proceeds in two steps. First, a solution is obtained for the stresses and displacements in a circular ring of constant thickness and any inner and outer diameters. Then the solution for the reinforced specimen is obtained by considering the reinforced parts as one such ring and the rest of the sheet as another. Symbols having the subscript "2" correspond to the reinforced sheet, whereas symbols having the subscript "1" correspond to the unreinforced sheet. Symbols without a subscript are general and apply to any ring of constant thickness.

The origin of coordinates, figure 1, is taken at the center of the hole with x, y as rectangular

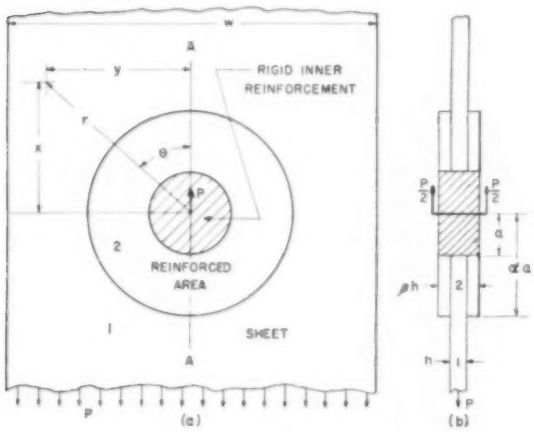

FIGURE 1. *Problem to be analyzed, (a) plan view of plate, (b) section at A–A.*

coordinates for points in the sheet and r,θ as polar coordinates. The positive direction of x will be taken in the direction of the applied load at the hole. The relations between the coordinates are,

$$\left.\begin{aligned} x &= r\cos\theta \\ y &= r\sin\theta \\ r &= \sqrt{x^2+y^2} \\ \theta &= \tan^{-1} y/x \end{aligned}\right\} \tag{1}$$

Normal and shearing stresses are denoted by the conventional symbols σ and τ. Radial displacements are denoted by u_r and circumferential displacements by v_θ.

Since the edge of the hole is assumed not to deform, the boundary conditions for displacements at the inner edge of the reinforcement can be taken as,

$$\left.\begin{aligned} u_{r2} &= 0, \quad r=a \\ v_{\theta 2} &= 0, \quad r=a \end{aligned}\right\} \tag{2}$$

and for forces,

$$\left.\begin{aligned} \beta h\int_0^{2\pi} [\sigma_{r2}\cos\theta - \tau_{r\theta 2}\sin\theta]_{(r=a)} a\,d\theta &= -P \\ \beta h\int_0^{2\pi} [\sigma_{r2}\sin\theta + \tau_{r\theta 2}\cos\theta]_{(r=a)} a\,d\theta &= 0. \end{aligned}\right\} \tag{3}$$

At the junction between the reinforced and unreinforced sheet, it is necessary that the displacements be the same for both the reinforced and unreinforced sheet, or,

$$\left.\begin{aligned} u_{r1} &= u_{r2}; \quad r=\alpha a \\ v_{\theta 1} &= v_{\theta 2}; \quad r=\alpha a, \end{aligned}\right\} \tag{4}$$

It is also necessary that, at the junction between the reinforced and the unreinforced sheet, the normal and shearing forces be the same, or

$$\left.\begin{aligned} \beta\sigma_{r2} &= \sigma_{r1}; \quad r=\alpha a \\ \beta\tau_{r\theta 2} &= \tau_{r\theta 1}; \quad r=\alpha a \end{aligned}\right\}. \tag{5}$$

The solution of the actual problem, figure 2, a, is the superposition of the solutions for the two subproblems, figure 2, b, and 2, c. For the problem in figure 2, b, the stresses at $r=a$ must satisfy eq 3, and far from the hole, the stresses must remain finite, i. e.;

$$\sigma_{r1},\ \sigma_{\theta 1},\ \text{and}\ \tau_{r\theta 1}\ \text{finite};\ r\to\infty. \tag{6}$$

For the problem in figure 2, c, the stresses at $r=a$ must satisfy the condition that the resultant load on the hole is zero

$$\left.\begin{aligned} \int_0^{2\pi} [\sigma_{r2}\cos\theta - \tau_{r\theta 2}\sin\theta]_{(r=a)} d\theta &= 0 \\ \int_0^{2\pi} [\sigma_{r2}\sin\theta + \tau_{r\theta 2}\cos\theta]_{(r=a)} d\theta &= 0 \end{aligned}\right\};\ r=a \tag{7}$$

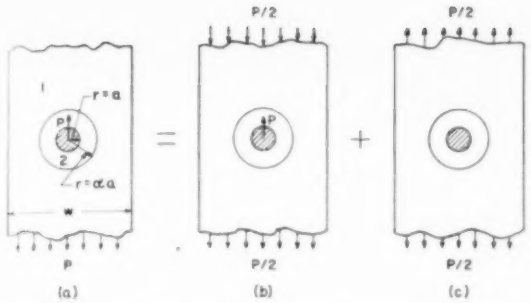

FIGURE 2. *Solution for the actual problem (a) by the superposition of the solutions for the subproblems (b) and (c).*

and that, far from the hole, the stress is a uniform tension in the x-direction of magnitude $P/2wh$, where w is the width of the specimen:

$$\left.\begin{aligned} \sigma_{r1} &= (P/2wh)\cos^2\theta \\ \sigma_{\theta 1} &= (P/2wh)\sin^2\theta \\ \tau_{r\theta 1} &= -(P/4wh)\sin^2\theta \end{aligned}\right\} ;\ r\to\infty, \tag{8}$$

For both the problem in figure 2, b, and the problem in figure 2, c, the stresses on the free longitudinal edges of the plate should be zero. Auxiliary stress functions of the type used by Howland [7] might be used to satisfy this boundary condition. This is not done, however, since for moderately small values of the ratio a/w of hole radius to plate width, the stress functions to be used reduce the unbalanced stresses on the free edges to a negligible amount.

III. Solution for Problem in Figure 2, b

By using the second line of the general stress function eq 77 [8, p. 114],

$$\phi = \frac{1-\nu}{4\pi} Mr\,(\log r)\cos\theta - \frac{Mr}{2\pi}\theta\sin\theta + \frac{T}{4\pi r}\cos\theta + \frac{Rr^3}{4\pi}\cos\theta \tag{9}$$

where

ν = Poisson's ratio,
M, T, R = arbitrary constants to be determined from boundary conditions,

it may be shown from eq 34 [8, p. 53] that the equations of equilibrium and of compatibility for the stresses in a ring of constant thickness are satisfied by

$$\left.\begin{aligned} \sigma_r &= -\frac{3+\nu}{4\pi}\frac{M\cos\theta}{r} - \frac{1}{2\pi}\frac{T\cos\theta}{r^3} + \frac{1}{2\pi}Rr\cos\theta \\ \sigma_\theta &= \frac{1-\nu}{4\pi}\frac{M\cos\theta}{r} + \frac{1}{2\pi}\frac{T\cos\theta}{r^3} + \frac{3}{2\pi}Rr\cos\theta \\ \tau_{r\theta} &= \frac{1-\nu}{4\pi}\frac{M\sin\theta}{r} - \frac{1}{2\pi}\frac{T\sin\theta}{r^3} + \frac{1}{2\pi}Rr\sin\theta \end{aligned}\right\} \tag{10}$$

By using the relations between strains and stresses given on pages 62 and 63 of [8], it may be shown that the corresponding displacements are

$$\left.\begin{aligned} u_r &= \frac{M}{4\pi E}(\nu^2-2\nu-3)(\cos\theta)\log r + \frac{T}{4\pi Er^2}(1+\nu)\cos\theta \\ &\quad + \frac{Rr^2}{4\pi E}(1-3\nu)\cos\theta + \frac{N}{4\pi E}\cos\theta \\ v_\theta &= \frac{M}{4\pi E}(1+2\nu+\nu^2)\sin\theta - \\ &\quad \frac{M}{4\pi E}(\nu^2-2\nu-3)(\sin\theta)\log r \\ &\quad + \frac{T}{4\pi Er^2}(1+\nu)\sin\theta + \frac{Rr^2}{4\pi E}(5+\nu)\sin\theta - \\ &\quad \frac{N}{4\pi E}\sin\theta \end{aligned}\right\} \tag{11}$$

where

E = Young's modulus,
N = integration constant to be determined from boundary conditions.

Applying the boundary conditions, eq 2, to eq 11 gives

$$M_2(\nu^2-2\nu-3)\log a + N_2 + \frac{T_2}{a^2}(1+\nu) + R_2a^2(1-3\nu) = 0 \tag{12}$$

and,

$$M_2(1+2\nu+\nu^2) + M_2(3+2\nu-\nu^2)\log a - N_2 + \frac{T_2}{a^2}(1+\nu) + R_2a^2(5+\nu) = 0 \tag{13}$$

Applying eq 3 to eq 10 gives

$$M_2 = P/\beta h. \tag{14}$$

Applying eq 4 to eq 11 gives

$$\left.\begin{aligned} M_2(\nu^2-2\nu-3)\log a a+N_2+\frac{T_2}{\alpha^2a^2}(1+\nu)+\\ R_2\alpha^2a^2(1-3\nu)=\\ M_1(\nu^2-2\nu-3)\log a a+N_1+\frac{T_1}{\alpha^2a^2}(1+\nu)+\\ R_1\alpha^2a^2(1-3\nu), \end{aligned}\right\} \quad (15)$$

and

$$\left.\begin{aligned} M_2(1+2\nu+\nu^2)+M_2(3+2\nu-\nu^2)\log\ \alpha a-N_2+\\ \frac{T_2}{\alpha^2a^2}(1+\nu)+R_2\alpha^2a^2(5+\nu)=\\ M_1(1+2\nu+\nu^2)+M_1(3+2\nu-\nu^2)\log\ \alpha a-N_1+\\ \frac{T_1}{\alpha^2a^2}(1+\nu)+R_1\alpha^2a^2(5+\nu). \end{aligned}\right\} (16)$$

Applying eq 5 to eq 10 gives

$$\beta[-(3+\nu)M_2-\frac{2}{\alpha^2a^2}T_2+2R_2\alpha^2a^2]=$$

$$-(3+\nu)M_1-\frac{2}{\alpha^2a^2}T_1+2R_1\alpha^2a^2, \quad (17)$$

and,

$$\beta[(1-\nu)M_2-\frac{2}{\alpha^2a^2}T_2+2R_2\alpha^2a^2]=$$

$$(1-\nu)M_1-\frac{2}{\alpha^2a^2}T_1+2R_1\alpha^2a^2. \quad (18)$$

Applying eq 6 to eq 10 gives

$$R_1=0 \quad (19)$$

Equations 12 to 19 may be solved for the eight constants M_2, N_2, T_2, R_2, M_1, N_1, T_1, and R_1.

IV. Solution for Problem in Figure 2, c

Reference [4] shows that the equations of equilibrium and compatibility in a ring of constant thickness are satisfied by the stresses

$$\left.\begin{aligned} \sigma_r&=F+Ka^2/r^2+(-A-3Ca^4/r^4-2Da^2/r^2)\cos 2\theta\\ \sigma_\theta&=F-Ka^2/r^2+(A+6Br^2/a^2+3Ca^4/r^4)\cos 2\theta\\ \tau_{r\theta}&=(A+3Br^2/a^2-3Ca^4/r^4-Da^2/r^2)\sin 2\theta, \end{aligned}\right\} (20)$$

where F, K, A, B, C, D, are constants to be determined from the boundary conditions. It also shows that the corresponding displacements are

$$\left.\begin{aligned} u_r&=(r/E)\{F(1-\nu)-K(1+\nu)a^2/r^2+[-A(1+\nu)\\ &\quad -2\nu Br^2/a^2+C(1+\nu)a^4/r^4+2Da^2/r^2]\cos 2\theta\}\\ v_\theta&=(r/E)[A(1+\nu)+B(3+\nu)r^2/a^2+C(1+\nu)a^4/r^4\\ &\quad -D(1-\nu)a^2/r^2]\sin 2\theta. \end{aligned}\right\} (21)$$

Applying the boundary conditions of eq 2 to eq 21 gives

$$(1-\nu)F_2=(1+\nu)K_2 \quad (22)$$

$$(1+\nu)A_2=-2\nu B_2+(1+\nu)C_2+2D_2 \quad (23)$$

$$(1+\nu)A_2=-(3+\nu)B_2-(1+\nu)C_2+(1-\nu)D_2 \quad (24)$$

Applying eq 4 to eq 21 gives

$$(1-\nu)\alpha^2F_2-(1+\nu)K_2=(1-\nu)\alpha^2F_1-(1+\nu)K_1, \quad (25)$$

$$-(1+\nu)\alpha^4A_2-2\nu\alpha^6B_2+(1+\nu)C_2+2\alpha^2D_2=$$

$$-(1+\nu)\alpha^4A_1-2\nu\alpha^6B_1+(1+\nu)C_1+2\alpha^2D_1, \quad (26)$$

$$(1+\nu)\alpha^4A_2+(3+\nu)\alpha^6B_2+(1+\nu)C_2-(1-\nu)\alpha^2D_2=$$

$$(1+\nu)\alpha^4A_1+(3+\nu)\alpha^6B_1+(1+\nu)C_1-(1-\nu)\alpha^2D_1. \quad (27)$$

Applying eq 5 to eq 20 gives

$$\beta\alpha^2F_2+\beta K_2=\alpha^2F_1+K_1, \quad (28)$$

$$\beta\alpha^4A_2+3\beta C_2+2\beta\alpha^2D_2=\alpha^4A_1+3C_1+2\alpha^2D_1, \quad (29)$$

$$\beta\alpha^4A_2+3\beta\alpha^6B_2-3\beta C_2-\beta\alpha^2D_2=$$
$$\alpha^4A_1+3\alpha^6B_1-3C_1-\alpha^2D_1 \quad (30)$$

Applying eq 8 to eq 20 gives

$$F_1=P/4wh, \quad (31)$$

$$A_1=-P/4wh, \quad (32)$$

$$B_1=0. \quad (33)$$

V. Solution for Problem in Figure 2, a

Combining eq 10 and 20, we obtain, for the stresses in a ring of constant thickness,

$$\left.\begin{aligned} \sigma_r&=F+Ka^2/r^2+\\ &\quad[-(3+\nu)M/4\pi r-T/2\pi r^3-Rr/2\pi]\cos\theta+\\ &\quad[-A-3Ca^4/r^4-2Da^2/r^2]\cos 2\theta,\\ \sigma_r&=F-Ka^2/r^2+\\ &\quad[(1-\nu)M/4\pi r+T/2\pi r^3+3Rr/2\pi]\cos\theta+\\ &\quad[A+6Br^2/a^2+3Ca^4/r^4]\cos 2\theta,\\ \tau_{r\theta}&=[(1-\nu)M/4\pi r-T/2\pi r^3+Rr/2\pi]\sin\theta+\\ &\quad[A+3Br^2/a^2-3Ca^4/r^4-Da^2/r^2]\sin 2\theta. \end{aligned}\right\} (34)$$

The values of the arbitrary constants, A, B, C, D, K, M, R, T for the sheet 1 and the reinforcement 2 can be determined as follows: M_2, R_1, F_1, A_1, B_1: From eq 14, 19, 31, 32, and 33

$$\left.\begin{aligned} M_2&=P/\beta h\\ R_1&=0\\ F_1&=P/4wh\\ A_1&=-P/4wh\\ B_1&=0 \end{aligned}\right\} \tag{35}$$

M_1: By combining eq 14, 17 and 18:

$$M_1=P/h. \tag{36}$$

T_1, T_2, R_2: By combining eq 12, 13, 15, 16, and 17, and making use of eq 35 and 36, three simultaneous equations are obtained:

$$\left.\begin{aligned} &2(1+\nu)T_2+2(3-\nu)a^4R_2=-(1+\nu)^2a^2P/\beta h\\ &2(1+\nu)T_2+2(3-\nu)\alpha^4a^4R_2-2(1+\nu)T_1=\\ &\quad(1+\nu)^2\alpha^2a^2(\beta-1)P/\beta h\\ &-2\beta T_2+2\beta\alpha^4a^4R_2+2T_1=0. \end{aligned}\right\} \tag{37}$$

K_1, F_2, K_2: By combining eq 22, 25, and 28 and making use of eq 35

$$\left.\begin{aligned} &(1-\nu)F_2-(1+\nu)K_2=0\\ &(1-\nu)\alpha^2F_2-(1+\nu)K_2+(1+\nu)K_1=(1-\nu)\alpha^2P/4wh\\ &\beta\alpha^2F_2+\beta K_2-K_1=\alpha^2P/4wh. \end{aligned}\right\} \tag{38}$$

C_1, D_1, A_2, B_2, C_2, D_2: From eq 23, 24, 26, 27, 29, and 30, and making use of eq 35,

$$\left.\begin{aligned} &(1+\nu)A_2+2\nu B_2-(1+\nu)C_2-2D_2=0\\ &(1+\nu)A_2+(3+\nu)B_2+(1+\nu)C_2-(1-\nu)D_2=0\\ &-(1+\nu)\alpha^4A_2-2\nu\alpha^6B_2+(1+\nu)C_2+2\alpha^2D_2-\\ &\quad(1+\nu)C_1-2\alpha^2D_1=(1+\nu)\alpha^4P/4wh\\ &(1+\nu)\alpha^4A_2+(3+\nu)\alpha^6B_2+(1+\nu)C_2-\\ &\quad(1-\nu)\alpha^2D_2-(1+\nu)C_1+(1-\nu)\alpha^2D_1=\\ &-(1+\nu)\alpha^4P/4wh\\ &\beta\alpha^4A_2+3\beta C_2+2\beta\alpha^2D_2-3C_1-2\alpha^2D_1=-\alpha^4P/4wh\\ &\beta\alpha^4A_2+3\beta\alpha^6B_2-3\beta C_2-\beta\alpha^2D_2+3C_1+\\ &\quad\alpha^2D_1=-\alpha^4P/4wh \end{aligned}\right\} \tag{39}$$

Combining eq 11 and 21, we obtain for the displacements in a ring of constant thickness,

$$\left.\begin{aligned} u_r&=(r/E)[F(1-\nu)-K(1+\nu)a^2/r^2]+\\ &\quad[(\cos\theta)/4\pi E][M(\nu^2-2\nu-3)\log r+\\ &\quad T(1+\nu)/r^2+Rr^2(1-3\nu)+N]+\\ &\quad[(r\cos 2\theta)/E][-A(1+\nu)-2\nu Br^2/a^2+\\ &\quad C(1+\nu)a^4/r^4+2Da^2/r^2]\\ v_\theta&=[(\sin\theta)/4\pi E][M(1+\nu)^2+M(3+2\nu-\nu^2)\log r+\\ &\quad T(1+\nu)/r^2+Rr^2(5+\nu)-N]+\\ &\quad[(r\sin 2\theta)/E][A(1+\nu)+B(3+\nu)r^2/a^2+\\ &\quad C(1+\nu)a^4/r^4-D(1-\nu)a^2/r^2] \end{aligned}\right\} \tag{40}$$

The additional arbitrary constants, N_1, N_2, are obtained by combining eq 12, 13, 15, and 16 with eq 35 giving:

$$\left.\begin{aligned} N_1&=-2(1+\nu)(\alpha^2-1)a^2R_2+[(1+\nu)\beta+\\ &\quad 2\beta(3-\nu)\log\alpha a-2(3-\nu)\log\alpha]\\ &\quad(1+\nu)P/2\beta h\\ N_2&=2(1+\nu)a^2R_2+[1+\nu+2(3-\nu)\log a]\\ &\quad(1+\nu)P/2\beta h \end{aligned}\right\} \tag{41}$$

VI. Comparison of Analysis With Experiment

The specimen, figures 3 and 4, was furnished for these tests by Chance-Vought Aircraft, Dallas, Texas It was of Metalite construction, consisting of two sheets of 0.013-in. 24S–T81 Alclad aluminum alloy bonded to a 0.5-in core of balsa wood, which had been cut with the grain normal to the sheet. The edges of the specimen were reinforced by pairs of $\frac{3}{8}$- by $\frac{3}{4}$- by $\frac{1}{8}$-in. 24S–T aluminum alloy angles bonded to the sheet.

The concentrated load was applied by a steel pin, of 1.25-in. diameter, making a snug, but turning, fit in a hole reamed in a steel bushing. The Metalite was reinforced to a radius of 5 in. from the center of the loading pin. A detail of the reinforcement is shown at section A–A, figure 3. The reinforcement to a radius of 2.5 in. was considered heavy enough to prevent distortion inside this circle.

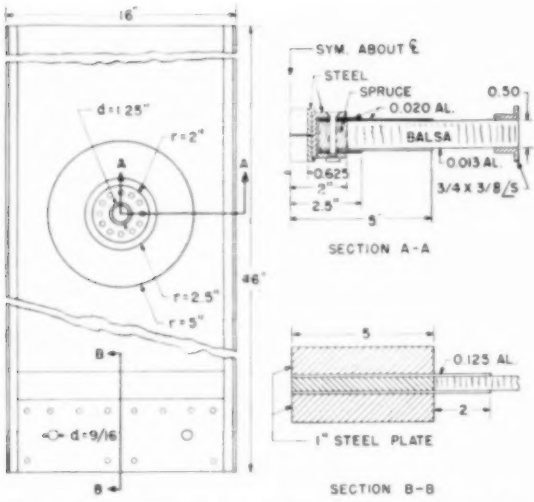

FIGURE 3. *Specimen tested, showing reinforcement near hole*

The following constants were taken from the specimen and were used in the analysis of the experiment:

$$a=2.5 \text{ in.}$$

$$\alpha a=5 \text{ in.}$$

$$h=0.026 \text{ in.}$$

$$\beta h=0.066 \text{ in.}$$

$$\nu=0.3.$$

The effective width, w, of the panel was obtained by dividing the gross cross section of the panel, including edge angles, by the sheet thickness, with the result

$$w=31.56 \text{ in.}$$

The arbitrary constants were determined by solving the simultaneous equations in section V, with the result:

$$A_1=-0.3049P \qquad A_2=-0.1295P$$

$$B_1=0 \qquad B_2=-0.001977P$$

$$C_1=1.194P \qquad C_2=0.06584P$$

$$D_1=-0.7572P \qquad D_2=-0.1275P$$

$$F_1=0.3049P \qquad F_2=0.1425P$$

$$K_1=0.426P \qquad K_2=0.0768P$$

$$M_1=38.46P \qquad M_2=15.15P$$

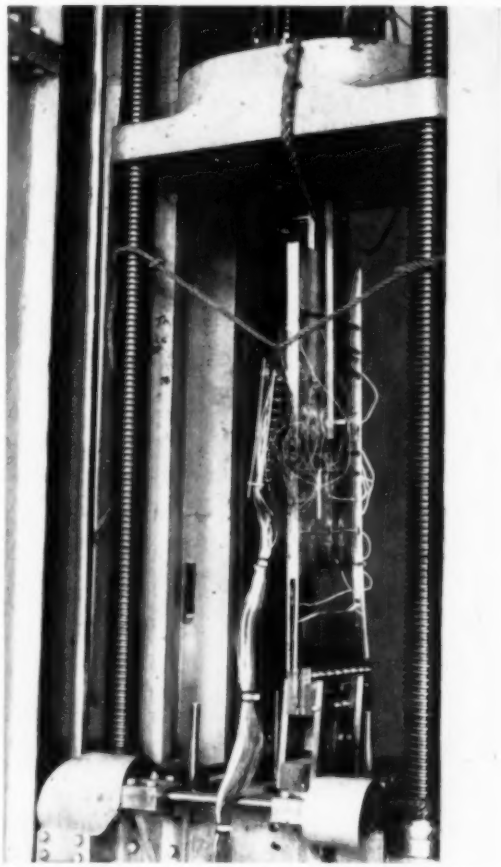

FIGURE 4. *Specimen in testing machine after failure.*

$$N_1=208.0P \qquad N_2=63.01P$$

$$R_1=0 \qquad R_2=0.09215P$$

$$T_1=-321.7P \qquad T_2=-69.04P$$

The stress in the unreinforced region 1 ($r>5$) was computed by substituting the constants with subscript 1 into eq 34; whereas the stress in the reinforced region 2 ($2.5<r<5$) was similarly computed using constants with subscript 2.

The radial and circumferential strains were computed from the stresses by the well-known formulas

$$\left.\begin{aligned}\epsilon_r&=\frac{1}{E}(\sigma_r-\nu\sigma_\theta)\\ \epsilon_\theta&=\frac{1}{E}(\sigma_\theta-\nu\sigma_r)\end{aligned}\right\} \tag{42}$$

taking

$E = 10.6 \times 10^6$ lb/in.^{2}

$\nu = 0.3$

Figure 5 shows the measured strains at a load of 10,000 lb, and figure 6 shows a comparison between measured and computed longitudinal strains for the longitudinal and transverse centerlines and for a transverse section 12 in. below the center of the hole. The computed maximum strain, just outside the reinforcement, differed only about 2 percent from the measured strain. Larger differences were found elsewhere. The agreement is as good as could be expected in view of the assump-

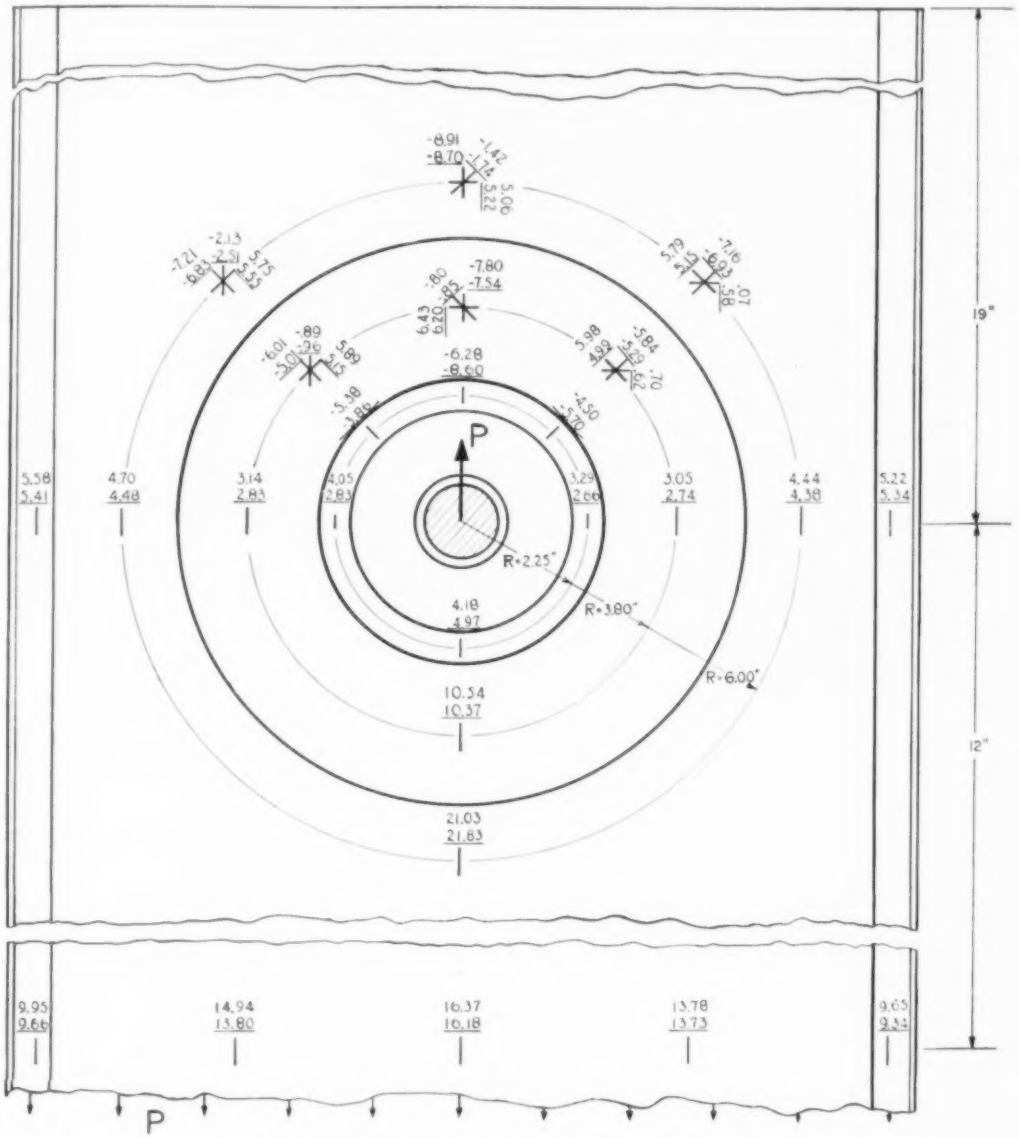

FIGURE 5. *Strain distribution at load of 10,000 lb (strains $\times 10^6$).*

Underlined strain values are based on measurements on front of specimen; other strain measured on back of specimen.

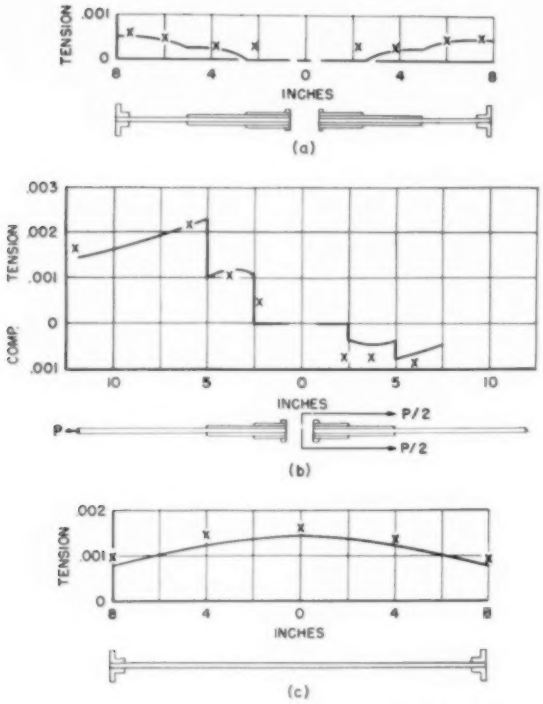

FIGURE 6. *Average longitudinal strain at 10,000-lb load.*

X, Measured; calculated. (a) Transverse center line; (b) longitudinal center line; (c) transverse line 12 in. below center of hole.

tions of the theory that a state of plane stress existed, that the central area was rigid, and that the hole and reinforcement were small compared to the width of the specimen.

VII. Conclusions

It is concluded that:

1. The plane stress theory may be used to compute the stress distribution in the neighborhood of a reinforced circular hole loaded by a pin in a plate of sandwich construction, in which practically all the load is carried by sheets of metal bonded to each other or to a light-weight core and in which a relatively rigid central reinforcement is used.

2. For large values of the ratio of plate width to hole diameter and with a nearly rigid central reinforcement for applying the load, the solution can be expected to be accurate in all parts of the plate.

3. For moderate values of plate width, the results for the stresses are not of very satisfactory accuracy near the free edges of the plate, but are reliable in the neighborhood of the hole near the places of largest stress.

4. The presence of the reinforcement is likely to move the point of highest stress from the edge of the hole to a point in the plate just outside the reinforcement.

Acknowledgment is made to the Bureau of Aeronautics, Navy Department, whose research projects on reinforcement of holes have provided the impetus and the necessary financial support for the work reported in this paper. The authors take this opportunity to acknowledge also the assistance of members of the Engineering Mechanics Section of the National Bureau of Standards, particularly Albert E. McPherson and Wilhelmina D. Kroll.

VIII. References

[1] E. G. Coker and L. N. G. Filon, Photo-elasticity, p. 524 to 530 (Cambridge Univ. Press, London, 1931).

[2] S. Timoshenko, Strength of materials, part II, p. 457 (D. Van Nostrand Co., Inc., New York, N. Y., 1930).

[3] K. Sezawa and K. Kubo, Stresses in a plate with a flanged circular hole, Rept. Aero. Res. Inst. Tokyo Imp. Univ., No. 84 (1932).

[4] C. Gurney, An analysis of the stresses in a flat plate with reinforced circular hole under edge forces, Brit. Res. Memo. No. 1834 (1938).

[5] L. Beskin, Strengthening of circular holes in plates under edge loads, J. Appl. Mech., p. A-140 (Sept. 1944).

[6] L. H. Donnell, Stress concentrations due to elliptical discontinuities in plates under edge forces (Th. v. Karman Anniversary Volume, Calif. Inst. Tech., 1941).

[7] R. C. J. Howland, Phil. Trans. Roy. Soc. London [A] **229,** 49 (1930).

[8] S. Timoshenko, Theory of elasticity (McGraw-Hill Book Co., Inc., New York, N. Y., 1934).

WASHINGTON, June 3, 1948.

U. S. Department of Commerce
National Bureau of Standards

Research Paper RP1980
Volume 42, April 1949

Part of the Journal of Research of the National Bureau of Standards

Volumetric Determination of Columbium

By Howard B. Knowles and G. E. F. Lundell

The quantitative determination of columbium based on reduction by amalgamated zinc and reoxidation with potassium permanganate has, in general, produced results that lack both accuracy and precision. A study of the various factors involved indicates that essential conditions require adequate duration of reduction in the presence of an excess of zinc and a proper concentration of both acid and columbium. A procedure is described whereby columbium, in a sulfuric acid solution, is quantitatively reduced by amalgamated zinc to the trivalent form and subsequently oxidized to the quinquevalent state.

I. Introduction

A method for the quantitative determination of columbium, depending on the reduction in acid solutions of quinquevalent columbium to the trivalent state by zinc, and subsequent titration with a standard solution of a suitable oxidant, has been the object of numerous investigations extending over a period of years. In brief, the procedures attempted have involved the treatment of a hydrochloric, a sulfuric, or a hydrofluoric acid solution of the columbium with zinc, usually amalgamated, and subsequent oxidation of the carefully protected solution directly, or indirectly through use of a ferric salt, with potassium permanganate. With but a single exception [1][1] no reliable procedure based on the foregoing principle has been established that permits the use of stoichiometric values. A critical study of the procedures advocated by earlier investigators [2], in conjunction with the results obtained, is of little aid in indicating the underlying reason or cause for failure to obtain a quantitative reduction of this element. The use of material of unknown purity, imperfect procedures, doubtful conclusions, and other factors such as inadequate data, have all served separately or collectively to retard the solution of a rather difficult problem.

The present article concerns only the question of consistently obtaining complete and uniform reduction of the columbium, such as would permit its use for quantitative determinations, and embodies results that have been obtained in an intermittent study of various related factors.

[1] Figures in brackets indicate the literature references at the end of this paper.

II. Experimental Details

1. Amalgamation of Zinc

A study of the reducing action of amalgamated zinc [3] indicates that for a number of elements it is requisite that the zinc be but lightly coated with mercury. Satisfactory amalgamation is accomplished as follows: Transfer 1,000 g of 20-mesh zinc metal (low in iron) to a stout, wide-mouthed glass bottle, add 500 ml of a 2-percent aqueous solution of mercuric chloride, mix continuously for 45 to 60 sec, discard the solution, and wash five times with distilled water. Treat the washed amalgamated zinc with 500 ml of warm, diluted sulfuric acid (1+99)[2], mix, discard the acid, and wash thoroughly with distilled water. The prepared amalgam is preferably preserved in water to which a few drops of hydrochloric acid have been added. The period of use of an amalgam thus prepared is limited. With continued use it eventually loses its efficiency and can no longer be used for this purpose.

2. Sources of Columbium

The two samples of columbium oxide used in the investigation were laboratory preparations. One was an oxide on which three different analysts

[2] Unless otherwise specified, concentrated reagents are meant.

obtained 96.45, 96.53, and 96.42 percent of Cb_2O_5 by the tannin method [5]. A preferred average value of 96.43 percent for this sample would, for the purpose of reduction, be increased to an apparent 97.10 percent by the presence of 0.32 percent of TiO_2, 0.40 percent of Fe_2O_3, and 0.08 percent of Cr_2O_3. A second sample of oxide was prepared from a specimen of columbium metal, spectroscopically free from titanium and tantalum. This specimen, however, contained traces of iron, copper, and tin, which were removed before preparation of the final Cb_2O_5. This sample was used on the basis of 100.00-percent purity.

3. Permissible Acidity

A study of the acid concentration necessary for the quantitative reduction of columbium indicates that the solution should contain preferably 20 percent by volume but never less than 15 percent by volume of sulfuric acid. With the latter concentration, there is a general tendency to slightly low but still satisfactory values. Under these conditions the reduced solution is clear and possesses an "amethyst-like" color. At lower concentrations of acid the reduced solution exhibits a dark (blackish) color and yields low values on titration.

The presence of small amounts of succinic acid, introduced as an aid to prevent hydrolysis, if not beneficial at least exerts no harmful influence.

4. Concentration of Columbium Solution and Duration of Reduction

Experiments indicate that essential factors for satisfactory reduction involve the time of contact of the solution with the amalgam, the amount of and concentration of the columbium to be reduced, and the amount of available zinc. The last, in turn, is a function of both the active area of the amalgam and the degree of amalgamation. In this study the time for the passage of *all* solutions through the reductor, unless otherwise noted, was not less than 25 min. No study was made of the rate of reduction, a factor conditioned by other variables; but where only a few milligrams of columbium is involved, satisfactory reductions can undoubtedly be effected in less time. Two Jones' reductors of the conventional type containing columns of amalgamated zinc slightly less than 1 inch in diameter were used. One column was 18 in. in length and the other 33 in.

Definite limitations regarding the maximum concentrations for use with these or similar reductors are difficult to define because the solution, when introduced into the reductor, undergoes dilution and, due to nonuniform mixing, lacks homogeneity. Although concentrations of as high as 1.7 mg of Cb_2O_5/ml have been reduced quantitatively at times with the long reductor, a study of all experiments indicates a concentration not greatly exceeding 1.0 mg/ml to be desirable. Similarly, the concentration for use with the short reductor should not exceed 0.7 to 0.8 mg/ml.

5. Temperature During Reduction

Although heat is not essential to quantitative reduction [4], all reductions were conducted at a temperature of 65°±5° C. This temperature facilitates the diffusion of zinc through the amalgam [3], and effects more vigorous action during passage of the solution through the reductor.

6. Results

The results of experiments obtained with two reductors under varying concentrations of acid and columbium are given in the following tables.

TABLE 1. *Reductions effected in reductor with 33-in. column of zinc*

Experiment Number	Cb_2O_5 taken	Error	Composition of Cb_2O_5 solution
	g	*g*	
1	0.1048	+0.0005	200-ml volume containing 30 ml of H_2SO_4, 2 g of succinic acid, and 1 ml of H_2O_2 (30 percent).
2	.1548	+.0005	
3	.1993	−.0003	
4	.2053	−.0001	
5	.2503	−.0002	
6	.2527	−.0016	
7	.2535	+.0004	
8	.3025	−.0002	
9	.3418	−.0004	
10	.3516	−.0008	
11	.3513	−.0017	
12	.3418	−.0127	
13	.0596	+.0002	200-ml volume containing 40 ml of H_2SO_4, 2 g of succinic acid, and 1 ml of H_2O_2 (30 percent).
14	.1017	+.0007	
15	.1511	+.0004	
16	.2062	+.0007	
17	.2502	+.0001	
18	.2535	+.0005	
19	.3021	+.0002	
20	.3405	+.0002	
21	.3505	−.0013	
22	.3512	−.0002	400 ml volume containing 60 ml of H_2SO_4, 3 g of succinic acid, and 2 ml of H_2O_2 (30 percent).
23	.3519	−.0002	

TABLE 2. *Reductions effected in reductor with 18-in. column of zinc*

Experiment number	Cb_2O_5 taken	Error	Composition of Cb_2O_5 solution	Remarks
	g	*g*		
1	0.0502	+0.0005		
2	.0971	−.0004	200-ml volume containing 30 ml of H_2SO_4, 2 g of succinic acid, and 1 ml H_2O_2 (30 percent)	0.1020 g of TiO_2 present during reduction in experiment 6.
3	.0971	−.0002		
4	.0991	−.0003		
5	.1017	+.0001		
6	.1006	−.0024		
7	.1973	−.0018		
8	.1978	−.0041		
9	.0495	.0000	200-ml volume containing 40 ml of H_2SO_4, 2 g of succinic acid, and 1 ml of H_2O_2 (30 percent)	Reduction effected at 25° C in experiment 12. Freshly amalgamated zinc used in experiments 20 and 21.
10	.0971	+.0006		
11	.0971	+.0005		
12	.0973	−.0006		
13	.0976	+.0004		
14	.0979	+.0006		
15	.1005	+.0005		
16	.1005	+.0003		
17	.1006	+.0005		
18	.1030	+.0005		
19	.1519	+.0004		
20	.1958	+.0006		
21	.1959	+.0004		
22	.0971	−.0011	300-ml volume containing 20 ml of H_2SO_4, 2 g of succinic acid and 1 ml H_2O_2 (30 percent)	
23	.0981	−.0007		
24	.0990	−.0018		
25	.0978	−.0005	100-ml volume containing 20 ml of H_2SO_4, 1 g of succinic acid and 1 ml H_2O_2 (30 percent).	Duration of reduction 12 to 15 min in experiments 25 to 28, inclusive. 0.1509 g, 0.1006 g and 0.1960 g of TiO_2 present during reduction in experiments 25, 26, and 27, respectively.
26	.0982	−.0006		
27	.1032	−.0006		
28	.1032	−.0012		
29	.1046	−.0001		
30	.1947	−.0018		
31	.1942	+.0001	300-ml volume containing 60 ml of H_2SO_4, 3 g of succinic acid, and 2 ml H_2O_2 (30 percent).	

III. Discussion

A study of the results recorded in tables 1 and 2 indicates that solutions containing 20 percent of sulfuric acid by volume tend to yield slightly positive values, whereas those containing 15 percent are somewhat low. No study of this variation was undertaken, but in a few experiments the presence of traces of hydrogen sulfide was indicated, notably in solutions of higher acid concentration, by a slight discoloration of moistened lead-acetate paper on contact with the gases evolved. A similar case has been noted during the reduction of chromium solutions [6].

The presence of added titanium dioxide, as recommended by some investigators [1, 7] as an aid in securing uniform and complete reduction, does not appear to be a requisite. Experiments 6, 25, 26, and 27 of table 2 yielded slightly low results in the presence of this constituent but gave, on repetition in the absence of titania, equally unsatisfactory values, thus indicating other factors as a source of error.

A reconciliation of the differences between experiments 6, 7, and 8 with 20 and 21 of table 2 and experiments 11 and 21 with 9 and 20 of table 1 is difficult because of the factors involved. The low and unsatisfactory values obtained in these experiments are believed to be largely due to the amount and concentration of columbium that each reductor is capable of handling, although other factors, such as a lower concentration of acid and the age of the reductors, may have exerted contributory effects. A repetition of the experiments yielding low results, in a somewhat larger volume of solution, gave satisfactory results as is shown by experiment 31 of table 2 and experiments 22 and 23 of table 1. A study of the results indicates that for a satisfactory reduction it is necessary to maintain the proper relationship between both the concentration and amount of columbium to be reduced and the size of the reductor that is to be used.

Experiments 6, 10, and 12 of table 1 indicate progressively the failure of an amalgam that had proved satisfactory in a series of 11 prior determinations involving a total of 2.66 g of Cb_2O_5. The smaller reductor, used in the experiments recorded in table 2, gave no indication of exhaustion at the conclusion of a series of 14 determinations involving 1.46 g of oxide.

With the reductors employed in the present investigation, desirable limits appear to be 300 mg of Cb_2O_5 contained in a volume of 200 ml for the 33-in. reductor and 175 mg in a similar volume for a reductor with an 18-in. column. The above quantities may be materially increased if larger volumes of the Cb_2O_5 solution to be reduced, at the appropriate acid concentration, are employed.

Solutions containing as impurities elements that are reduced to metal by zinc should not be introduced into the reductor, since their presence tends to result in an unnecessarily violent evolution of hydrogen.

IV. Recommended Procedure

The following procedure describes conditions suitable for solutions that may contain as much as 300 mg of Cb_2O_5 and requires the use of a reductor having a long column of amalgamated zinc. With solutions containing not more than 175 mg of the oxide, satisfactory reductions can be effected in a shorter reductor, such as one with an 18-in. column.

Fuse a dry weighed sample of not more than 300 mg of the oxide in a 25-ml covered silica (or equivalent) crucible with 3 to 5 g of potassium pyrosulfate. Cool, transfer the covered crucible with contents to a covered 250-ml beaker, add 20 ml of sulfuric acid, and heat moderately to dissolve the melt. Cool, add 1 to 2 ml of hydrogen peroxide (30%), cautiously dilute with 100 ml of water, and rinse and remove the crucible and cover. Cool, add 20 ml of sulfuric acid, dilute to 200 ml with water, add 2 g of succinic acid, and heat moderately, while stirring, until the succinic acid dissolves.

Reduce the columbium in a reductor having a 33-in. column in the following manner: First clean and preheat the reductor by pouring through it hot diluted sulfuric acid (1+19) and then hot water (90° C). Discard the washings. Place a three-fold excess of ferric iron in the receiver and attach to the reductor. Pour into the reductor 100 ml of sulfuric acid (1+4) heated to 65°±5° C. With the aid of suction draw the foregoing solution, the solution of the columbium, 150 ml of sulfuric acid (1+4) containing 1 percent of succinic acid, each at 65°±5° C, and 200 to 250 ml of cold water slowly through the reductor without interruption at such a rate (unchanged) that the total time for the passage of all solutions is not less than 25 min.[3] Cool the solution of reduced columbium by immersion of the receiver in ice water during the operation. Remove the receiver from the reductor, rinse and drain the outlet tube in the customary manner. Add 10 ml of phosphoric acid (85%) and titrate with a 0.1-*N* solution of potassium permanganate (0.0066455 g of Cb_2O_5/ml) [8], using orthophenanthroline as an indicator. Correct the titration by deducting the amount of potassium permanganate consumed by a blank determination, involving all reagents, obtained under identical conditions. To insure absence of oxidizable impurities each of the acid-wash solutions is permanently tinted, while hot, by the addition of a few drops of a solution of potassium permanganate.

[3] During reduction, particularly during passage of the columbium solution the reductor alternately fills and empties due to formation of gas. This condition, although resulting in a nonuniform rate of passage of the solution, is normal and should not be disturbed. With volumes of columbium solution exceeding 200 ml, the time of reduction is materially increased.

V. References

[1] T. R. Cunningham, Ind. Eng. Chem., Anal. Ed. **10,** 233 (1938).

[2] W. R. Schoeller and E. F. Waterhouse, Analyst, **49,** 215 (1924).

[3] H. W. Stone and D. N. Hume, Ind. Eng. Chem., Anal. Ed. **11,** 598 (1939); H. A. Liebhafsky, J. Am. Chem. Soc. **59,** 452 (1937).

[4] G. E. F. Lundell and H. B. Knowles, Ind. Eng. Chem. **16,** 823 (1924).

[5] W. R. Schoeller, Analyst **57,** 750 (1932).

[6] J. R. Branham, J. Research NBS **21,** 45 (1938) RP1112.

[7] W. D. Treadwell, Helv. Chim. Acta **5,** 806 (1922).

[8] R. M. Fowler and H. A. Bright, J. Research NBS **15,** 493 (1935) RP843.

WASHINGTON, December 13, 1948.

U. S. Department of Commerce
National Bureau of Standards

Research Paper RP1981
Volume 42, April 1949

Part of the Journal of Research of the National Bureau of Standards

Effect of Concentration on the Viscosity of Dilute Solutions*

By Robert Simha

A theory of the higher coefficients of the viscosity-concentration curve of a suspension of nonspherical particles is presented. Starting with the simple model of a dumbbell, the flow around a single particle and its modification due to interaction with other particles are considered. It is shown that the coefficients a_i in the equation

$$\eta=\eta_0(1+a_1c+a_2c^2+a_3c^3+\ldots)$$

are related to each other, namely,

$$a_2=k_1a_1^2,\ a_3=k_2a_1^3\ldots,$$

where the k's are independent of molecular size, in agreement with empirical equations. An explicit value for k_1 is obtained that applies also to models consisting of various arrays of spheres. The variation of k_1 with molecular shape is discussed, and various factors affecting the numerical values and the validity of the last-mentioned equation are pointed out.

I. Introduction

The dependence of the viscosity η of a dilute solution on the concentration c (expressed as volume fraction or as weight by volume) can be represented as a power series of the type

$$\eta=\eta_0(1+a_1c+a_2c^2+a_3c^3+\ldots), \qquad (1)$$

if the solute is a nonelectrolyte. η_0 is the viscosity of the pure solvent. Considerable experimental and theoretical effort has been devoted to a determination of the coefficient a_1, the so-called intrinsic viscosity, for suspensions of particles of various shapes since Einstein's [1][1] original hydrodynamic treatment of spheres. In these hydrodynamic theories, a_1 is a measure of the disturbance of the flow of the solvent due to the presence of the solute particles at infinite dilution. The total effect under such conditions is the sum of the effects of the individual particles. For the range of higher concentrations, a number of empirical equations have been proposed. They can all be expressed as a power series of type given in eq 1. As one can readily see, the theoretical calculation of the higher coefficients a_2, a_3, etc., becomes increasingly complicated. It has been carried out explicitly first for the coefficient a_2 of a spherical suspension by the author [2]. a_2, a number independent of size for spheres, measures the disturbance of the flow around a particle by a second one at a finite distance from the first. The method applied in the particular case is analogous to the procedure first developed by Smoluchowski [3] to obtain the modification of Stokes' law for the resistance of a sphere caused by the presence of a second one. Smoluchowski's results, of which we shall make use, are obtained by a perturbation in terms of inverse powers of the distance between the two spheres.

Empirically it has been suggested [4, 5] that the coefficients a_1 and a_2 are related in polymer solutions by the equation

$$a_2=ka_1^2, \qquad (2)$$

where the factor k is independent of the dimensions

[1] Figures in brackets indicate the literature references at the end of this paper.

* Awarded an A. Cressy Morrison Prize in Natural Science in 1948 by the New York Academy of Sciences.

826086—49——6

of the solute particle but may vary with the solute-solvent system. In several instances, although not always, this rule seems to apply satisfactorily. It is the purpose of this paper to examine the validity of the proportionality (eq 2), using first the simplest model for a nonspherical particle, namely, that of a dumbbell considered originally by Kuhn in his treatment of intrinsic viscosity [6]. This model can be extended to that of a pearl string currently used by various authors in the description of hydrodynamic properties of chain molecules.

In section II the velocity distribution around a single particle and the intrinsic viscosity a_1 are obtained because the results are needed for what follows. In sections III and IV, interaction effects between solute molecules are considered. In section V attention is devoted to the nature of the approximations used and to the effect of various factors on the validity of eq 2 and the magnitude of the parameter k.

II. Flow around an isolated particle. Intrinsic viscosity

Figure 1 illustrates the notations and reference axes used. $2L$ is the length of the dumbbell and a the radius. It will be assumed that $a/L \ll 1$. Let the flow of the pure solvent be represented by a simple shearing motion in the X_1X_2-plane, namely,

$$u_1^0 = qX_2,\ u_2^0 = u_3^0 = 0, \tag{3}$$

where q is the velocity gradient and u_i^0 the velocity component parallel to the X_i-axis. If the dumbbell is held in a given orientation relative to the reference system X_i, the centers P and Q have the coordinates $x_k(P)$ and $x_k(Q) = -x_k(P)$, respectively. Equation 3 then gives for the velocities at P and Q

$$u_1(P) = qx_2(P);\ u_1(Q) = -u_1(P), \tag{3a}$$

where the $x_k(P)$ are functions of the length L and the direction cosines of the particle axis. In the absence of rotatory Brownian motion, this flow will rotate the particle axis into preferred directions. If one superimposes upon the motion (eq 3) a second one resulting from the spins of the particle and considers the resulting force and torques acting on the spheres P and Q, one arrives at a result corresponding in three dimensions to Kuhn's [6] and identical with Jeffery's [7] formulae

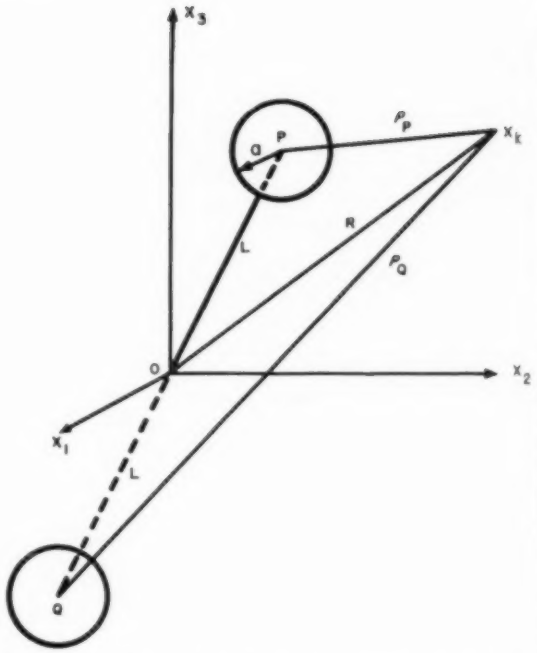

FIGURE 1. *Dumbbell model and reference axes used and geometric relations involved.*

for the rate of change of the orientation specialized for a thin rod. Here however we shall be concerned only with the case of so-called complete Brownian motion, where any orientation tendency is absent. Following a previous procedure [8] we shall consider only the effects of the velocities (eq 3) and (eq 3a) on the particle.

The change in the unperturbed flow (eq 3) due to a single dumbbell is obtained as a solution of the hydrodynamic equations of motion, which neglecting inertia terms, assume in this case the form

$$\left.\begin{aligned} \eta_0 \nabla^2 u_i &= \frac{\partial p}{\partial X_i} \\ \frac{\partial u_m}{\partial X_m} &= 0. \end{aligned}\right\} \tag{4}$$

Here, as in the following, summations from one to three are performed over twice occuring indices m. p is the pressure. At infinite distance R, u_i has to assume the form shown in eq 3. If the velocity u_i is transformed to a reference system $X_i(P)$ parallel to the first but with its origin at P, such that $X_2 = X_2(P) + x_2(P)$, it is seen that

the velocities u_l consist of two parts if the mutual disturbance between the two spheres is neglected. The first satisfies the condition imposed by the $X_2(P)$—term. The required solution is of the type given by Einstein [1]. The second part, satisfying the constant velocity $qx_2(P)$ is of the type given by Stokes [9] for translational flow. Now for the calculation of the dissipated energy of the system particle plus solvent, it is sufficient to consider the velocity and pressure distribution at large distances compared with the dimensions of the solute molecule, and therefore a fortiori large compared with the radii a of the spheres. As Einstein's solution contains terms of the order $a^3/\rho_P{}^2$ (multiplied by a velocity gradient) and higher, while in Stokes' solution terms of the order a/ρ_P (multiplied by a velocity) are found, the former can be neglected for our immediate purposes. Physically this amounts to concentrating the effect of each sphere on the solvent flow in its center P or Q. The calculation of the perturbing field of flow then bears a certain formal similarity to that of the field of a rigid dipole, and including hydrodynamic interaction, to the calculation of dipole-dipole interaction. It should be remembered, however, that at distances close to the particle the equations given below are invalid. For the disturbance due to sphere P, we find in this manner from Stokes' solution neglecting terms of the order $a^3/\rho_P{}^3$:

$$\left.\begin{aligned} u_l{}^P &= -\frac{3}{4}\,u_1(P)\,\frac{a}{\rho_P}\,\delta_{1l} - \frac{3}{4}\,u_1(P)\,\frac{aX_1(P)X_l(P)}{\rho_P{}^3} \\ p &= \text{const.} - \frac{3}{2}\,\eta_0 u_1(P) a\,\frac{X_1(P)}{\rho_P{}^3}, \end{aligned}\right\} \quad (5)$$

where

$$\delta_{1l} = \begin{cases} 1 & l=1 \\ 0 & l\neq 1. \end{cases}$$

The additional velocity $u_l{}^Q$ around sphere Q is given by an analogous equation. From eq 3a and 5 it will be seen that the total velocity obtained by superposition of $u_l(P)$ and $u_l(Q)$ will contain terms

$$\frac{1}{\rho_P} - \frac{1}{\rho_Q}$$

and

$$\frac{X_1(P)X_l(P)}{\rho_P{}^3} - \frac{X_1(Q)X_l(Q)}{\rho_Q{}^3}.$$

At points in the field of flow for which not only $\rho_P,\ \rho_Q \gg a$, but also $R \gg L$, it is permissible to expand these quantities in terms of the ratio L/R (see fig. 1) and to discard the third and higher powers of L. Omitting details, one finds

$$\left.\begin{aligned} \frac{1}{\rho_P} - \frac{1}{\rho_Q} &= \frac{2}{R^3}\sum_k X_k x_k(P) \\ \frac{X_1(P)X_l(P)}{\rho_P{}^3} - \frac{X_1(Q)X_l(Q)}{\rho_Q{}^3} &= \\ \frac{6X_1X_l}{R^5}\sum_k X_k x_k(P) - \frac{2}{R^3}&\left[X_1 x_l(P) + X_l x_1(P)\right] \\ \frac{X_1(P)}{\rho_P{}^3} - \frac{X_1(Q)}{\rho_Q{}^3} &= \frac{6X_1}{R^5}\sum_k X_k x_k(P) - \frac{2x_1(P)}{R^3}. \end{aligned}\right\} \quad (6)$$

The velocity to be added to eq 3 is then given by

$$\left.\begin{aligned} u_l &= -\frac{3}{2}\,\frac{u_1(P)a}{R^3}\left\{\sum X_k x_k(P)\delta_{1l} - \right. \\ &\qquad \left.[X_1 x_l(P) + X_l x_1(P)] + \frac{3X_1X_l}{R^2}\sum X_k x_k(P)\right\} \\ p &= \text{const.} - 3\eta_0\,\frac{u_1(P)a}{R^3}\left[\frac{3X_1\sum X_k x_k(P)}{R^2} - x_1(P)\right]. \end{aligned}\right\} \quad (5a)$$

Equation 5a is, of course, a solution of the equations of motion (eq 4). It is useful to write it in the form of Lamb's [9] general solution in terms of spherical harmonics. It is easily found that eq 5a corresponds, using his notation, to:

$$p_{-3} = p,\ \chi_{-2} = -\frac{3}{2}\,\frac{au_1(P)}{R^3}\,[X_2 x_3(P) - X_3 x_2(P)]. \quad (5')$$

In order to obtain the dissipation of energy caused by the flow (eq 5a), one considers a large spherical volume $V = \frac{4\pi}{3}\,R_0{}^3$ around the particle. Let $p_{rX_l}{}^0$ and p_{rX_l} denote the components of the radial stresses exerted per unit area on the surface of this sphere. Then one derives from eq 3 and the definition of the stresses:

$$p_{rX_1}{}^0 = \eta_0 q\,\frac{X_2}{R_0};\ p_{rX_2}{}^0 = \eta_0 q\,\frac{X_1}{R_0};\ p_{rX_3}{}^0 = 0. \quad (3b)$$

Equation 5′, together with an expression cited in [9] yield

$$p_{rx} = \frac{18\eta_0 u_1(P)a}{R^3}\left\{\frac{2X_1{}^2}{R^2}\sum X_k x_k(P) - X_1 x_1(P)\right\}. \quad (7)$$

The rate of dissipation per unit volume is given by:

$$\frac{dW}{dt}=\frac{1}{V}\int(p_{rx_m}{}^0+p_{rx_m})(u_m{}^0+u_m)dS \qquad (8)$$

where the integral is extended over the surface of the sphere R_0. The result is, omitting terms of the order $1/R_0$ and using eq. 3, 3a, 3b, 5a, and 7:

$$\frac{dW}{dt}=\eta_0 q^2\left[1+\frac{36\pi}{5}\frac{ax_2(P)^2}{V}\right], \qquad (8a)$$

if the particle is held in a fixed orientation. If the solution consists of n particles dissolved in the volume V, such that $N=n/V$ represents their average number per unit volume, one has

$$2\,\frac{4\pi}{3}\,a^3N=c, \qquad (9)$$

where c is the volume concentration. In the present case all effects are additive, and hence the dissipation of the whole solution is obtained by combining eq. 8a and 9 to

$$\frac{dW}{dt}=\eta_0 q^2\left(1+\frac{27}{10}\frac{x_2(P)^2}{a^2}c\right) \qquad (8b)$$

In order to obtain the viscosity η of the solution we follow the method of reference [1].[2] It will be assumed that the solute molecules are randomly distributed in the volume V. Let particle i have its center situated at a point $\xi_k(i)$ in the X_k-system, $k=1, 2, 3$; $i=1, 2, \ldots n$. Its contribution $u_l(i)$ to the flow disturbance at a point X_k is obtained from eq 5a if the coordinates X_k are replaced by the relative coordinates $X_k-\xi_k(i)$. Hence we can write for the velocity distribution in the whole solution

$$u_l=\delta_{1l}qX_2+\sum_{i=1}^{n}u_l(i). \qquad (5b)$$

The viscosity of the pure solvent can be defined by the relation

$$\left(\frac{dW}{dt}\right)\text{solvent}=\eta_0 q^2=\eta_0\left[\frac{\partial u_1{}^0}{\partial X_2}+\frac{\partial u_2{}^0}{\partial X_1}\right]^2_{X_k=0}. \qquad (10)$$

In the same manner we regard the solution as a liquid with effective viscosity η subject to an effective gradient q_s defined as

$$\frac{dW}{dt}=\eta q_s{}^2=\eta\left[\frac{\partial u_1}{\partial X_2}+\frac{\partial u_2}{\partial X_1}\right]^2_{X_k=0}$$
$$=\eta\left\{q+\sum_{i=1}^{n}\left[\frac{\partial u_1(i)}{\partial X_2}+\frac{\partial u_2(i)}{\partial X_1}\right]_{X_k=0}\right\}^2 \qquad (10a)$$

where the left-hand side is given by eq 8b. As $\partial/\partial X_k=-\partial/\partial\xi_k(i)$, the sum in eq 10a may be replaced by

$$-\sum_{i=1}^{n}\left[\frac{\partial u_1(i)}{\partial\xi_2(i)}+\frac{\partial u_2(i)}{\partial\xi_1(i)}\right]_{X_k=0}\doteq$$
$$-N\int_V\left(\frac{\partial u_1}{\partial\xi_2}+\frac{\partial u_2}{\partial\xi_1}\right)_{X_k=0}d\tau$$

if an integral is substituted for the sum. The integration is to be carried out over the whole volume V. The expression can be transformed into an integral over the surface S, namely,

$$-N\int_S\left(u_1\frac{\xi_2}{R_0}+u_2\frac{\xi_1}{R_0}\right)_{X_k=0}dS.$$

Substitution from eq 5a then leads to the result:

$$q_s=q\left(1-\frac{9}{10}\frac{x_2(P)^2}{a^2}c\right). \qquad (11)$$

Thus the viscosity η of the solution follows from eq 10a as

$$\eta=\eta_0\left[1+\frac{27}{10}\frac{x_2(P)^2}{a^2}c\right]\left[1-\frac{9}{10}\frac{x_2(P)^2}{a^2}c\right]^{-2}. \qquad (12)$$

Equation 12 gives the correct viscosity up to linear terms in the concentration c. Averaging over-all (random) orientations, $\langle x_2(P)^2\rangle=(L^2/3)$, we finally obtain

$$\eta=\eta_0\left(1+\frac{3}{2}\frac{L^2}{a^2}c\right). \qquad (13)$$

The intrinsic viscosity for the model under consideration is proportional to the ratio L^2/a^2 in concordance with the familiar result obtained for infinitely thin ellipsoids or rods not subject to any orientation effects by the flow gradient.

The quadratic and higher terms in c obtained from eq 12 have to be discarded as long as hydrodynamic interaction effects that give contributions of the same character and order of magnitude [2], are not taken into account. This has sometimes not been observed in the literature when Einstein's results have been extended to higher concentrations. However, it can be seen that the higher terms in eq 12 will, after averaging the powers of $x_2(P)$, contain successively higher powers

[2] The procedure given in reference [7] can equally well be made use of when interaction effects are absent.

of the ratio L^2/a^2, thus confirming the empirical relation (eq 2) which may now be written as

$$a_2=k_1a_1^2;\ a_3=k_2a_1^3\ldots., \qquad (2a)$$

where the k's are, for the present model, pure numbers and independent of the dimensions of the molecule.

Equation 13 could, of course, have been derived in a much more straight-forward manner by considering the frictional resistance to the flow offered by each of the two spheres. The rate of dissipation arising in this way is given by the product of frictional force and relative velocity. If the latter quantity is taken from eq 3a, we have by application of Stokes' law

$$\frac{dW}{dt}=\eta_0q^2+6\pi\eta_0aq^2\ [x_2(P)^2+x_2(Q)^2]\ N.$$

Elimination of N by means of eq 9 leads at once to eq 13.

III. Interaction between two particles

The influence of a second particle on the viscous flow around a first has been considered first by Smoluchowski [3] for spheres in translational motion, leading to a modification of Stokes' law. The effect so obtained is a function of the ratio between radii and mutual distance of the two spheres. More exact calculations are reviewed in Oseen's treatise [3]. Rotating spheres have also been treated [2] and calculations for nonspherical particles have been presented [3, 10]. The principle of Smoluchowski's method consists in seeking to fulfill by successive "reflections" the hydrodynamic boundary conditions on the surfaces of all solid bodies involved. That is, additional flow distributions are superimposed on the previous flow, to compensate for the additional disturbance at the boundary between particle and fluid induced by the neighbors of the former. Thus the boundary conditions are fulfilled to successively higher degrees of approximation. The first approximation that is sufficient for our present purpose has been shown [3] to fulfill the boundary conditions not at each point of the surface, which would make it an exact solution, but on the average over the whole surface. The velocity distribution is in other words such that, if averaged over the surface of the sphere, it gives no relative motion between the sphere and the liquid at their boundary. The solution previously employed by the author [2] in the viscosity treatment is of the same degree of accuracy.

Smoluchowski's original equations refer to spheres moving in the same direction with equal speeds. His results are modified slightly if this equality does not hold. Let the position of the centers of two spheres be given by $\xi_k^{(1)}$ and $\xi_k^{(2)}$ in a coordinate system fixed in space, their mutual distance by R_{12} and their respective velocities in the ξ_1-direction by $U_1^{(1)}$, $U_1^{(2)}$. At a point ξ_k (fig. 2) the velocity and pressure distribution pro-

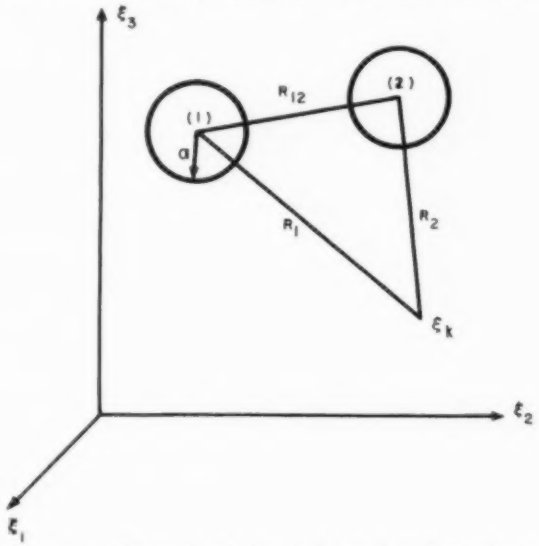

FIGURE 2. *Geometric relations in interaction of two spheres, equations 14 and 15.*

duced by sphere 1 at large distances R_1 has the following form:[3]

$$\left.\begin{aligned} u_i^{(1)}&=U_1^{(1)}U_{i1}^{(1)}(\xi_k)-U_1^{(2)}U_{m1}^{(1)}(\xi_k^{(2)})U_{im}^{(1)}(\xi_k)\\ p^{(1)}&=\frac{3}{2}\eta_0a\ \frac{(\xi_m-\xi_m^{(1)})}{R_1^3}\ [U_1^{(1)}\delta_{m1}-U_1^{(2)}U_{m1}^{(1)}(\xi_k^{(2)}],\\ U_{ij}^{(1)}(\xi_k)&=\frac{3}{4}\frac{a}{R_1}\delta_{ij}+\frac{3}{4}\frac{a}{R_1^3}(\xi_i-\xi_i^{(1)})\ (\xi_j-\xi_j^{(1)}) \end{aligned}\right\} \qquad (14)$$

where

[3] The author is indebted to E. O. Knox for checking eq 14.

$U_{ij}^{(1)}(\xi_k^{(2)})$ represents this function at the point $\xi_k^{(2)}$.

An analogous expression results for $u_i^{(2)}$ and $p^{(2)}$. It is seen that $u_i^{(1)}$ and $p^{(1)}$ each consist of two terms. The first is, of course, Stokes' expression. The second one is a function of the mutual distance and represents the interaction. Equation 14 leads to a frictional resistance

$$F_i^{(1)}=6\pi\eta_0 a\left[U_1^{(1)}\delta_{i1}-\frac{3}{4}\frac{a}{R_{12}}U_1^{(2)}\delta_{i1}-\frac{3}{4}\frac{a}{R_{12}^3}(\xi_1^{(2)}-\xi_1^{(1)})(\xi_i^{(2)}-\xi_i^{(1)})U_1^{(2)}\right] \quad (15)$$

Thus the resultant resistance is no longer in the direction of motion.

Let us now consider a second dumbbell (M, N) as shown in figure 3. Relative to its center the points M and N have the coordinates $x_k(M)$ and $-x_k(M)$, which are functions of the orientation of the axis MN in respect to the X_k-system. They determine $u_i(M)$ and $u_i(N)=-u_i(M)$, the respective velocities of the undisturbed solvent flow relative to the particle at points M and N. As in section II we shall be concerned with distances R, which are large in comparison with L. Considering furthermore only molecules that are far apart, the modification of the Einstein-type of motion which gives rise to terms of the order a^6 [2], will be omitted and only a^3-terms retained. With these approximations one can make use of eq 14 and write the velocity around P to be superimposed on u_i^P in eq 5

$$\left.\begin{aligned}\Delta u_i^P=u_1(M)U_{m1}^P(M,P)\,.\,U_{lm}^P(X,P)+\\ u_1(N)U_{m1}^P(N,P)U_{lm}^P(X,P)\end{aligned}\right\}$$

with

$$\left.\begin{aligned}U_{ik}^P(X,P)=\frac{3}{4}\frac{a}{\rho_P}\left\{\delta_{ik}+\frac{[X_i-x_i(P)][X_k-x_k(P)]}{\rho_P^2}\right\}.\end{aligned}\right\} \quad (16)$$

$U_{ik}^P(M, P)$ is obtained from the last equation by replacing ρ_P by ρ_{PM} and the coordinates X_j by $\xi_j+x_j(M)$. The last term in eq 16 is obtained in a corresponding manner. An expression analogous to eq 16 results for Δu_i^Q. We define the interaction coefficients p_{jl} and q_{jl} by means of the relations:

$$p_{jl}=U_{jl}^P(M,P)-U_{jl}^P(N,P);\quad q_{jl}=U_{jl}^Q(M,Q)-U_{jl}^Q(N,Q) \quad (17)$$

and obtain from eq 16 for the total velocity distribution around the molecule P, Q

$$u_i=u_i(\text{Stokes})+u_1(M)p_{m1}U_{lM}^P(X,P)+u_1(M)q_{m1}U_{lm}^Q(X,Q) \quad (16a)$$

where the first term is given by eq 5a. The remainder contains functions of the mutual distance and orientation of the two interacting molecules. As stated previously, one sums over m from one to three.

The quantities U_{lm}^P and U_{lm}^Q in eq 16a are of the same type as Stokes' velocity distribution and can be transformed in the same manner for large distances R. One finds in this manner in analogy to eq 5a

$$\left.\begin{aligned}u_i=u_i(\text{Stokes})+\frac{3}{4}\frac{au_1(M)}{R^3}(p_{m1}-q_{m1})\left\{\sum_k X_kx_k(P)\delta_{lm}-[X_mx_l(P)+X_lx_m(P)]+\frac{3X_lX_m}{R^2}\sum_k X_kx_k(P)\right\}\\ p=p(\text{Stokes})+\frac{3}{2}\eta_0\frac{au_1(M)}{R^3}(p_{m1}-q_{m1})\left\{\frac{3X_m}{R^2}\sum X_kx_k(P)-x_m(P)\right\}.\end{aligned}\right\} \quad (16b)$$

In analogy to eq 7 this makes a contribution to the X_1—component of the radial stress

$$p_{rX1}=p_{rX1}(\text{Stokes})-\frac{9}{2}\eta_0 a\frac{u_1(M)}{R^4}(p_{m1}-q_{m1})\left\{\frac{4X_1X_m}{R^2}\sum X_kx_k(P)-[X_mx_1(P)+X_1x_m(P)]\right\}. \quad (18)$$

Application of eq 8 now yields for the total rate of dissipation per unit volume of the system consisting of solvent plus one particle (P, Q) acted upon by a second one (M, N):

$$\frac{dW}{dt}=\eta_0q^2\left\{1+\frac{36}{5}\frac{\pi a}{V}x_2(P)^2-\frac{6}{5}\frac{\pi a}{V}x_2(M)[3x_2(P)(p_{11}-q_{11})-2x_1(P)(p_{21}-q_{21})]\right\}. \quad (19)$$

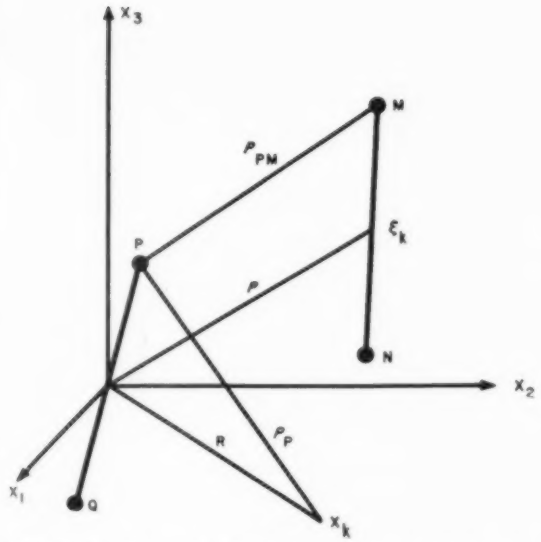

FIGURE 3. *Geometric relations in interaction between two molecules, equation 16.*

The interaction coefficients p_{j1} and q_{j1} can be evaluated for pairs sufficiently far apart in terms of the mutual distance ρ (see fig. 3). A series expansion in terms of $1/\rho$ gives, using eq 17 and discarding higher powers in L/ρ:

$$(p_{j1}-q_{j1}) \doteq -\frac{3a}{\rho^3}\left\{\frac{15}{\rho^4}\,\xi_1\xi_j\sum\xi_k x_k(P)\cdot\sum\xi_k x_k(M)-\right.$$

$$3\,\frac{\xi_1\xi_j}{\rho^2}\sum x_k(P)x_k(M)-\frac{3}{\rho^2}\,[\xi_1 x_j(P)+\xi_j x_1(P)].$$

$$\sum\xi_k x_k(M)-\frac{3}{\rho^2}\,[\xi_1 x_j(M)+\xi_j x_1(M)]\sum\xi_k x_k(P)+$$

$$x_1(P)x_j(M)+x_j(P)x_1(M)+\delta_{j1}\left[\frac{3}{\rho^2}\sum\xi_k x_k(P)\cdot\right.$$

$$\left.\left.\sum\xi_k x_k(M)-\sum x_k(P)x_k(M)\right]\right\}. \qquad (20)$$

Equations 16b and 20 constitute the complete solution of the interaction problem for two particles.

IV. Viscosity of Solution

To obtain the quadratic concentration term in the viscosity one computes first from eq 19 the dissipation of the mixture. If we visualize again the centers of the solute molecules randomly distributed over the volume V, then for the ith particle (P_iQ_i) situated at a point $\xi_k(i)$ and acted upon by a fixed particle (M, N), $p_{j1}(i)-q_{j1}(i)$ becomes a function of the relative coordinates $\xi_k-\xi_k(i)$. It is to be summed over all (P_iQ_i) species interacting with one (M, N) and then multiplied by the total number of particles. In this manner eq 19 yields

$$\frac{dW}{dt}=\left(\frac{dW}{dt}\right)_{\text{Stokes}}-$$

$$\frac{9}{20}\,\eta_0 q^2 c\,\frac{x_2(M)}{a^2}\,\{3x_2(P)\sum_i[p_{11}(i)-q_{11}(i)]-$$

$$2x_1(P)\sum_i[p_{21}(i)-q_{21}(i)]\}, \qquad (19a)$$

where the first term is given by relation (eq 8b). The summations may be replaced by integrations over the volume V. The use of the expression eq 20 in the whole region amounts to neglecting the influence of particles close to a given one. The error so committed increases, of course, at higher concentrations where the average distances between solute molecules become small. The two integrals can easily be transformed into surface integrals by means of Gauss' theorem. Omitting all terms that vanish on integration because of reasons of symmetry, one finds for instance, that the remainder in $(p_{21}-q_{21})$ can be written as

$$(p_{21}-q_{21})=-\frac{3a}{2}\,[x_1(P)x_2(M)+x_2(P)x_1(M)]$$

$$\left[\frac{\partial}{\partial\xi_1}\left(\frac{\xi_1}{\rho^3}-\frac{3\xi_1\xi_2^2}{\rho^5}\right)+\frac{\partial}{\partial\xi_2}\left(\frac{\xi_2}{\rho^3}-\frac{3\xi_1^2\xi_2}{\rho^5}\right)\right]$$

with a similar expression for $p_{11}-q_{11}$. The final result for the dissipation due to particles oriented in a given direction $x_k(P)$ interacting with particles in another direction $x_k(M)$ is

$$\left.\begin{aligned}\frac{dW}{dt}=\eta_0 q^2\Big\{1+\frac{27}{10}\,\frac{x_2(P)^2}{a^2}\,c-\\ \frac{27}{50a^4}\,[4x_1(P)x_2(P)x_1(M)x_2(M)+\\ 6x_2(P)x_2(M)\,(x_2(P)x_2(M)+\\ x_3(P)x_3(M))+x_1(P)^2x_2(M)^2]\,c^2\Big\}.\end{aligned}\right\} \qquad (19b)$$

The next step consists in calculating the effective velocity gradient q_s defined in eq 10a. The velocity distribution around molecule i in the presence of a perturbing molecule at an arbitrary point ξ_k is derived from eq 16b and 20 by replacing X_k by $X_k-\xi_k(i)$ and ξ_k by $\xi_k-\xi_k(i)$.

The corresponding result for the whole mixture follows again from eq 5b. q_s is then derived as in section II. The expression

$$u_1 \frac{\xi_2}{R_0} + u_2 \frac{\xi_1}{R_0}$$

to be integrated over the sphere R_0 now involves terms of the order $\frac{\xi_k^6}{R_0^{11}}$ and $\frac{\xi_k^4}{R_0^9}$. The integration requires the values of the following integrals over the surface of the spherical enclosure:

$$\int \xi_1^2 \xi_2^2 dS = \frac{4\pi}{15} R_0^6; \quad \int \xi_1^4 \xi_2^2 dS = \frac{4\pi}{35} R_0^8; \quad \int \xi_1^2 \xi_2^2 \xi_3^2 dS = \frac{4\pi}{105} R_0^8.$$

The integrand written above depends upon the mutual orientation in each molecule pair. On averaging independently the $x_k(P)$ and $x_k(M)$ terms, there remains after a lengthy but straight forward calculation, omitting all terms which vanish for random orientation:

$$nN \int \left(u_1 \frac{\xi_2}{R_0} + u_2 \frac{\xi_1}{R_0} \right) dS =$$

$$nN \frac{162}{5} \pi q \frac{a^2}{R_0^3} x_1(P)^2 x_2(M)^2.$$

Instead of eq 12, one finds now, using eq 19b, that

$$\eta = \eta_0 \frac{\left[1 + \frac{27}{10} \frac{x_2(P)^2}{a^2} c - \frac{27}{10} \cdot \frac{7}{5} \frac{x_2(P)^2 x_2(M)^2 c^2}{a^4} \right]}{\left[1 - \frac{9}{10} \frac{x_2(P)^2}{a^2} c - \frac{9}{10} \cdot \frac{27}{4} \frac{x_2(P)^2 x_2(M)^2}{a^4} c^2 \right]^2}, \tag{12a}$$

where the denominator represents q_s^2. Expanding up to quadratic terms in the concentration and averaging over the direction cosines, we arrive at the following result for the viscosity of the solution:

$$\eta = \eta_0 \left(1 + \frac{3}{2} \frac{L^2}{a^2} c + \frac{87}{50} \frac{L^4}{a^4} c^2 \right). \tag{13a}$$

On the other hand, eq 12 would have given for the coefficient of the quadratic term the smaller value 81/100.

V. Discussion

Equation 13a yields for the coefficient k_1 defined in 2a the value

$$k_1 = 0.77. \tag{21}$$

Had interaction effects not been taken into consideration, eq 12 would have given

$$k_1 = 0.36. \tag{21a}$$

These results refer so far to the model of a dumbbell. Let the molecule be represented next by a linear array of length $2L$, consisting of a number of spheres with radii a, ν per unit length, arranged evenly. The simple considerations at the conclusion of section II, which lead to eq 13, indicate that now the factor L^2 is replaced by an average value $\langle L^2 \rangle < L^2$. This is seen as follows: The contribution to the dissipated energy by a sphere located at a distance y from the center of the molecule is proportional to y^2. This is to be summed over all groups in the molecule and multiplied by N, the number of molecules in unit volume. N is inversely proportional to $2\nu L$. Thus the intrinsic viscosity a_1 becomes proportional to

$$\frac{2\nu}{2\nu L} \int_0^L y^2 dy = \langle L^2 \rangle.$$

In the case of a randomly coiled chain one averages over all internal configurations of the chain in addition to averaging over all orientations of the whole molecule. As long as coiling is not extensive the determining quantity has been shown repeatedly to be the mean square separation of chain ends. Reverting to the linear array, it can be seen from eq 19 and 20 that the interaction of parts of two molecules at distances y_1 and y_2 from their respective centers will contribute terms proportional to $y_1^2 y_2^2$ to the dissipation rate. Consequently, the coefficient a_2 will be proportional to the square of $\langle L^2 \rangle$ as one could have surmised. A corresponding result obtains for a solution consisting of moderately coiled chains. Thus the numerical values (eq 21 and 21a) should be valid also for a long extended molecule and a coil.

The value (eq 21) is larger than those derived experimentally from suitable extrapolations of viscosity-concentration curves, the latter being usually of the order of 0.3-0.7 and more nearly comparable with the value (eq 21a). On the

other hand, the theory in its present form can reproduce only approximately the contribution of the hydrodynamic interaction to the k_1 coefficient or rather to its excess over 0.36. It has been stressed previously that the evaluation of the interaction coefficients p_{j1}, q_{j1} (eq 17) as a series (eq 20) and therefore eq 19b are valid only for large intermolecular distances. One could improve the situation by dividing the volume V around the center of a molecule into three parts. The first comprises all particles with spherical groups so close to those of the center particle, that an expansion of the mutual disturbance in terms of the ratio a/R_{12} (fig. 2) becomes altogether meaningless. In other words, solute molecules are practically touching each other whatever their relative orientation. From a hydrodynamic point of view, these complexes would be treated as single molecules. Such conditions, frequent at higher concentrations for large molecules will be disregarded here (see also below). In the second region intermolecular distances are large in comparison with the size of the individual group in the molecule, but are of the order of magnitude of the dimensions of the molecule. This would permit the application of Smoluchowski's equation (eq 14), but not of the expansion (eq 20). All further summations are to be performed in terms of individual group to group distances without using expansions in terms of molecular center to center distances. In the third region the current approximations are valid. Of course, the subdivision is somewhat arbitrary. The conditions in region two affect both the numerator and denominator in eq 12a. They should be more important in the calculation of the dissipated energy (see eq 19a) than in that of the effective velocity gradient q_s (compare eq 10a), because of the direct summations over the $(p_{j1}-q_{j1})$ occurring in the former. Also in this region a disturbance of the random mutual orientation of particles merely because of geometric reasons is possible.

The treatment in section II took no account of the hydrodynamic interaction between groups in the same molecule. For the dumbbell a simple calculation based on the result (eq 15) leads in a first approximation to a correction factor in the expression (eq 13) for a_1 equal to

$$1+\frac{9}{20}\frac{a}{L}$$

for $a/L \ll 1$. Also as a first approximation, a_2 remains unaltered. Thus only a decrease of k_1 by a few percent results from this effect. In an array of spheres the interaction of neighboring spheres with velocities of the same sign relative to the surrounding liquid will actually give a correction factor that is smaller than unity. The interaction between different groups within a strongly coiled molecule changes the flow pattern pronouncedly, as has been shown recently by several authors, and this influences also the total mutual disturbance between two different molecules.

It is perhaps noteworthy that the calculation in section II already gives as large a value of k_1 as 0.36. Effects other than purely hydrodynamic ones may contribute to the slope of the viscosity-concentration curve even at relatively moderate concentrations. Experimentally the reported initial slopes have sometimes been obtained by extrapolation at concentrations at which the conditions inherent in our derivation are no longer fulfilled; the solute molecules of large molecular weights are no longer sufficiently far apart on the average. There are indications in the literature that at concentrations roughly below 0.1 g/100 ml solutions of chain polymers exhibit steeper slopes than the extrapolated straight lines. Qualitatively similar effects have been observed in tobacco mosaic virus solutions [11]. In the latter case one is dealing with long rod-like particles and the possibility of aggregation is strongly increased at higher concentrations. Orientation effects are then relatively more important and this reduces the viscosity at higher concentrations. Systematic measurements of the viscosity of very dilute polymer solutions as function of velocity gradient and solvent character are desirable to decide the nature of the apparent downward curvature, found on approaching the region of high dilution.

It is obvious that the present considerations do not apply directly if the nature or the identity of the individual molecule changes with concentration. For instance if formation of aggregates occurs which can be expressed, say, by an equilibrium constant K between double and single molecules it is seen that this makes an additional contribution to the coefficient a_2, namely,

$$+K\,(a_1^{(2)}-a_1)$$

where $a_1^{(2)}-a_1$ is the difference between the intrinsic viscosity of double and single molecules.

Thus the higher coefficients in the expansion (eq 1) cannot be found solely by hydrodynamic considerations and therefore eq 2a is then not valid. This is particularly the case when the effect of velocity gradient in concentrated solutions is to be examined. However, even in dilute solution the interaction is more affected by orientation than the intrinsic viscosity.

Finally the present results for asymmetric particles may be compared with those previously obtained for compact spheres. The author's method of calculation [2] leads to a value $a_2=14.1$ [10]. Einstein's results give a value of 4 for a_2. Thus, for spherical particles, the corresponding values are $k_1=2.26$ and 0.64, respectively. It would be of interest to calculate the gradual increase in the k_1-values with increasing symmetry by considering ellipsoidal particles of finite thickness. Such results would be of value in the case of protein solutions and also of chain polymers. One should expect a parallelism between k_1 and other parameters characterizing shape such as the exponent in the modified Staudinger equation. Also branching and cross-linking should result in an increase of k_1. Such changes have been reported. It appears from the foregoing considerations that, leaving aside other factors, the parameter k_1 will remain independent of molecular weight as long as the degree of coiling does not change markedly.

VI. Conclusions

In treating the concentration dependence of η_{sp}, two effects may be considered at low concentrations. Aggregation, or entanglements, and hydrodynamic interaction of distinct molecular entities. The first makes a contribution to the viscosity of the solution, which depends on the frequency of the aggregates and can be described in terms of the intrinsic viscosity of an aggregate. The second one leads to results that are in agreement with empirical relations proposed for dilute solutions. Without explicit calculation of the cubic and higher terms in c it cannot be seen whether η_{sp} is represented by the binomial formulas given by various authors. The present work indicates that they probably are not strictly valid.

The numerical value derived for k_1 (eq 2a and 21) is of the correct order of magnitude but somewhat larger than those encountered for solutions of chain molecules in good solvents, to which the model used is applicable under certain conditions. It seems to be more nearly in agreement with some numerical results for globular proteins. Possible experimental and theoretical reasons for this divergence have been outlined.

The parameter k_1 depends in a characteristic manner on the shape, as determined for coiling molecules by their structure, the solvent environment, and also on the molecular weight. This conclusion can be reached on the basis of the results obtained for two extreme cases treated here and in previous work, respectively. In this connection it is noteworthy that globular proteins appear to give larger values for k_1 than chain polymers. The region between the two extremes of an "open" coil, or dumbbell, and a sphere remains to be treated. On the basis of such a treatment it may become possible to derive information about the properties of the solute similar to that presently obtained from intrinsic viscosities.

It is of interest to examine the influence of the mutual disturbance on the viscosity at finite velocity gradients, when partial orientation in the field of flow occurs. Effects present at infinite dilution should be more pronounced.

VII. References

[1] A. Einstein, Ann. Physik **19,** 289 (1906); **34,** 591 (1911).
[2] E. Guth and R. Simha, Kolloid-Zeits. **74,** 266 (1936).
[3] M. Smoluchowski, Bul. Acad. Sci. de Cracovie **1A,** 28 (1911); C. W. Oseen, Hydrodynamik, Akademische Verlagsgesellschaft (Leipzig, 1927).
[4] G. W. Schulz and F. Blaschke, J. prakt. Chem. **158,** 130 (1941).
[5] M. L. Huggins, J. Am. Chem. Soc. **64,** 2716 (1942).
[6] W. Kuhn, Z. physik. Chem. [A] **161,** 1 (1932).
[7] G. B. Jeffery, Proc. Roy. Soc. [A] **102,** 163 (1923).
[8] R. Simha, J. Phys. Chem. **44,** 25 (1940).
[9] H. Lamb, Hydrodynamics (6th ed. p. 596 and 598, Dover Publications, New York, N. Y., 1945).
[10] O. Gold, Thesis (Vienna, 1937).
[11] H. K. Schachman, J. Am Chem. Soc. **69,** 1841 (1947).

Washington, December 23, 1947.

U. S. GOVERNMENT PRINTING OFFICE, 1948